National Aeronautics and Space Administration

PLANETARY MISSION CONCEPT STUDY FOR THE 2023–2032 DECADAL SURVEY
7 June 2021

Journey to an Ice Giant System

URANUS
ORBITER & PROBE

Amy Simon
Science Co-Lead
NASA Goddard Space Flight Center
amy.simon@nasa.gov

Francis Nimmo
Science Co-Lead
University of California Santa Cruz
fnimmo@ucsc.edu

Richard C. Anderson
Study Lead
Johns Hopkins University
Applied Physics Laboratory
richard.c.anderson@jhuapl.edu

www.nasa.gov/...

Data Release, Distribution & Cost Interpretation Statements

This document is intended to support the 2023–2032 Planetary Science and Astrobiology Decadal Survey.

The data contained in this document may not be modified in any way.

Cost estimates described or summarized in this document were generated as part of a preliminary concept study, are model-based, assume an APL in-house build, and do not constitute a commitment on the part of APL.

Cost reserves for development and operations were included as prescribed by the NASA ground rules for the Planetary Mission Concept Studies program. Unadjusted estimate totals and cost reserve allocations would be revised as needed in future more-detailed studies as appropriate for the specific cost-risks for a given mission concept.

Acknowledgments

The Johns Hopkins Applied Physics Laboratory would like to thank all of the Uranus Orbiter and Probe (UOP) team members, the National Academies of Sciences, Engineering, and Medicine Planetary Science and Astrobiology Decadal Survey 2023–2032 (especially the Giant Planet Systems Panel and the Ocean Worlds and Dwarf Planets Panel), and the NASA Planetary Science Division for supporting this study.

ROLE	NAME	AFFILIATION
Science Champions	Amy Simon	NASA/GSFC
	Francis Nimmo	UC Santa Cruz
Science Points of Contact	Ian Cohen	APL
	Debra Buczkowski	APL
Science/Engineering Consultant	Rob Gold	APL
Study Program Manager	Art Azarbarzin	APL
Systems Engineering	Richard Anderson (Study Lead)	APL
	Debarati Chattopadhyay	APL
	Max Harrow	APL
Mission Design	Juan Arrieta	Nabla Zero Labs
	Martin Ozimek	APL
	Chris Scott	APL
Operations	Andy Calloway	APL
Ground	Alice Berman	APL
	Patrick McCauley	APL
Probe Entry/Descent Analysis	Helen Hwang	NASA Ames
	Dinesh Prabhu	NASA Ames
	Gary Allen	NASA Ames
	Josh Monk	NASA Ames
	John Thornton	NASA Ames
	Soumyo Dutta	NASA Langley
	Alejandro Pensado	NASA Langley
Payload	Kim Slack	APL
	David Coren	APL
	Katherine Rorschach	APL
Instrument Performance	Hari Nair	APL
Propulsion	Jeremy John	APL
Mechanical/Structures	Erich Schulze	APL
Spacecraft Design	Dave Weir	APL
Thermal	Bruce Williams	APL
RF & Radio Science	Reza Ashtari	APL
Power	Dan Gallagher	APL
Guidance & Control	John Wirzburger	APL
	Rebecca Foust	APL
Avionics	Kirk Volland	APL
	Steve Cho	APL
	Christian Campo	APL
	Justin Kelman	APL
Flight Software	Adrian Hill	APL
Harness	Vince Bailey	APL
	Jackie Perry	APL
Integration & Test	Elliott Rodberg	APL
Radiation Assessment	Michelle Donegan	APL
Scheduling	Faith Kahler	APL
Cost Estimation	Kathy Kha	APL
Document Manager	Marcie Steerman	APL

URANUS ORBITER & PROBE

JOURNEY TO AN ICE GIANT SYSTEM

A Journey Whose Time Has Come ...

A Uranus Orbiter & Probe mission was highly ranked in both the *Visions and Voyages* and *Solar and Space Physics* Decadal priorities. The Uranus Orbiter & Probe enables broad multi- and cross-disciplinary science across nearly all Decadal thematic questions and provides a case study for ice giant mass exoplanets.

Q1	Q2	Q3	Q4	Q5	Q6	Q7	Q8	Q9	Q10	Q11	Q12
✓	✓	✓	✓	✓	✓	✓	✓		✓	✓	✓

This mission fully (green) or partially (yellow) addresses most of the thematic questions posed for the 2023–2032 Planetary Decadal Survey.

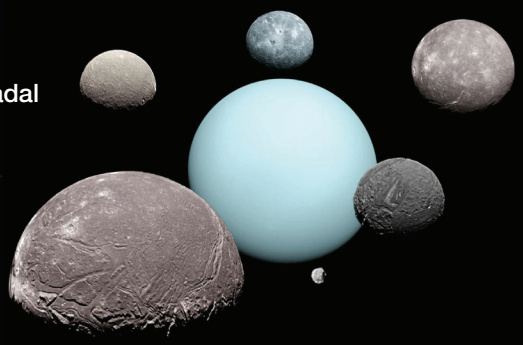

Mission Goals Reveal the Secrets of an Ice Giant System

Origins
Formation
Composition
Migration

Processes
Impacts
Rings
Satellites
Interior
Atmosphere
Magnetosphere
Seasonal Extremes

Habitability
Ocean Worlds
Astrobiology

Interconnections
Exoplanets
Heliophysics

The Uranus Orbiter & Probe mission would deliver an in situ probe into Uranus's atmosphere, then complete a multi-year orbital tour of all aspects of the Uranian system including: atmosphere, interior, magnetosphere, rings, and satellites.

Understanding Solar System Origins: Decadal Thematic Q1–Q3, Q12

- When and where did Uranus form in the protosolar nebula?
- Did Uranus and Neptune migrate or swap positions?
- Did a catastrophic giant impact tilt Uranus, rearrange its interior, and form satellites?

Studying Processes: Decadal Thematic Q4–Q8, Q12

- What mechanisms are transporting heat / energy in the planet and satellites today?
- How do the components within the Uranian system interact with each other?
- What external factors are altering the planet, satellites, and ring compositions?
- What interior structure produces Uranus's complex magnetosphere?

Exploring Habitability: Decadal Thematic Q10, Q11

- Did any of Uranus's moons have substantial heat flux or oceans in the past?
- Are any of the moons presently ocean worlds?

Informing Interconnections

- How do ice giant-mass planets form and evolve in exoplanetary systems?
- How does solar wind couple to a magnetosphere with a rapidly changing orientation?

Orbital Operations: probe insertion followed by 4-year tour, including polar and equatorial campaigns observing Uranus and rings, with multiple targeted flybys of the outer four satellites

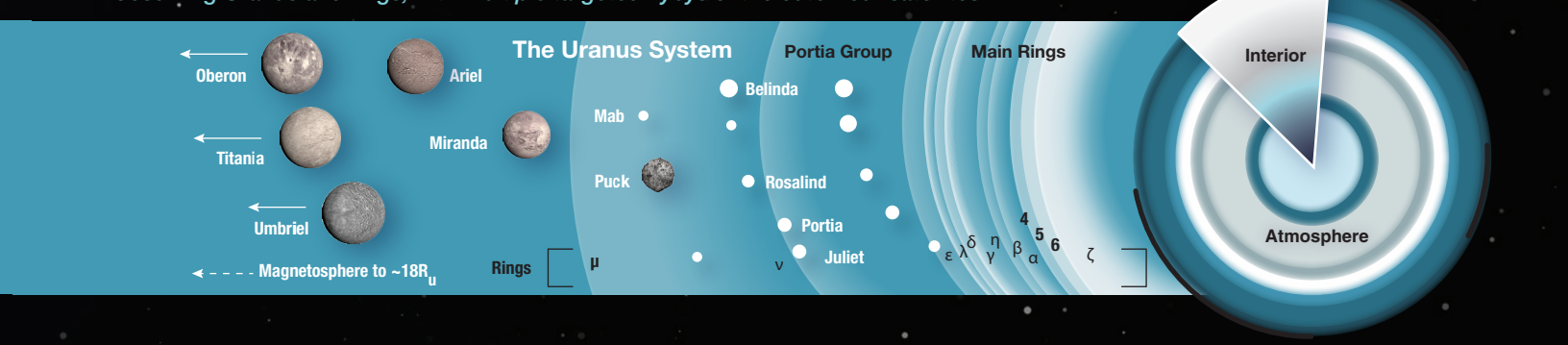

Designed to Be NASA's Next Flagship Mission

- Mission provides context of an entire ice giant system
- Target-rich environment makes for very flexible tour design
- Efficient spacecraft design gives ample margin on launch vehicle
- No new technology is required for mission
- Descopes available
  (removal of WAC, ortho-para hydrogen sensor; reduce tour length)

	Phase A–D (FY25$K)	Phase E–F (FY25$K)	Total (FY25$K)
Total w.o Reserves	1,275,940	542,034	1,817,974
Reserves	634,157	135,508	769,665
Launch Vehicle	236,000		236,000
Total	2,146,097	677,542	2,823,640

Mission-Enabling Launch Windows Occur Every Year, With or Without a Jupiter Flyby

	Launch Date	C3 (Km²/s²)	Path	Inserted Mission Mass (kg)	Time of Flight (years)
Primary	**6/13/2031**	**27.1**	**E(ΔV)EJU**	**4919**	**13.4**
Secondary	**4/29/2032**	**28.8**	**E(ΔV)EJU**	**5111.5**	**12.8**
	10/31/2029	11.3	EVEEJU	6665.4	13.1
	3/7/2031	17.5	EVEEJU	6068.7	12.5
	8/1/2031	18	EVEJU	4855	12.3
	5/3/2032	29.2	E(ΔV)EJU	4527.2	12.2
	1/8/2033	23.6	EVEEU	5933.3	15.3
	5/27/2034	23.1	EVEEU	5626.4	15.2
	2/28/2036	28.2	EVEEU	5240.5	15.3
	1/8/2038	35.5	EVEEU	4812.3	14.2

Instrument Suite

Orbiter Instrument Suite

Magnetometer

Narrow Angle Camera

Wide Angle Camera

Thermal IR Camera

Visible-Near IR Imaging Spectrometer

Comprehensive Fields & Particle Suite

Radio Science + UltraStable Oscillator

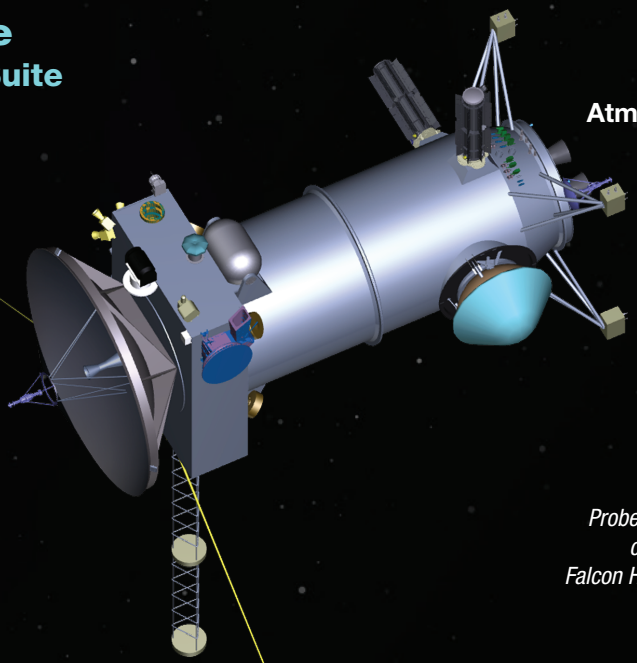

Probe Instrument Suite

Atmospheric Structure Instrument

Mass Spectrometer

UltraStable Oscillator

Ortho-Para Hydrogen Sensor

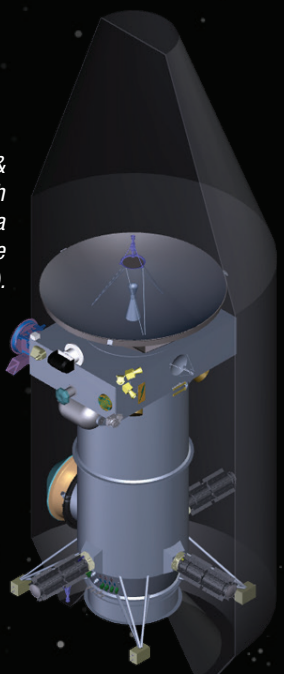

Uranus Orbiter & Probe shown in launch configuration on a Falcon Heavy Expendable (baselined).

Spacecraft Characteristics

- Total flight system mass (including probe): 2756 kg (dry), 7235 kg (wet)
- 30% dry mass and power margins
- 3-axis stabilized, except for passive spin during cruise hibernation
- Uses 3 Next-Gen Mod 1 Radioisotope Thermal Generators
- Planned mission data volume return: 51.9 GB

URANUS ORBITER & PROBE

Planetary Science Decadal Survey

Uranus Orbiter & Probe (UOP) Mission Concept Design Study Final Report

Graphic Cover i
Acknowledgements iii
Fact Sheet iv
Table of Contents vi
Executive Summary 1
1. Scientific Questions & Objectives 2
1.1. Atmosphere & Interior 2
1.2. Magnetosphere 6
1.3. Rings & Small Satellites 7
1.4. Large Satellites & Ocean Worlds 8
1.5. Science Traceability Matrix 9
1.6. Driving Functional Requirements & Tour Design Considerations 12
2. High-Level Mission Concept 14
2.1. Study Request & Ground Rules 14
2.2. Overview & Concept Maturity Level (CML) 14
2.3. Technology Maturity 15
2.4. Key Trades 15
3. Technical Overview 16
3.1. Instrument Payload Description 16
3.2. Flight System 19
3.2.1. Orbiter Element 19
3.2.2. Probe Element 22
3.2.3. Flight System Element Summary 23
3.3. Mission Design & Concept of Operations 25
3.3.1. Interplanetary Cruise 25
3.3.2. Interplanetary Trade Space 26
3.3.3. High Fidelity Analysis 28
3.3.4. Uranus Capture & Probe Release 29
3.3.5. Satellite Tour 31
3.3.6. Mission Design Summary 33
3.3.7. Mission Operations 34
3.4. Risk List 35
4. Development Schedule & Schedule Constraints 36
4.1. High-Level Mission Schedule 36
4.2. Technology Development Plan 36
4.3. Development Schedule & Constraints 36
5. Mission Life Cycle Cost 37
5.1. Introduction 37
5.2. Mission Ground Rules & Assumptions 37
5.3. Cost Benchmarking 38
5.4. Costing Methodology & Basis of Estimate 38
5.5. Confidence & Cost Reserves 40
Appendix A: Acronyms & Abbreviations 42
Appendix B: References 49
Appendix C: Additional Details 53

Executive Summary

The ice giant Uranus is one of the most enigmatic and least explored bodies in the solar system. Many of its characteristics, including its axial tilt, energy balance, atmospheric dynamics and complex magnetic field, present major puzzles. Its five large icy satellites represent potential ocean worlds, with some displaying surprising degrees of geological activity. And Uranus is arguably the closest analog we have to the most common exoplanets. Yet only one spacecraft has explored Uranus, thirty-five years ago; a return to Uranus was a high priority of the 2012–2022 Planetary Decadal Survey and the 2013 Solar and Space Physics Decadal.

The Uranus Orbiter and Probe (UOP) is a Flagship-class mission concept ($2.15B FY$25, Phase A–D, including launch vehicle) developed in response to the 2023–2033 Planetary Science and Astrobiology Decadal Survey with the aim of answering the top-level science questions concerning Uranus, its rings and moons. The mission deploys an atmospheric probe into Uranus shortly after orbit insertion, followed by multiple flybys of Titania to reduce the orbital inclination to the equatorial plane, carrying out observations of the planet as it does so. An equatorial tour of all five major moons follows, completing a 4.5-year science mission phase at Uranus. The tour is highly flexible, with different options available depending upon which moon is used for equatorialization.

The probe carries four instruments to measure atmospheric composition and isotopic ratios, temperature structure and winds. The orbiter carries six instruments – magnetometer, narrow-angle camera, thermal-IR camera, Vis-NIR imaging spectrometer, and a fields and particles suite – plus a radio science capability. This modest payload was selected to address the top-priority science questions concerning Uranus's atmosphere, interior, magnetosphere, rings and small satellites, and large satellites. In doing so it addresses all of the Decadal Survey's twelve questions, with the single exception of Insights from Terrestrial Life.

Mission science questions address three overarching goals – Origins, Processes, and Habitability – and include: When and where did Uranus form in the protosolar nebula? Did a catastrophic giant impact tilt Uranus? What mechanisms transport heat/energy in the planet and satellites? How does the solar wind interact with Uranus's magnetosphere? What external factors are altering the planet, satellites and ring compositions? Are any moons currently ocean worlds, or have they been in the past? These questions are intimately connected to questions of exoplanet system formation and evolution, as well as heliophysics objectives.

The objective of this study was to update the prior Uranus Orbiter and Probe concepts, including a project start between 2023–2030, with refined science goals and payload complement, updated launch vehicles, and a chemical-only mission design. The study was also directed to increase concept maturity/fidelity where possible, at a concept maturity level (CML) of 4.

Alternative Earth-to-Uranus interplanetary trajectories were analyzed to satisfy multiple, competing objectives. Numerous options were identified for launches throughout the 2030s, taking advantage of newer, higher-performing launch vehicles. Optimal prime and backup launch opportunities were identified for Jun 2031 and Apr 2032 with a 13.4-year cruise to Uranus, baselining a Falcon Heavy Expendable with a launch energy (C_3) of 29.36 km^2/sec^2. Both use a Jupiter gravity assist (JGA) to achieve the most cost-efficient solution; however, numerous other viable alternatives without JGA exist, either with modestly increased flight times or the use of Venus. Significant emphasis was placed on optimizing the atmospheric probe deployment while developing an integrated, end-to-end trajectory from launch through disposal, in response to technical feedback from previous ice giant concept studies. The mission design team, in collaboration with NASA Langley and NASA Ames EDL experts, developed a high-fidelity Uranus capture and probe deployment design to demonstrate feasibility. A significant finding of this study is that significant mission risk reduction is possible by deploying the probe after orbital insertion rather than on approach, all while incurring minimal performance penalties. The stacked flight system dry mass of 2756 kg includes 30% margin, with launch mass of 7235 kg. The orbiter is powered by three Mod 1 Next-Generation RTGs (NGRTGs), and is spin stabilized during most of cruise to reduce cost.

As a Flagship mission, UOP has the imprimatur of a broad community. The mission would answer fundamental questions about the origin and evolution of our own solar system, and the characteristics of planets elsewhere. The mission concept requires no new technologies or launch vehicle, and has a highly flexible tour design and ample mass and power margins. The 60th anniversary of the Voyager 2 flyby could be celebrated by the arrival of the next visitor to Uranus.

1. Scientific Questions & Objectives

Uranus and Neptune are mysterious worlds that comprise the only class of planet – ice giants – not yet intensively studied by spacecraft; these worlds hold important clues about our solar system's formation and evolution. Uranus and Neptune are distinctly different than Jupiter and Saturn; their smaller size, chemical enrichments, slower rotation, asymmetric magnetospheres, and diverse satellite-ring systems set them apart from their larger, hydrogen-dominated, cousins. The Uranian system, in particular, is of great interest due to its extreme obliquity, apparent dearth of internal heat, complex magnetic field, and regular ring and satellite system containing possible ocean worlds. Most exoplanets are ice-giant sized; detailed study of this system is vital. The unique Uranian system is also key for understanding solar wind-magnetosphere interactions. Prioritized in the 2013–2022 Planetary Decadal Survey after MAX-C and Europa [Vazan & Helled 2020], and of great international interest [Arridge et al. 2011, 2014; Atreya et al. 2020; Fletcher et al. 2020a], the Uranus Orbiter & Probe (UOP) mission provides broad, multidisciplinary science. There are three overarching science goals of this mission, along with interconnections to astrophysics and heliophysics, with a myriad of discipline-specific questions as described in the next sections (a small subset is shown here):

Origins:

- When and where did Uranus form in the protosolar nebula?
- Did Uranus and Neptune migrate or swap positions?
- Did a catastrophic giant impact tilt Uranus and rearrange its interior?

Processes:

- What mechanisms are transporting heat / energy in the planet and satellites today?
- How do all the components in the Uranian system interact with each other?
- What external factors are altering the planet, satellites, and ring compositions?
- What interior structure produces Uranus's complex magnetosphere?

Habitability:

- Did any of Uranus's moons have oceans in the past?
- Are any of the moons presently ocean worlds?

Interconnections:

- How do ice giant-mass planets form and evolve in exoplanetary systems?
- How does solar wind couple to a magnetosphere with a rapidly changing orientation?

Exhibit 1-1. *The Uranus Orbiter & Probe mission enables broad multi- and cross-disciplinary science across nearly all Decadal thematic questions. This mission was also a high priority in the last Planetary and Heliophysics Decadal Surveys.*

1.1. Atmosphere & Interior

Uranus has a higher proportion of ices than Jupiter and Saturn, though its actual bulk composition is not yet well constrained. Uranus is unique in that it appears to have much less internal heat than the other planets, perhaps due to a catastrophic impact during its formation, or owing to sluggish convection [Friedson & Gonzalez 2017; Guillot 1995; Reinhardt et al. 2020]. However, the structure and dynamics of Uranus's deep interior, as well as the circulation, chemistry, and clouds in its atmosphere, remain poorly constrained. Convection is predicted to be inhibited in its methane cloud layer [Friedson & Gonzalez 2017; Guillot 1995; Leconte et al. 2017], yet the hazy atmosphere of Uranus is variable, not the constant calm blue atmosphere imaged by Voyager 2; frequent, violent storms develop, and the polar caps become more or less opaque with the seasons [Hueso, Guillot & Sanchez-Lavega 2020] (Ex. 1-2). Understanding the interplay between low internal heat, large chemical enrichments of volatile species, seasonal storms on a planet far distant from the Sun, and a perhaps impact-stirred interior structure leads to a series of questions about the atmosphere and interior of Uranus addressable by an orbital mission and atmospheric probe.

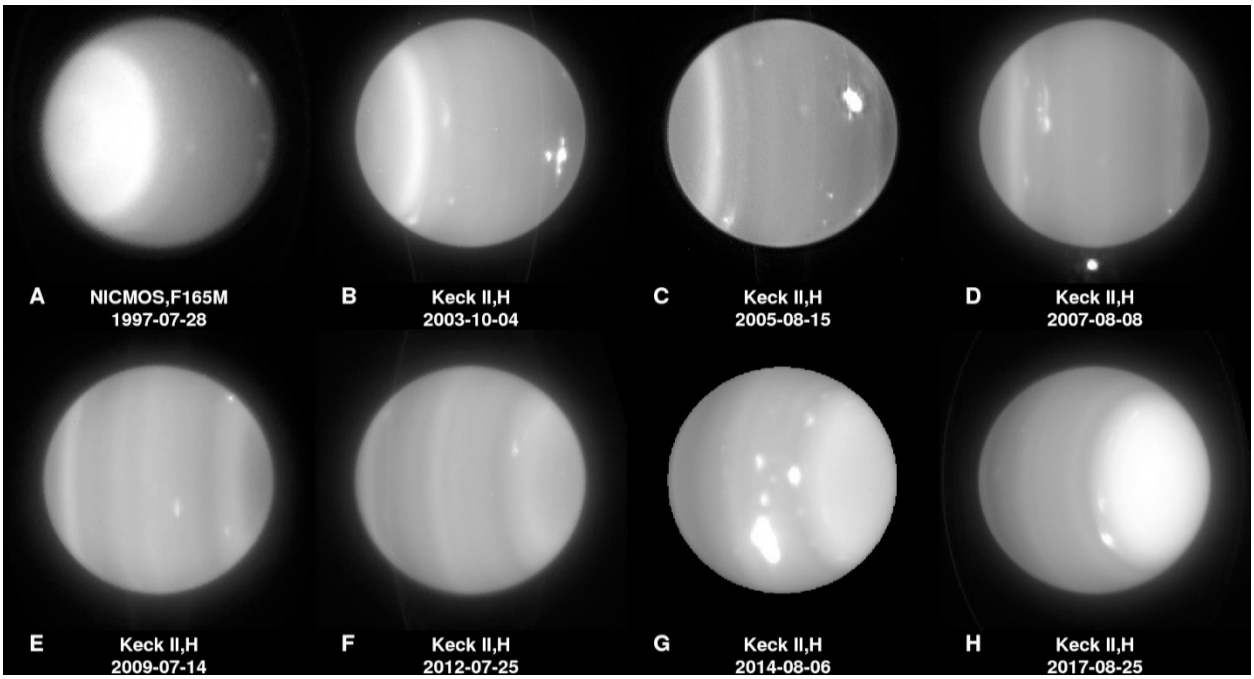

Exhibit 1-2. *Uranus's polar haze and atmospheric variability from Hubble and Keck imaging.*
Credit: L. Sromovsky, P. Fry, I. de Pater, and H. Hammel.

A1. How does atmospheric circulation function, from interior to thermosphere, in an ice giant? Giant planet atmospheric circulation is a complex system that effectively transports energy, momentum, and chemical elements between the interior, weather layer, and upper atmosphere through a combination of radiation, convection, wave propagation, condensation, and precipitation. However, Uranus has the least constrained wind profile of any of the giant planets, simply due to the lack of cloud features easily observable from Earth [Hammel et al. 2005]. Spacecraft measurements of the cloud top winds via imaging, vertical wind shear and lapse rate via thermal imaging, and direct in situ measurement provide information on the weather layer circulation. In situ measurement of disequilibrium species, along with thermal mapping, constrains vertical mixing and its influence on photochemistry [Moses et al. 2020]. Additionally, measuring latitudinal gradients in temperatures, composition, and aerosols can correlate how the banded circulation patterns vary as a function of pressure [Fletcher et al. 2020b]. Lastly the depths of the winds may be measurable with radio science measurements of high order gravitational moments from close planetary passes.

A2. What is the 3D atmospheric structure in the weather layer? Cloud features in Uranus's weather layer are thought to be composed primarily of methane, and possibly hydrogen sulfide, ices. Methane is so abundant that moist convection should be locally inhibited in the methane cloud layer [Guillot 1995], with potentially very strong consequences for the deeper temperatures of the planet [Friedson & Gonzales 2017; Leconte et al. 2017]. Yet, bright storms most often appear suddenly and are quickly sheared apart and dissipate, but without sufficient wavelength coverage and spatial resolution, we cannot resolve their vertical extent; extremely few were visible during the Voyager 2 flyby [Hueso & Sanchez-Lavega 2019; Smith et al. 1986]. Other small storms, particularly near the edge of the polar haze caps, appear to be long lived, but again originate from unknown depths. The importance of precipitation and downdrafts of storms should be assessed as it may lead to the formation of long-lasting, deep abundance variations as observed in Jupiter [Li et al. 2017; Guillot et al. 2020]. Temporal variations in polar haze may be due to variations in dynamics or photochemical reaction rates, but both the stratospheric and tropospheric circulations are poorly constrained due to a lack of small, traceable atmospheric features and the very low signals associated with low atmospheric temperatures. The full 3D circulation can be measured with repeated atmospheric views of varying phase angle, as well as with in situ ground truth measurements of the vertical temperature and wind profiles. Thermal contrasts associated with the banded structure, discrete meteorology, and polar vortices can be provided by thermal-IR mapping, in addition to spectroscopic observations of reflected sunlight to measure contrasts in aerosol properties and composition. Lapse rates, atmospheric stability, and shear on the winds are crucial for determining the dynamics of the atmosphere and the relation to the deeper sub-cloud layers. Vertical structure and waves can be identified in radio occultations. Radio science might help identify lightning.

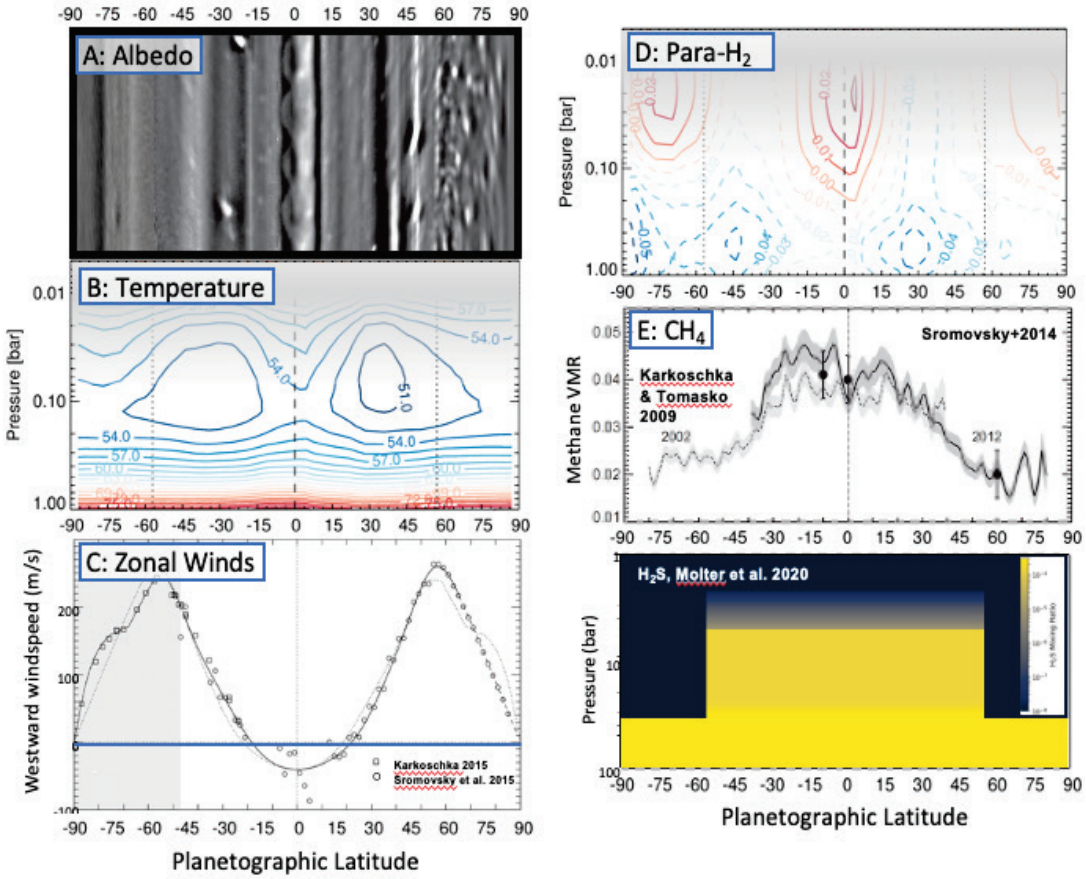

Exhibit 1-3. *Current best knowledge of Uranus's cloud-level variations in albedo, temperatures, zonal winds, para hydrogen fraction, methane and hydrogen sulfide [Fletcher et al. 2020b].*

A3/I1. When, where, and how did Uranus form, and how did it evolve both thermally and spatially, including migration? Uranus's bulk composition traces early solar system formation: ratios of elemental abundances and isotopic ratios in the planets are clues to the types and source regions of the accreted gas; pebbles, and planetesimals, the relative timing of planet formation and disk evolution; and the orbital interactions among the giant protoplanets [Frelikh & Murray-Clay 2017; Helled & Stevenson 2017; Lissauer et al. 2009; Mousis et al. 2020; Velleta & Helled 2020]. Key questions regarding Uranus's growth rate and formation location also remain unsolved [Helled, Nettelman & Guillot 2020; Helled & Fortney 2020]. Measurements of the concentrations of CO in the troposphere, plus noble gases, are needed to determine whether Uranus is a volatile-rich ice giant or a rock-dominated super-Earth [Feuchtgruber et al. 2013; Teanby et al. 2020]. Ex. 1-4 illustrates our current state of knowledge of the giant planets compared with two analogs for their possible solid building blocks

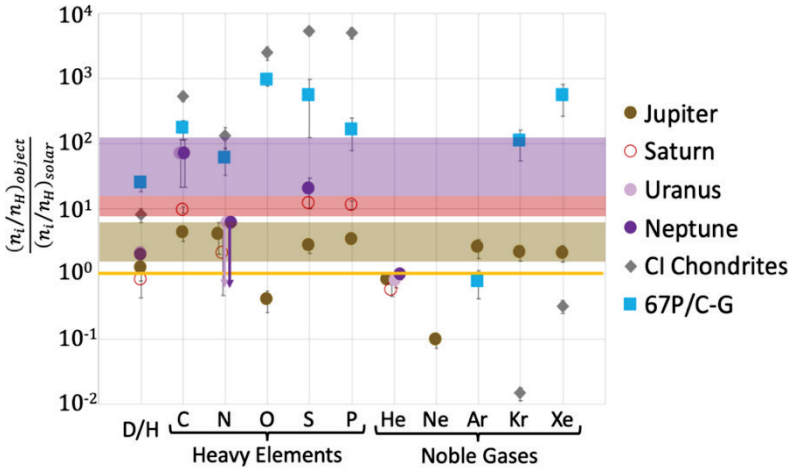

Exhibit 1-4. Current knowledge of giant planet composition. *The colored bars show the predicted heavy element enhancement if the Jupiter (brown), Saturn (red), and Uranus/Neptune (purple) building blocks were solar relative to carbon. The nitrogen estimate for Uranus and Neptune is an upper limit [Mandt et al. 2020].*

[Mahaffy et al. 2000; Mandt et al. 2020; Niemann et al. 1998]. Thanks to the Galileo probe, Jupiter is the only planet for which most key measurements have been made [Niemann et al. 1998]. The He/H_2 ratio is a particularly important compositional ratio that can only be adequately constrained by atmospheric probe data [von Zahn, Hunten & Lehmacher 1998]; at Uranus, almost a factor of two separates the most extreme He/H_2 ratios invoked by remote sensing studies [Orton et al. 2016; Sromovsky, Fry & Kim 2011] delineating the need for in situ measurement. In addition to bulk compositional uncertainties, Uranus has a much lower heat flux than that of the other giant planets indicating that convection in the deep interior may be inhibited by the presence of strong compositional gradients [Podolak, Weizman & Marley 1995; Podolak, Helled & Stevenson 2019; Rosenblum et al. 2011]. In turn, the heat flux is also key to understanding the planet's evolution, internal structure, and atmospheric dynamics. An atmospheric probe will provide direct measurements of noble gas abundances and isotope ratios at Uranus. Of particular importance are the isotope ratios of helium and xenon, which vary significantly in solar system materials and provide direct links to solid building block materials and the early evolution of the protosolar disk [Atreya et al. 2020; Mandt et al. 2020]. Accurate determination of heat flux requires measurement of the planet's Bond albedo and global energy balance from visible to near-infrared wavelengths.

I2. What is the bulk composition and its depth dependence? As in **I1**, the bulk composition of the planet provides evidence for how and where Uranus formed, and protosolar nebula conditions. Variation of composition with depth depends provides information not only on how the planet formed, but also how it has evolved since formation and about its current interior structure. Currently, Uranus's composition must be determined indirectly from interior models. The ratio between H-He and heavy-elements in Uranus is still unknown. In addition, it is still unclear whether Uranus is a water-rich or silicate-rich planet. Interior models of Uranus and Neptune assuming adiabatic temperature profiles with distinct layers predict extremely high water-to-rock ratios in Uranus (19–35× solar) and a total H-He mass of 2 M_{Earth}. The exact estimates are highly model-dependent but also suffer from the high uncertainties in the gravity measurements and other physical properties [Helled, Nettelmann & Guillot 2020; Helled & Fortney 2020]. To further constrain the planetary bulk composition, and its depth dependence, measurements of Uranus's gravity field with high accuracy (ideally up to J_{10} with uncertainty of 10^{-6}) are required. These, along with the measurements in **A3/I1**, can further constrain interior gradients and structure models.

I3. Does Uranus have discrete layers or a fuzzy core, and can this be tied to its formation and tilt? Recent giant planet formation models indicate that the deep interiors of gaseous planets are expected to consist of composition gradients, resulting in fuzzy cores [Helled & Stevenson 2017]. Currently, it is unknown whether Uranus possesses distinct layers or a gradual change in composition. On one hand, ab-initio simulations indicate that rock-and-water and water-and-hydrogen are miscible [Soubiran & Militzer 2015; Soubiran et al. 2017]. On the other hand, laboratory experiments indicate that water and hydrogen may not be fully miscible under Uranian conditions and various structure and evolution models are consistent with Uranus without distinct layers [Helled et al. 2011; Vazan & Hellad 2020; Bailey & Stevenson 2021]. Identifying the existence of a fuzzy core in Uranus not only constrains its formation history but is also critical for understanding its evolution (thermal) history and its measured low luminosity [Podolak, Helled & Stevenson 2019; Scheibe, Nettelmann & Redmer 2019]. In addition, the occurrence of a grazing giant impact, probably relatively early in the evolution of the planet (while Neptune may have suffered a head-on collision), may account for the planet's low luminosity, tilt, and system of moons [Kegerreis et al. 2018; Reinhardt et al. 2020]. Identifying traces of this event through a determination of the amount of mixing in the planetary interior would be a milestone in understanding the formation of the solar system. Measurements of Uranus's gravity field with high accuracy, as in **I2**, can constrain the planet's density structure, as they have for Jupiter. Furthermore, Uranus's complex ring system provides opportunities for using ring seismology to constrain the planet's internal structure, as has been done at Saturn [Mankovich et al. 2018; Fuller 2014]. Composition and thermal balance measurements complement this investigation.

I4. What is the true rotational rate of Uranus, does it rotate uniformly, and how deep are the winds? Uranus's rotational rate, as inferred from the Voyager 2 flyby, may not represent the deep interior as measured radio signals may be affected by local concentration of ions in the planetary magnetosphere [Helled, Anderson & Schubert 2010]. In addition, the complex multi-polar magnetic field signal is expected to originate from relatively shallow depths [Stanley & Bloxham 2004; Stanley & Bloxham 2006], and its instantaneous measurement may not be representative of the deeper rotation period. Determining the rotation rate from a minimization of dynamical heights leads to a significantly faster deep rotation [Helled, Anderson & Schubert 2010] and to significant differences in Uranus's inferred composition and internal structure [Nettelmann et al. 2013]. Additionally, close periapse passes of Jupiter and Saturn by Juno and Cassini, respectively, have revolutionized our understanding of the depth of gas giant zonal winds, by measuring the odd and even gravity

coefficients to high precision. These showed that a potential boundary exists, where differential rotation experiences drag forces in the electrically conducting metallic hydrogen [Kaspi et al. 2018; Guillot et al 2018]. With a smaller internal pressure, but a potential ionic water ocean at great depth, Uranus is likely to be very different, and Voyager's close flyby provided only an upper limit on the wind depths (<1000 km) [Kaspi et al. 2013]. Constraining the true rotation period of Uranus requires accurate measurements of its gravitational field, magnetic field, zonal flow and shape via close periapse passes.

1.2. Magnetosphere

While the global size of Uranus's magnetosphere is intermediate between giant Jupiter and modest Earth, more important is that the large tilt (59°) of the dipole from the spin axis plus a large obliquity (98°) makes the dynamics of Uranus's magnetosphere profoundly weird [Bagenal 1992; Bagenal 2013]. The brief Voyager 2 flyby gave a glimpse of a magnetospheric configuration when the planet's spin axis was roughly aligned with the solar wind flowing from the Sun: the effects of rotation (that dominate Jupiter's vast magnetosphere) were decoupled from the solar-wind-driven convection (that control dynamics at Earth) (Ex. 1-5). At Uranus, both processes occurred simultaneously. Modeling Voyager 2 observations indicated the source of ~10^{24} particles per second produced a tenuous (<1 cm^{-3}) plasma (10s eV protons, electrons) that convects through the system with a timescale of ~days [Selesnick & McNutt 1987]. The magnetotail spiraled downstream with Uranus's 17.3-hour spin period [Toth et al. 2004; Vasyliunas 1986; Voigt, Behannon & Ness 1987]. The unusual geometry of Uranus's magnetic field provoked interest in how the dynamics might change between solstice (Voyager 2 epoch with the spin axis parallel to the solar wind) and equinox (with the spin axis perpendicular). Modeling such geometries showed the equinox period to be particularly dynamic due to the changing angle between the external interplanetary magnetic field (carried from the Sun by the solar wind) and the internal field [Cao & Paty 2017; Cowley 2013]. The process of reconnection between the internal and external fields can drive convection and acceleration of plasma within the magnetosphere via a process derived to explain Earth's magnetosphere call the Dungey Cycle. For Uranus around equinox, models suggest this Dungey Cycle would likely turn on and off multiple times per 17.3-hour spin period [Cao & Paty 2017; Cowley 2013].

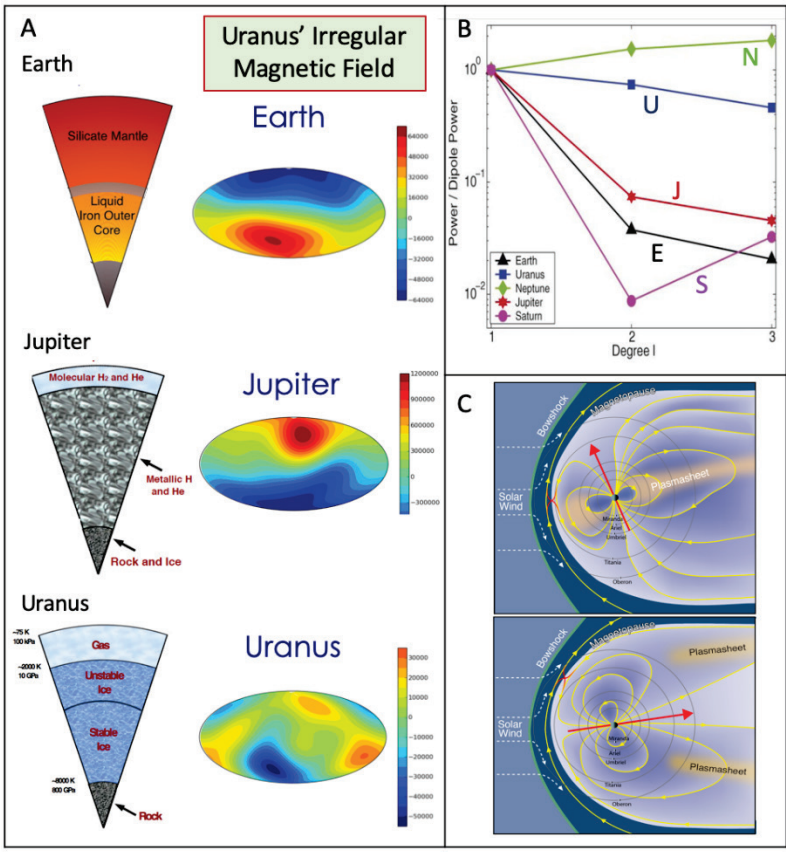

Exhibit 1-5. *(A) Uranus has a very irregular magnetic field that is generated in the shallow unstable ice layer. (B) Unlike regular magnetic fields of Earth, Jupiter and Saturn, at Uranus and Neptune the power in the higher degree moments is comparable to the dipole moment. (C) Around the equinox epoch the magnetosphere geometry shows dramatic changes in structure over the 17.3-hour spin period with the (yellow lines) magnetic field reconnecting (red Xs) in changing locations around the magnetopause boundary with the solar wind.*

M1. What dynamo process produces Uranus's complex magnetic field? To constrain Uranus's dynamo requires quantifying both the internal properties (density, temperature, composition, flows) plus the high-order structure of the magnetic field [Stanley & Bloxham 2004; Stanley & Bloxham 2006]. Multiple close passes by UOP at different longitudes will tie down the magnetic field structure while gravity measurements, combined with physical-chemistry models [Helled, Nettelmann & Guillot 2020], constrain the internal structure and flows. If the orbiter is able to make more than ~20 passes and last more than ~3 years, it will detect secular variation in the

magnetic field (certainly since the Voyager epoch and perhaps over the mission duration), as expected for highly non-dipolar magnetic fields, which provides estimates of flow speeds in the conductive region [Moore et al. 2019].

M2. What are the plasma sources and dynamics of Uranus's magnetosphere, and how do they interact with the solar wind? The plasma measured by Voyager 2 comprised only protons and electrons, creating a major mystery as to why a system believed to be solar wind-driven is lacking heavier solar wind ion species [Selesnkick & McNutt 1987]. On a more extended orbital tour, modern instruments on a UOP mission could measure the extent of material produced by the rings and/or moons. Key to understanding Uranus's dynamic magnetosphere will be continuous measurements of magnetic fields and plasma properties by an orbiting spacecraft made within the system for multiple spin periods and under varying upstream solar wind and interplanetary magnetic field conditions.

M3. How does the magnetosphere interact with Uranus's upper atmosphere and satellite surfaces? Auroral emissions can provide valuable diagnoses of magnetosphere dynamics, as they can be traced back to the electrical currents generated by the magnetospheric interactions. The sources of charged particles responsible for exciting auroral emissions (from UV to radio wavelengths) are largely unknown. Voyager 2 provided the only spatially resolved observation of Uranus's ultraviolet (UV) aurora to date [Herbert 2009] with patches roughly aligned with the magnetic poles, at the solstice geometry. Observations of Uranus's UV aurora taken with the Hubble Space Telescope around the time of the equinox suggest a very different geometry [Lamy 2012]. A UOP mission will monitor Uranus's aurora while measuring the magnetospheric dynamics and the charged particles that precipitate into the atmosphere and excite aurora. At the same time, the charged particles that convect through the magnetosphere also bombard the moons. Radiolysis of icy surfaces also changes the composition and ice structure [Cassidy et al. 2010]. UOP will measure the charged particle fluxes in the environment of the moons and how they vary under magnetospheric geometries, while measuring the surface properties of the moons via spectroscopy.

1.3. Rings & Small Satellites

Uranus is surrounded by a remarkably complex ring-moon system containing nine exceptionally narrow, dense rings and over a dozen small moons, as well as a wide variety of dust populations [Nicholson et al. 2018; Showalter 2020]. Many aspects of this system are still not well understood and pose significant challenges to our understanding of circumplanetary material. For one, we still do not know why so many of Uranus's rings are so narrow. Collisions among ring particles and interactions with magnetospheric plasma should cause ring material to spread out over time. While this natural spreading can be counteracted by gravitational perturbations from either nearby or distant satellites, these specific outside forces can only account for a limited subset of the observed ring features. The forces responsible for sculpting most of Uranus's narrow ring features, therefore, remain yet to be discovered. Meanwhile, the many small moons found just outside the main rings orbit so close to each other that their mutual gravitational interactions are likely to lead to collisions on timescales far less than the age of the solar system [French & Showalter 2012; French, Dawson & Showalter 2015]. Some of the dusty rings within this system may even represent debris from similar collisions that happened in the most recent past. This system of small moons is therefore likely to have had a dynamic recent history. Finally, over longer timescales most of these moons should migrate inwards until they get close enough to the planet to be torn apart to form rings. Indeed, material in this region may have cycled between rings and moons multiple times over the history of the solar system [Hesselbrock & Minton 2017]. The current composition and configuration of these rings and moons may therefore hold clues to how material can accrete into larger objects or fragment into small particles under different conditions. A Uranus orbiter would enable significant advances in our understanding of this ring-moon system by addressing the following two questions:

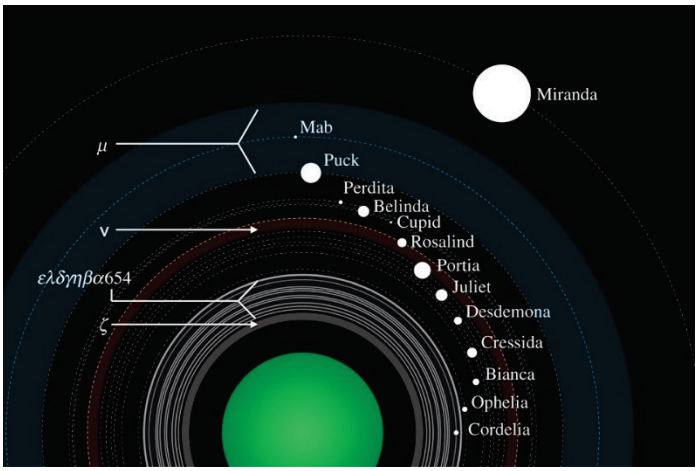

Exhibit 1-6. *Diagram of the system of rings and small moons surrounding Uranus. Credit M. Showalter.*

R1. What processes sculpted the ice giant rings and small moons into their current configuration? The narrowness of Uranus's rings strongly implies that unknown outside forces are acting on these rings, while both the distribution of small moons and their associated dusty rings suggests that there are more objects orbiting Uranus in this region. A spacecraft orbiting Uranus would be able to perform comprehensive surveys for objects less than 1-km wide anywhere is this region. The size distribution and locations of such objects would provide information about the recent dynamical history of the Uranian system. Furthermore, if moons can be found in close proximity of the narrow rings, they could even help explain the current architecture of those rings. An orbiting spacecraft would also be able to track longitudinal variations in the rings' structure and make high-resolution observations of the rings' fine-scale radial structure. Both these structures encode information about any outside forces acting on these rings, and so should clarify the origins of these forces, be they nontrivial gravitational interactions with the moons or something more exotic arising from structures within the planet itself. Furthermore, high resolution imaging of the rings' structure can constrain the particle size and velocity distributions, both of which influence the rings' long-term evolution.

R2. What are the compositions, origins and history of the Uranian rings and inner small moons? The limited spectral data on the rings and small moons indicates that they have a very different surface composition from the larger moons [de Kleer et al. 2013; Dumas, Smith & Terrile 2003; Karkoschka 2001; Karkoschka 2003], which is surprising given their common history and environment. These differences could potentially reflect a primordial compositional gradient across the Uranus system, variations in how quickly objects of different sizes are covered with exogenous debris, or even the material in the rings and small moons being less geologically processed than the material currently visible on the surfaces of the larger moons. An orbiting spacecraft would provide detailed spectral data on both the rings and small moons that could distinguish between these options by properly documenting variations in the surface texture and composition between different rings and moons and even across individual objects. For example, systematic trends in composition with distance from Uranus could reflect primordial compositional gradients, while more localized variations could reflect more discrete events like recent collisions. In this context, spectra of Mab and its associated dusty mu ring are likely to be particularly informative, since the mu ring has an unusually blue color and Mab also appears to be bluer than other nearby objects. This indicates that there is something unusual about the material in this particular region that merits further investigation.

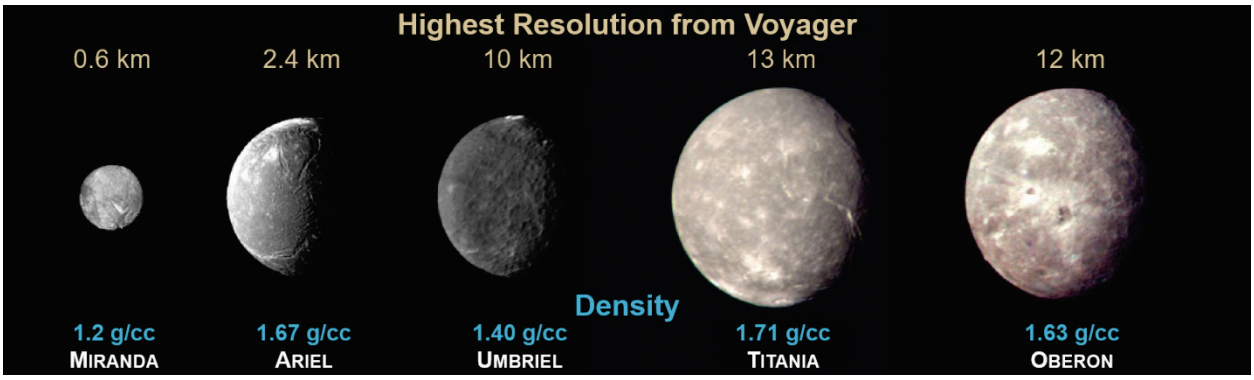

Exhibit 1-7. *Photo montage of Uranus's five major satellites in order of distance from planet. Satellites are shown to scale and at relative brightness. Resolutions are in kilometers per line pair. Credit: NASA*

1.4. Large Satellites & Ocean Worlds

The Uranian moons comprise the only regular satellite system that has not been intensively studied by spacecraft. Voyager 2 and Earth-based spectroscopy have provided some glimpses of these moons, but without a dedicated mission, many fundamental questions remain unanswered. In particular, given the recently recognized astrobiology potential of other icy moons, a key question is: ***Do, or did, any of the Uranian satellites harbor habitable environments?*** Habitability requires liquid water, an energy source and raw materials, and time; existing data provide hints of surface organics and high heat fluxes, and theory permits present-day oceans on the larger moons. To move from hints to an answer, we have defined four science objectives:

S1. What are the internal structures and rock-to-ice ratios of the large Uranian moons? And which ones possess substantial internal heat sources or possible oceans? The magnetic field of Uranus is complex and rotating, resulting in a time-variable magnetic field experienced by each satellite. As at the Galilean satellites, a

subsurface ocean will result in an induced field which will be detected by the magnetometer on multiple passes [Weiss et al. 2021]. Simultaneous plasma measurements will reduce the noise. The satellites' gravity fields (from radio science) and shapes (from limb profiles and stereo) can be used to determine the internal distribution of mass [Iess et al. 2014], thus indicating whether rock-ice differentiation has happened or not. Like Triton or Enceladus, some of the Uranian moons, particularly extensively resurfaced and lightly cratered Ariel, may also have active geology at present. Geologic and topographic mapping suggest internal convection on Miranda [Pappalardo, Reynolds & Greeley 1997] and high heat fluxes and chaotic overturn on Ariel [Peterson, Nimmo & Schenk 2015; Schenk & Moore 2020], but the level of geologic activity on Umbriel, Titania and Oberon is poorly known. High phase angle images will be taken to search for evidence of plumes or outgassing. Such activity would likely be driven by tidal heating; anomalous surface heat flows will be searched for using thermal infrared, while the magnitude of tidal heating can be assessed by using images to look for changes in satellite orbital position with time, as at Io [Lainey et al. 2009].

S2. How do the compositions and properties of the Uranian moons and ring system constrain their formation and evolution? The surfaces of the moons may contain organics or salts [Cartwright et al. 2018], leading to the speculation that these materials come from interior oceans [Sohl et al. 2010]. To determine if such is the case and whether more volatile ices such as ammonia or methane related to internal activity are present, Vis/NIR spectroscopy will be used. Correlation with geologic features will help identify the source, distribution and origin of different species. Volatiles, such as CO_2, and their potential for migration or sublimation will be investigated using imaging and spectroscopy. Spectroscopy can also be used to determine D/H ratios [Clark et al. 2019], which provide a link to protoplanetary disk conditions. The global distribution of surface materials will also be used to assess whether there is a significant contribution from external dust and/or plasma bombardment, particularly when compared with the smaller moons and rings (see **R2**). The moon rock-to-ice ratios and differentiation state (see **S1**) provide constraints on how fast the moons accreted, and whether they were subject to large impacts.

S3. What geological history and processes do the surfaces record, and how can they inform outer solar system impactor populations? Limb profiles and stereo images will provide topography which can be used to infer heat fluxes (which hint at a possible ocean on Ariel [Peterson, Nimmo & Schenk 2015]) and strain magnitudes. Topography, imaging and spectroscopy will be used together to search for and confirm proposed cryovolcanic resurfacing [Schenk et al. 2011]. High resolution crater counts will be used to determine how recently these units and structures formed. The size-frequency distribution of impact craters will be compared with known populations elsewhere (e.g., Saturn, Pluto) to determine if similar populations occur across the outer solar system, while their spatial distribution will constrain the moons' rotation state. The moons' crater population may also record signatures of the Uranus-tilting impact.

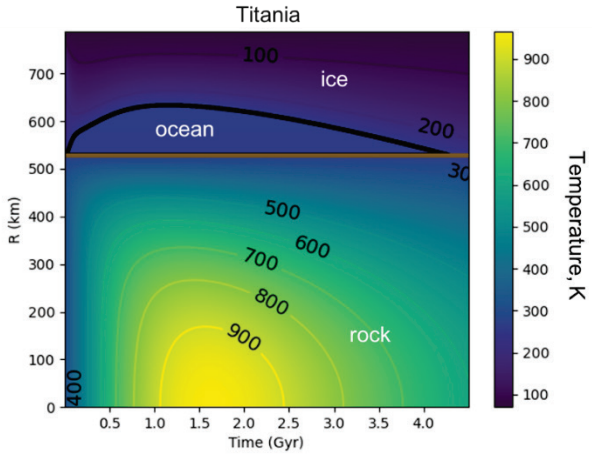

Exhibit 1-8. *Thermal evolution of a differentiated Titania subject to radiogenic heating. The interior heats up and heat conducted out melts the ice shell, resulting in a long-lived ocean.*

S4. What evidence of exogenic interactions do the surfaces contain? Vis/NIR spectroscopy will be used to determine whether plasma bombardment (which is expected to have a characteristic asymmetric spatial distribution) has modified the surface composition. Darkening of the surfaces from irregular satellite dust is thought to occur and can be assessed with imaging and spectroscopy. Plumes or outgassing, if present, will certainly modify the plasma characteristics, as at Enceladus. Equatorial circum-satellite ring deposits might also have formed on some satellites, as likely occurred at Iapetus [Ip 2006] and Rhea [Schenk et al. 2011].

1.5. Science Traceability Matrix

Each of the above discipline-specific science objectives flow into required measurements and were used to define a notional payload. In turn, these instrument drive specific mission requirements and operations. It is recognized that other instruments can be used to meet these science objectives. The full science traceability matrix (STM) used in this study is shown in Ex. 1-9.

Exhibit 1-9. *Science Traceability Matrix by Discipline (page 1 of 2).*

	Science Objective	Measurement	Nominal Instrument	Mission Functional Requirement
Atmospheres	**A1. How does atmospheric circulation function, from interior to thermosphere, in an ice giant?**	A. Cloud top zonal and 2D winds, waves to ~10 m/s resolution	NAC, imaging at 50 km/pixel	Repeated views of same features over timescales of minutes to hours
		B. *In situ* vertical wind profile to 10–20 m/s resolution	USO (probe), 10 measurements per scale height	Probe to 5 bars
		C. Resolved composition, disequilibrium species mapping (to P < 3 bars): CH_4, H_2S, H_3^+, C_2H_2, C_2H_6, etc., hydrogen ortho/para fraction to mixing ratio ±20%	Vis/NIR, 1000 km/pixel	
			TIR, ~1000 km horizontal spatial resolution	
			MS (probe)	Probe to 5 bars, 10 bars preferred
			Ortho/para sensor (probe)	Probe to 5 bars
		D. Depth of atmospheric winds (gravity moments)	Radio Science, gravity passes	Polar and equatorial passes, distances of 1.1 R_u
	A2. What is the 3D atmospheric structure in the weather layer?	A. Cloud tomography and aerosols	Vis/NIR imaging spectra at 500–1000 km/pixel	Repeated views of same features over timescales of hours
			WAC or NAC imaging at 500–1000 km/pixel	Repeated views of same features over minutes to hours
		B. Vertical temperature profile to ±1K	ASI (probe), 4 measurements per scale height	Probe to 5 bars
			Ortho/para sensor (probe)	Probe to 5 bars
			Radio Sci + UltraStable Oscillator, occultations	Atmospheric occultations
		C. Global temperature variations in troposphere, stratosphere, thermosphere	TIR, 500-1000 km/px mapping	Global coverage, repeated views
			Vis/NIR spectra at 500–1000 km/pixel	
	A3/I1. When, where, and how did Uranus form, and how did it evolve both thermally and spatially, including migration?	A. Noble gas (& isotopes of He, Xe) abundances to ± 5%	MS (probe)	Probe to 5 bars
		B. Elemental (& isotopes of H, C, S, N & O (stretch goal)) abundances, lower bounds on CH_4, H_2S, NH_3, H_2O, and the variation with depth	MS (probe)	Probe to 5 bars, 10 bars preferred
		C. Global distribution of atmospheric composition	*Same as A1.C above*	
		D. Global energy balance (Bond albedo and thermal emission) to 1%	TIR, 1000 km/pixel	Repeat orbiter ~yearly to determine variability
			Vis/NIR spectra at 500-1000 km/pixel	Repeat ~yearly to determine variability
Interiors	**I2. What is the bulk composition and its depth dependence?**	A. Gravity field to at least J_8, uncertainties on J_2-J_6	Radio Science + UltraStable Oscillator, gravity passes	
	I3. Does Uranus have discrete layers or fuzzy core, and can this be tied to its formation and tilt?	A. Gravity field to at least J_8, uncertainties on J_2-J_6	*Same as I2.A above*	Polar passes, distances of 1.1 R_u require validation of safe passage inward of rings
		B. Ring oscillations	NAC imaging of rings (<1 km/pix)	
			Radio Sci + UltraStable Oscillator, occultations	
	I4. What is the true rotation rate of Uranus, does it rotate uniformly, and how deep are the winds?	A. Internal magnetic field structure	MAG, 0.1 to 20,000 nT, 1-second cadence	Many close passes
		B. Planet shape and gravity to J_8	Radio Sci + UltraStable Oscillator, occultations	
		C. Gravity field to J_8	*Same as I2.A above*	
Magnetospheres	**M1. What dynamo process produces Uranus's complex magnetic field?**	A. Internal magnetic field structure	*Same as I4.A above*	Close passes
	M2. What are the plasma sources & dynamics of Uranus's magnetosphere and how does it interact with the solar wind?	A. Particles & fields over range of space (distance, longitude, latitude, local time) and time (spin, solar wind variability)	Fields & Particles package	Multiple passes
	M3. How does the magnetosphere interact with Uranus's upper atmosphere and satellite surfaces?	A. Energetic particle fluxes at satellite orbital ranges	Fields & Particles package	
		B. Plasma/energetic particle fluxes over Uranus polar regions	Fields & Particles package	Polar passes

Exhibit 1-9. *Science Traceability Matrix by Discipline (page 2 of 2).*

	Science Objective	Measurement	Nominal Instrument	Mission Functional Requirement
Rings and Small Satellites	**R1. What processes sculpted the ice giant rings and small moons into their current configuration?**	A. Fine-scale structures in the dense rings at multiple times and longitudes	WAC or NAC imaging (100 m/pixel)	Repeat views of rings
			Radio Sci + UltraStable Oscillator, occultations	
			WAC or NAC stellar occultations	
		B. Measure longitudinal variations in the ring structure (including normal modes and arcs)	WAC or NAC imaging (1 km/pixel)	Image all co-rotating longitudes in the main ring system multiple times
		C. Inventory and shape of small moons > 0.5 km in radius within 500,000 km of the planet's center	WAC or NAC imaging (100 m/pixel)	Large area coverage
	R2. What are the compositions, origins and history of the Uranian rings and inner small moons?	A. Ring (color) imaging at a wide range of phase angles	WAC multi-band imaging	Phase angle > 160
		B. Ring and small moon spectra (Cordelia to Mab), 1-5 μm	Vis/NIR imaging and spectroscopy	
Large Satellites and Ocean Worlds	**S1. What are the internal structures and rock-to-ice ratios of the large Uranian moons? Which ones possess substantial internal heat sources or possible oceans?**	A. Magnetic field intensity and direction	MAG, 0.1-20,000 nT, 1s cadence	Sample variable magnetic lat & long, altitude <0.5 satellite radii
		B. Static gravity coefficients	RS, 0.1 mm/s at 60s integration	Earth-pointing HGA ±30 mins of C/A; flyby velocities < 10 km/s at each satellite
		C. Global shape	NAC, global images, < 1 km/pix	Include limb
		D. Energy distribution of bulk plasma flow, 10eV–10 keV	F&P package	Point in plasma flow (ram) direction, <300 km baseline altitude
		E. Plume/activity searches	NAC, <1 km/pix; thermal anomalies TIR	High phase
		F. Satellite orbital positions	NAC	Distant imaging
	S2. How do the compositions and properties of the Uranian moons and ring system constrain their formation and evolution?	A. Reflectance spectra from 0.8-5 μm, detect features 1% of continuum from 0.8-2.6 μm and 2% of continuum from 2.6-5.0 μm	Vis/NIR, < 3km/pix	
		B. Static gravity coefficients	*See S1B above*	
		C. Global shape	*See S1C above*	
	S3. What geological history and processes do the surfaces record and how can they inform outer solar system impactor populations?	A. Distribution and topography of surface features	NAC, global images & stereo, <0.5 km/pix	Non-targeted flybys of each satellite for global mapping and stereo
		B. Variations in surface composition	Vis/NIR, < 3 km/pix	Non-targeted flybys of each satellite for global mapping
		C. Energy distribution of bulk plasma flow, 1eV-1 keV	Fields & Particles package	
		D. High-phase plume-search images	NAC, <1 km/pix	Phase angle > 150
	S4. What evidence of exogenic interactions do the surfaces contain?	A. Energy distribution of bulk plasma flow, 10keV–10 MeV	Fields & Particles package	Point in plasma flow (ram) direction, <300 km baseline altitude
		B. Variations in surface composition in reflectance spectra	*Same as S2.A above*	
		C. Evidence of radiation processing of surface ices	Vis/NIR, < 3 km/pix	

This mission can address questions across most of the Decadal Survey's thematic questions. By understanding Uranus's thermal history, bulk composition, migration and evolution, we can learn more about the solar system's origins in the protosolar nebula (Q1), accretion in the outer and inner solar system (Q2, Q3), and giant impacts past and present, which are also recorded on satellite surfaces (Q4). Further studies of the satellites will inform our understanding of solid body surfaces, interiors, and atmospheres/exospheres (Q5, Q6). Detailed exploration of the Uranian gravity field, ring seismology, and in situ composition will also inform models of giant planet evolution (Q7). All aspects of the system: rings, satellites, magnetosphere represent a complex circumplanetary system (Q8). This mission will investigate past and present satellite heat fluxes and the potential for subsurface oceans and habitable conditions (Q10, Q11). Lastly, Ice Giant mass planets are ubiquitous in exoplanet systems, but are distinctly different than Jupiter and Saturn, so our understanding of exoplanet formation and structure requires exploration of Uranus (Q12). This is a brief, and incomplete, summary of the broad, interdisciplinary, science that will be accomplished by the UOP.

1.6. Driving Functional Requirements & Tour Design Considerations

Adequate study of all aspects of the Uranian system requires an orbiter with time allotted to meet each objective, as well as temporal coverage to characterize variations, as shown in the STM. Additionally, it is desirable to have both polar and equatorial orbital phases to allow complete study of the planetary gravity field and magnetosphere, as well as provide satellite surface coverage. Mission functional requirements for nominal baseline and threshold cases are described in Ex. 1-10. Additionally, earlier mission studies released the atmospheric probe very close to orbit insertion, tightly constraining several critical events. Those trajectories also resulted in design imbalances between entry loads and communications with the orbiter. One goal of this study was to complete a trajectory and meshed tour design, while accounting for the probe entry. Another prime objective was to determine the feasibility of progressing from a polar orbit after orbit insertion to an equatorial phase for a satellite tour by using satellite passes to pump down the inclination. This is described further in § 3.3.5.

Category	Baseline Requirement	Threshold Requirement	Goal
Orbital Tour	4 Years	2 Years	Adequate sampling of magnetosphere, satellite flybys, rings, atmospheric observations, satellite gravity
	Polar phase, followed by low inclination phase	Polar only	Obtain Uranus gravitational moments
Satellite Flybys	3 targeted, 2 non-targeted, flybys of each of the major moons @ <10 km/s	2 targeted,1 non-targeted, flybys of each of the major moons @ <10 km/s	80% surface coverage (incl. w/ Uranus-shine)
	Targeted and non-targeted flybys of small moons	Non-targeted flybys only	Inventory and characterize small moons
	Polar and low inclination passes	Polar only	Gravitational moments and coverage
Uranus Orbits	Close (1.1 R_u) polar & low inclination dayside passes	Polar only	Gravitational moments and coverage
Probe Depth Range	From 0.1 to 5 bars (10 bars preferred, but not a driver)	From 0.1 to > 1 bar	Reach depths past certain condensation levels
Payload	Full Complement	Remove WAC from orbiter and ortho-para sensor from probe	

Exhibit 1-10. *Driving mission functional requirements.*

The trajectory and tour are described in detail in a later section of this report, but we summarize key aspects here, particularly those changed from previous studies. First, probe release occurs one petal after orbit insertion, allowing sufficient separation of all critical events during the orbit insertion burn. This allows for a good telecommunication link, enabling probe measurements to 10 bars of pressure. The mission duration is sufficient to track Uranus atmospheric evolution/changes over multi-year timescales. The orbit also allows multi-phase-angle views of reflected sunlight for aerosol tomography; global views with moderate resolution sampling at low and high latitudes, plus regional high-resolution views; and radio occultations spread over a wide range of latitudes and local times. Additionally, there is sufficient data volume for all of the remote sensing objectives, as well as fields and particles measurements.

For satellites, the orbital tour focuses initially on Titania, because it was poorly imaged by Voyager, because it is large enough to sustain a present-day ocean (Ex. 1-8), and because it sits inside the magnetopause, facilitating searching for an ocean via induction [Weiss et al. 2021]. Additionally, it can be used to pump the orbit down to the equatorial plane. Later in the tour, multiple flybys of all other satellites are carried out to image their surfaces, probe their internal structures via gravity and induction studies and determine their interactions with the external environment. Although the mission tour can be refined later, Ex. 1-11 shows most objectives are met by this mission design without any optimization yet applied; the rest can be easily accommodated with small tour tweaks. Occultations are also feasible in this tour but are not shown here.

***Exhibit 1-11**. Measurement coverage with notional tour design.*

Measurement	Instrument	Concept of Operations (Notional Payload)	Coverage (Notional Tour)
A1A. Cloud top zonal and 2D winds, waves to ~10 m/s resolution	NAC, imaging at 50 km/pixel	Scan across planet from ~5×10^9 km range or lower, phase angle < 45°	Many opportunities
A1C. Resolved composition, disequilibrium species mapping	Vis/NIR, 1000 km/pixel	Scan across planet from ~4x10^6 km range, phase angle < 45°	Many opportunities
	TIR, ~1000 km horizontal spatial resolution	3 strip scans across planet from ~3x10^5 km range, any phase angle	Many opportunities
A2A. Cloud tomography and aerosols	Vis/NIR imaging spectra at 500–1000 km/pixel	Scans across planet from ~2 to <4x10^6 km range, phase angle < 45°	Many opportunities
	WAC or NAC imaging at 500–1000 km/pixel	Scans across planet from ~1 to 2 x10^7 km range, phase angle < 45°	Many opportunities
A2C. Global temperature variations in troposphere, stratosphere, thermosphere	TIR, 500-1000 km/px mapping	6 strip scans across planet from ~1.5 to 3 x 10^5 km range, phase angle > 90°	Many opportunities
	Vis/NIR spectra at 500–1000 km/pixel	Covered in A2A observations	Many opportunities
A3D. Global energy balance (Bond albedo and thermal emission) to 1%	TIR, 1000 km/pixel	Covered in A1C observations	Many opportunities
	Vis/NIR spectra at 500–1000 km/pixel	Covered in A2A observations	Many opportunities
I3B. Ring Oscillations	WAC or NAC imaging (1 km/pixel)	Same as R1B below	Many opportunities
I4A/M1. Internal magnetic field structure	MAG, 0.1 to 20,000 nT, 1-second cadence	Many close passes, sample field	Opportunities near periapse
M2A. Particles & fields over range of space (distance, longitude, latitude, local time) and time (spin, solar wind variability)	Fields & Particles package	Multiple passes	Many opportunities
M3A. Energetic particle fluxes at satellite orbital ranges	Fields & Particles package		Opportunities during satellite tour phase
M3B. Plasma/energetic particle fluxes over Uranus polar regions	Fields & Particles package	Polar passes	Opportunities during polar phase
S4A. Bulk plasma flow	Fields & Particles package	Point in ram direction, <300 km altitude	Many opportunities
R1A. Fine-scale structures in the dense rings at multiple times and longitudes	WAC or NAC imaging (100 m/pixel)	Ring mosaics from ~1x10^7 km range or lower, phase angle < 90°	Rare opportunities, tour needs to be optimized
R1B. Measure longitudinal variations in the ring structure (including normal modes and arcs)	WAC or NAC imaging (1 km/pixel)	Ring mosaics from ~1x10^8 km range or lower, phase angle < 90°	Many opportunities
R1C. Inventory and shape of small moons > 0.5 km in radius within 500,000 km of the planet's center	WAC or NAC imaging (100 m/pixel)	Non targeted observations (range varies)	Rare opportunities, tour needs to be optimized
R2A. Ring (color) imaging at a wide range of phase angles	WAC multi-band imaging	Best effort resolution, scan across ring plane, Phase angle > 160°	Many opportunities
R3B. Ring and small moon spectra (Cordelia to Mab)	Vis/NIR imaging and spectroscopy	Best effort resolution, scan across rings, Phase angle < 90°	Many opportunities
S1B. Static gravity coefficients	Radio Science	Earth-pointing HGA +/- 30 mins of C/A	Several opportunities, more possible during satellite tour phase
S1C. Global Shape	NAC, global images < 1km/pix	Framing at ~300,000 km and ~200,000 km range, terminator should be visible	Many opportunities
S1E. Plume activity searches	NAC, < 1km/pix	Framing at ~200,000km, phase angle > 150°	Many opportunities
	TIR	Scan across satellite range ~25,000 km, any phase angle	Many opportunities
S1F. Satellite positions	NAC, global images, < 10 km/pix	Framing other satellites at ~2,000,000 km range	Many opportunities
S2A. Satellite composition	Vis/NIR, < 3km/pix	Scan across disk, range ~35,000 km	Several opportunities, more possible during satellite tour phase
S3A. Geology & Topography	NAC, <0.5 km/pix	Framing at ~100,000 km range, (stereo pairs, parallax angle <30°)	Rare opportunities, more possible during satellite tour phase
		Framing at ~15,000 km range	2 images inbound, 2 images outbound
S3B. Surface composition.	Vis/NIR, < 3 km/pix	Covered in S2A observations	Many opportunities
S3D. Plume search	NAC, < 1km/pix	Covered in S1E observations	Many opportunities
S4A. Bulk plasma flow	Fields & Particles package	Point in ram direction, <300 km altitude	Several opportunities, more possible during satellite tour phase

2. High-Level Mission Concept

2.1. Study Request & Ground Rules

The objective of this study was to update the prior UOP study conducted for the 2011 *Visions and Voyages* Decadal Survey [Iess et al. 2014]. Initial direction included the incorporation of new launch dates corresponding to a project start between 2023 and 2030, as well as refined science goals and payload complement (see also § 1). The study was also directed to increase mission maturity/fidelity where possible, and to develop a chemical-only mission design, thereby removing the solar electric propulsion (SEP) stage that was used in the 2011 UOP concept. The use of radioisotope power systems is assumed. The overall study goal was to mature a comprehensive, but low-cost, technologically-ready Flagship mission.

2.2. Overview & Concept Maturity Level (CML)

The study began by assessing alternative Earth-to-Uranus interplanetary trajectories that would satisfy multiple, competing objectives with an all-chemical implementation. Minimizing the time of flight, and thereby mission duration overall, provides numerous advantages given Uranus's large heliocentric distance (18.9 AU on average). Shorter transit times generally minimize mission cost and complexity, and also maximize the radioisotope thermoelectric generator (RTG) power available for the science phase, since their output degrades over time. However, shorter cruise durations compete with the time penalties associated with ΔV-reduction strategies such as gravity assists, and with the need for relatively low Uranus approach velocities to enable chemical capture. Despite these challenges, numerous feasible cruise trajectories for UOP were identified for launch opportunities in the upcoming decade taking advantage of significantly higher performing new launch vehicles (LV), such as Vulcan and Falcon Heavy Expendable (FHE). Prime and backup launch opportunities using an FHE LV were identified for Jun 2031 and Apr 2032, respectively. The prime launch requires a mission-driving launch energy (C_3) of 29.36 km^2/sec^2 and includes a 13.4-year cruise.

The prime and backup trajectories both use a Jupiter gravity assist to achieve the most cost-efficient solution; however, numerous other viable alternatives were found that do not require Jupiter, using combinations of Earth and/or Venus flybys. These alternate sequences extend launch availability through the mid- to late 2030s at the possible expense of increased overall mission duration (up to 16 years, see § 3.3.1), and would require updating the spacecraft design to accommodate the thermal challenges associated with Venus flybys.

A major focus of this study was to identify an optimal approach for deploying an atmospheric probe that penetrates Uranus's atmosphere and relays scientific data to the orbiter for a duration of one hour after entry, the time needed to reach an atmospheric pressure of 10 bar. After having selected the prime interplanetary trajectory, the mission design team, via multiple design iterations with NASA Langley and NASA Ames EDL experts, focused on developing a high-fidelity Uranus capture and probe deployment design to demonstrate feasibility. This emphasis on probe deployment and trajectory, as well as the development of an integrated, end-to-end trajectory from launch through disposal, is in response to technical feedback on previous Uranus orbiter and probe concept studies.

A significant finding of this study is that substantial mission risk reduction is possible by separating Uranus orbit insertion and probe deployment operations, all while incurring minimal performance penalties. Previous studies for both Uranus and Neptune have been based on deploying the probe on hyperbolic approach to the planet. While that approach minimizes ΔV requirements and overall mission duration, it also results in higher probe entry velocities and the coupling of three critical events: approach targeting, the operation of the orbiter-probe communication link, and Uranus orbit insertion (UOI) execution. Additional factors in play further complicate planning for this period of the mission, including ring avoidance constraints, the establishment of suitable probe-orbiter geometries, and insufficient time between the completion of probe operations and the start of UOI. In contrast, this study proposes a deployment on elliptic post-capture paradigm (see § 3.3.4), where the orbiter carries the probe through UOI. With this approach, the targeting of probe entry interface, probe deployment, and orbiter divert are addressed independently, after successful capture into Uranus's orbit. The approach does result in a modest but tolerable increase in mission ΔV and lengthens overall mission duration by one period of the capture orbit (120 days). In return, lower probe entry velocities are achieved and the decoupling of critical events is realized, also enabling the potential for probe deployment backup opportunities.

Having adopted the post-capture probe deployment approach, the study team focused on two parallel tracks: Developing a reference design for the subsequent 4-year tour of the Uranian system, and developing the full mission concept, including flight and ground segments, mission operations, and schedule and cost estimates, with an integrated design team. A wide array of compelling moon tour options was found to be possible. This study presents one possible reference tour design (§ 3.3.5) in a high-fidelity model.

This updated version of the UOP mission concept has been developed to CML-4 as a preferred design point. The proposed flight system design includes details to the subsystem level, with 30% margin for mass and power as defined by the PMCS guidelines. Cost, schedule, and risk assessments were conducted and are shown to fall within acceptable ranges as outlined by the PMCS guidelines. The result provides a comprehensive, high-heritage, flexible, feasible, and cost-effective mission concept.

2.3. Technology Maturity

The UOP mission, as specified in this study, can be executed without the need for technology development, with all orbiter spacecraft and probe components being at TRL 6 or greater. All of the reference science instruments chosen for this study have flight heritage, except for the ortho-para hydrogen detector on the probe. The Ortho-Para H_2 Detector, currently in development, is assessed at TRL 6. The device uses capacitive transducers to measure sound speed, having been matured in the development of an acoustic anemometer for Mars. It uses two TRL 6 transducers, one transmit and one receive, in a simple implementation. Supporting electronics will be implemented on a field-programmable gate array (FPGA), per the Mars anemometer application under development.

2.4. Key Trades

A number of key trades were performed during this study to arrive at a preferred concept, summarized in Ex. 2-1. Should this concept be selected for additional mission formulation in Phase A, the most optimal interplanetary trajectory solution should be reevaluated, based on updated budget profiles, launch dates, and launch vehicle performance information. The selection of particular RTGs options, with potentially higher output power, would also be driven by their scheduled availability relative to a revised launch date.

Area	Trade Options	Results / Justification
Interplanetary Trajectory	**Earth/Jupiter Gravity Assists;** Earth/Venus Gravity Assists	• Use of JGA was most cost-efficient solution and provided shortest transit durations to Uranus. • Shielding accommodations for Jupiter flyby radiation dose less challenging than thermal accommodations needed for Venus flybys.
Probe Deployment	During Uranus Approach; **Deployment After UOI**	• Deployment post-capture allows probe entry interface targeting, probe deployment, and orbiter divert maneuvers to be conducted independently of UOI, deconflicting execution of overlapping critical events. Refer also to discussion in § 2.2 and 3.3.5. • Selected option adds minimal added delta-v cost and about 120 days of mission duration, but adds potential for backup deployment opportunities.
Data Return	4-m vs **3.1-m HGA**; 50-W vs **100-W TWTAs**	• Combination of smaller high gain antenna and higher-powered transmitters were best choice to maximize downlink rates while remaining within RTG-limited power budget and minimizing pointing requirements at Uranus solar distances.
Number of RTGs	**Three Next-Gen Mod 1 RTGs**; Four Next-Gen Mod 1 RTGs	• The mission was able to close using three RTGs along with a supplemental battery to support higher-load cases such as maneuvers. This option was also preferable in terms of total flight system mass, cost, spacecraft accommodation/layout, and launch-site integration complexity. • Note: Dynamic RPS systems and Next-Gen Mod 2 generators were not selected for this study due to expected availability dates, despite higher power availability. The Next-Gen Mod 0 was not selected due to the expectation that only one would be made available.
Cruise Hibernation	**Passive-Spin Cruise Hibernation**; Exclusively 3-Axis Spacecraft	• The ability to passively spin the spacecraft during quiescent cruise periods offers significant savings in Phase E operations cost, but requires a spacecraft configuration that is rotationally stable throughout cruise despite its overall size and propellant load. • A spacecraft configuration was successfully designed that could accommodate both 3-axis operation as well as passive or active spin modes during cruise.

Exhibit 2-1. *Significant mission concept trade studies. Selected options are shown in bold text.*

3. Technical Overview

3.1. Instrument Payload Description

The notional payload was chosen for its ability to meet a broad set of science objectives for the diverse range of targets in the Uranian system. For remote sensing of Uranus from the orbiter, imaging and spectroscopy over the visible to near-IR range are needed for composition, cloud-tracked winds, cloud structure studies, and observations of thermospheric emission. Panchromatic reflected light imaging, plus thermal IR data, are needed to determine the heat balance of the planet and the circulation of the atmosphere. These wavelengths characterize the ice giant atmosphere from the cloud-forming troposphere, into the stratosphere and thermosphere. Additional wavelengths, either from orbiter instruments or contemporaneous Earth-based observations are of value, as well (Ex. 3-1). For maximum flexibility, we assumed wider fields of view and lower spatial resolutions than in the corresponding heritage instruments, but these parameters can be easily traded as remote sensing observations can be accommodated at multiple spacecraft ranges.

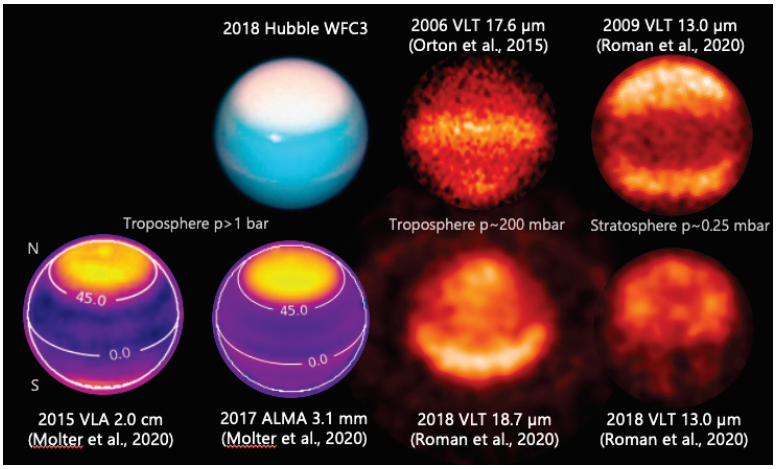

Exhibit 3-1. *State-of-the-art Earth-based visible, thermal IR, and microwave images are complementary to the UOP payload.*

The rings and satellites disciplines have similar composition and mapping science goals as the atmospheric science; most rings and satellites requirements are met with the same system tour and notional payload, including filtered visible and thermal imaging, and visible to near-IR imaging spectroscopy. However, several rings imaging objectives, in particular, require higher spatial resolution and would benefit from an optimized tour or instruments with finer resolution. Additionally, stereo viewing of the satellites will require specific views in the tour design, but likely no changes to the payload. The highest resolution views of the rings and rapid flybys of the satellites might further benefit from motion compensation, but this is not assumed in the notional payload, as that would be captured in trades between the final tour and the instrument capabilities. Scan mirrors are assumed in several of the instruments, however, to achieve ground coverage and this is in line with heritage capabilities.

Instrument	Capability/Performance	Priority	Mass (kg)	Power (W)
Orbiter				
Magnetometer	3-axis	Threshold	4.2	4
Narrow Angle Camera	framing, 10- µrad/pix, panchromatic	Threshold	8.8	5.8
Thermal IR	filters from ~7–100 µm, (higher priority at longward end, H_2-He continuum near Planck function peak)	Threshold	11	24.7
Fields & Particles Package	1eV-10 MeV range (ions & electrons); kHz-MHz	Threshold	11.8	11
Radio Science - UltraStable Oscillator		Threshold	2	2
Visible/NIR Imaging Spec	250 µrad/pix, ~0.8–5 micron	Threshold	15	10
Wide Angle Camera	pushbroom, 50 µrad/pix pan + broadband filters (0.4 to 1 micron)	Baseline	12	10
Total (baseline)			**64.8**	**67.5**
Total (threshold)			**52.8**	**57.5**
Probe				
Mass Spectrometer	1 - 150 amu, mass resolution >1,000	Threshold	16.2	19
Atmospheric Structure		Threshold	2.5	3.5
UltraStable Oscillator		Threshold	1	1
Ortho-para Hydrogen Sensor		Baseline	1	3.5
Total (baseline)			**20.7**	**27**
Total (threshold)			**19.7**	**23.5**

Exhibit 3-2*. Notional payload suite.*

Because of Uranus's unique magnetospheric configuration, and the desire to search for the signatures of ocean worlds, we include both a triaxial magnetometer and a robust fields and particles (F&P) package consisting of a number of sensors: energetic particle detectors, plasma spectrometers, a Langmuir probe and waves sensor, and a search coil magnetometer. An UltraStable Oscillator (USO) is also included as part of the radio science communication subsystem for high accuracy gravity measurements and occultations. The full notional orbiter payload is shown in Ex.3-2. On the orbiter, only the Wide-Angle Camera (WAC) is descopable, but it is included in the baseline mission design. In the future, it could also be traded for another instrument.

For the probe science requirements, the primary measurements come from ground truth vertical profiles of temperature and zonal winds, necessitating a standard atmospheric structure package (temperature, pressure and acceleration sensors) and a USO for Doppler wind tracking. In situ measurements of the noble gas, elemental and isotopic abundances require a minimum of a mass spectrometer with mass resolution of >1000. Lastly, we include an ortho-para hydrogen fraction sensor to understand the partitioning of energy within the troposphere and to provide essential "ground-truth" for understanding Uranus's infrared spectrum. This measurement is notionally accomplished with a simple sound speed (anemometer-type) measurement. The ortho-para sensor is the only descopable element on the probe science payload, though other instruments are also possible for the probe, as well.

To keep the mission affordable, and demands on resources as low as possible, the instruments chosen for the notional payload met the most science objectives or were the least resource intensive. However, a suite of other instrument types was considered for both the orbiter and the probe. Several of the candidate instruments ranked high scientifically but were not included in the notional payload (Ex. 3-3). These other instruments can meet or enhance specific science objectives, as listed. Should mass and power be available for them, they should also be considered as part of a more extensive instrument suite.

Instrument	Science Goal
Orbiter	
Microwave Radiometer	Deep atmospheric structure
UV Spectrometer	Aurorae, composition, upper atmospheric structure, exospheres
Mid-IR Spectrometer	Temperature mapping, Uranus stratospheric circulation/chemistry
Energetic Neutrals Analyzer	Neutral particle environment and abundance
Doppler Imager	Planetary oscillations, deep wind and core structure
Probe	
Nephelometer	In situ cloud detection
Net Flux Radiometer	In situ flux balance
Helium Abundance Detector	High accuracy helium abundance

Exhibit 3-3. *Enhanced payload suite.*

For each instrument, heritage options were identified. The exact accommodation of each instrument used in the design study are shown in the exhibits below:

Reference Instrument / Heritage Mission	Mass			Average Power		
	CBE (kg)	% Cont.	MEV (kg)	CBE (W)	% Cont.	MEV (W)
Orbiter						
Magnetometer (MESSENGER MAG)	1.43	10	1.57	2.0	10	2.2
Magnetometer Boom (Galileo/Cassini scaled to 5-m length)	0.47	20	0.56	--	--	--
Narrow Angle Camera (New Horizons LORRI)	8.80	10	9.68	8.0	10	8.8
Thermal IR Camera (LRO Diviner)	11.00	10	12.10	4.5	10	5.0
Fields and Particles Package (Suite Subtotal)	11.78	10	12.96	9.9	10	10.9
MAVEN LPW	*3.58*	*10*	*3.94*	*2.7*	*10*	*3.0*
TRACERS MSC (also Van Allen Probes)	*0.80*	*10*	*0.88*	*0.8*	*10*	*0.9*
MESSENGER FIPS	*1.40*	*10*	*1.54*	*1.9*	*10*	*2.1*
Parker Solar Probe SWEAP/SPAN-B	*2.50*	*10*	*2.75*	*2.0*	*10*	*2.2*
Parker Solar Probe EPI-Lo	*3.50*	*10*	*3.85*	*2.5*	*10*	*2.8*
Vis/NIR Imaging Spectrometer & WAC (Lucy L'Ralph)	27.00	10	29.70	5.3	10	5.8
Radio Science Experiment (RS) – *USO Included in Spacecraft*	--	--	--	--	--	--
Total Payload Mass & Power -- Orbiter	**60.5**	**10**	**66.60**	**29.7**	**10**	**32.7**
Probe						
Mass Spectrometer (Rosetta DFMS)	16.20	10	17.82	19.0	10	20.9
Atmospheric Structure Instrument (Cassini-Huygens HASI, others)	2.50	10	2.75	3.5	10	3.9
Ortho-Para H_2 Sensor (sound speed, capacitive transducers)	1.00	30	1.30	3.5	30	4.6
Total Payload Mass & Power -- Probe	**19.70**	**11**	**21.87**	**26.0**	**11**	**29.3**

Exhibit 3-4. *Orbiter and Probe Reference Payload Mass & Power.* *Contingency percentages based on TRL and APL institutional practice*

Characteristics	Value	Units
Size/Dimensions	8.1 × 4.8 × 4.6	cm × cm × cm
Average Science Data Rate	1.5	kbps
FOV	360	deg
Range	0.1–2000	nT

Exhibit 3-5 *Orbiter Magnetometer: MESSSENGER MAG.*

Characteristics	Value	Units
Number of Channels	5	
Size/Dimensions	13.5 x 45.5 x 17	cm × cm × cm
Avg. Science Data Rate	3.0	kbps
Pointing Requirements (knowledge)	350	µrad
Pointing Requirements (control)	0.1	deg
Pointing Requirements (stability)	5	µrad/s

Exhibit 3-6 *Orbiter Narrow Angle Camera (NAC): LORRI.*

Characteristics	Value	Units
Number of Channels	9	
Size/Dimensions	37.3 × 48.5 × 30.5	cm × cm × cm
Average Science Data Rate	0.18	kbps
FOV	3/84 × 0.384	deg
Pointing Requirements (knowledge)	350	µrad
Pointing Requirements (control)	0.1	deg
Pointing Requirements (stability)	0.05	deg/sec

Exhibit 3-7 *Orbital Thermal IR Camera: LRO Diviner.*

Characteristics	Value	Units
Spectral Range	Vis-NIR: 0.4–0.975	µm
	IR Spec: 1.0-5.0	
Number of Channels	Vis-NIR: 6	
Size/Dimensions	37.3 × 48.5 × 30.5	cm × cm × cm
Average Science Data Rate	3	kbps
FOV	Vis-NIR: 8.3 × 0.85	deg
	IR Spec: 4.6 × 3.2	
Pointing Requirements (knowledge)	0.4	deg
Pointing Requirements (control)	0.833	deg
Pointing Requirements (stability)	3.3E-3	deg/s

Exhibit 3-8. *Orbiter Vis/NIR & WAC: Lucy L'Ralph.*

Characteristics	Value	Units
Number of Electric Field Channels	3	
Size/Dimensions	40 × .635 × .635	cm × cm × cm
Average Science Data Rate	1	kbps
FOV	360	degrees
Electron Density Range	100 to 10^6	cm^-3
Electron Temperature Range	500 to 5000	K
Electric Field Frequency Range	.05 to 10	Hz
Electric Field Sensitivity (f_0=10 Hz)	10^-8	(V/m)^2/Hz (f_0/f)^2

Exhibit 3-9. *Orbiter Fields & Particles Package: MAVEN Langmuir Probe & Waves (LPW).*

Characteristics	Value	Units
Number of Channels	6	
Size/Dimensions	40 × 40 × 40	cm × cm × cm
Average Science Data Rate	3	kbps
FOV	360	degrees
Measurement Range	10 to 12,000	Hz

Exhibit 3-10. *Orbiter Fields & Particles Package: TRACERS Search Coil Magnetometer (MSC).*

Characteristics	Value	Units
Size/Dimensions	17 × 20.5 × 18.8	cm × cm × cm
Average Science Data Rate	.08	kbps
FOV	1.4*pi	steradians
Energy Measurement Range	50 to 20,000	eV
M/Q Measurement Range	1–40	amu/e

Exhibit 3-11. *Orbiter Fields & Particles Package: MESSENGER Fast Imaging Plasma Spectrometer (FIPS).*

Characteristics	Value	Units
Size/Dimensions	15 × 17.2 × 16	cm × cm × cm
Average Science Data Rate	<2	kbps
FOV	360 × 120	deg
Measurement Range	5–20,000	eV

Exhibit 3-12. *Orbiter F&P Package: PSP SWEAP/SPAN-B.*

Characteristics	Value	Units
Energy Range	Ions: 20–15000	keV
	Electrons: 25–1000	
Energy Resolution	11	%
Size/Dimensions	30 × 30 × 8	cm × cm × cm
Average Science Data Rate	3.1	kbps
FOV	360 × 90	deg

Exhibit 3-13. *Orbiter Fields & Particles Package: Parker Solar Probe Energetic Particle Instrument (EPI-Lo).*

Characteristics	Value	Units
Detector Size/Dimensions	63 × 63 × 26	cm × cm × cm
DPU Dimensions	16 × 14 × 14	cm × cm × cm
Average Science Data Rate	<20	kbps
Ion Source	±20 and ±2	degrees
Ion Detector	MCP	
Mass Range	12-150	amu
Dynamic Range	10^10	
Sensitivity	10^-5	A/mbar
Pressure Range	10^-5 to 10^-15	mbar

Exhibit 3-14. *Probe Mass Spectrometer: Rosetta Double Focusing Mass Spectrometer (DFMS).*

Characteristics	Value	Units
Number of sensors	T: 2; P:3; Acc: 4	
Size/Dimensions	6 d × 6 l	cm x cm
Average Science Data Rate	0.05	kbps
Range	Temp: 0-500	K
	Pres: 0.1–10	bar
	Accel: 3 µg–200 g	

Exhibit 3-15. *Probe Atmospheric Structure (p, t, accels).*

Characteristics	Value	Units
Size/Dimensions	32.2 × 7.2 × 7.2	cm × cm × cm
Average Science Data Rate	0.05	kbps

Exhibit 3-16. *Probe Ortho-Para H_2 Detector.*

3.2. Flight System

3.2.1. Orbiter Element

The UOP flight system is composed of Orbiter and Probe elements. The Orbiter architecture is in family with other Class A, outer-planet Flagship missions in terms of capability, redundancy, and operation over an 18.5-year mission lifetime. The Orbiter spacecraft features a 3.1-m High-Gain Antenna (HGA), three Next-Generation (Mod 1) RTGs, and is capable of both 3-axis stabilization and operating in a passive spin cruise hibernation mode. The use of reaction wheels provides for fine pointing for science observation and the use of dual mode X/Ka band communications. The equipment layout and thermal design are intended to minimize heater power requirements, including the utilization of RTG waste heat within the spacecraft. The body-fixed instrument payload layout supports operating scenarios developed for the science tour phase, and the antenna layout was selected to support all operational modes, including Probe deployment. Ex. 3-17 indicates the Orbiter layout and overall dimensions, and Ex.3-18 shows the block diagram. Descriptions of each Orbiter subsystem are included below, with additional information provided in Appendix C.

Orbiter Structures & Mechanisms. The Orbiter's structural design is largely based on that of the Europa Clipper spacecraft, featuring a primary structure, secondary structure, and launch vehicle interface. The primary structure consists of a cylindrical structure and honeycomb instrument and electronics module. The cylindrical structure is comprised of four segments: tapered adaptor, lower cylinder, upper cylinder, and instrument & electronics cylinder. The tapered adaptor transitions from the 60-inch diameter payload adapter fitting (PAF) to the 70.5-inch cylinder structure and is machined using 7075-T6 aluminum. The lower cylinder houses the hydrazine tank and is constructed from four 7075-T6 sheet metal segments joined with riveted splice plates and with machined 7075-T6 fittings on each end. The upper cylinder is similarly constructed, with a series of internal ribs to strengthen the structure. The instrument and electronics module consists of a honeycomb outer structure with removable side panels and an inner cylinder that houses an RF mini vault and supports the HGA. The inner cylinder is constructed of two 6061-T6 sheet metal segments joined with a riveted splice plate and machined 6061-T6 fittings on each end. The secondary structure consists of brackets that support the two externally mounted pressurant tanks, three RTGs, Probe, X-Band antennas, thrusters, propellant lines, and many of the instruments. The primary structure design is largely based upon the Europa spacecraft design. Many of the secondary structure components are based upon existing designs.

Orbiter Propulsion. The propulsion subsystem is baselined as a pressurized, bi-propellant system, operating at a maximum expected operating pressure (MEOP) of 350 psi. The system consists of two fixed-mounted 645-N bi-propellant main engines, four 22-N monopropellant steering thrusters, sixteen 4-N monopropellant attitude control system (ACS) thrusters, one custom fuel tank, two custom oxidizer tanks, two custom pressurant tanks, and plumbing as needed to support the main component layout. The custom tanks will be based on existing designs to the extent possible to minimize qualification costs. The system is sized to provide a total of 2708 m/s ΔV for a maximum launch mass of 7235 kg.

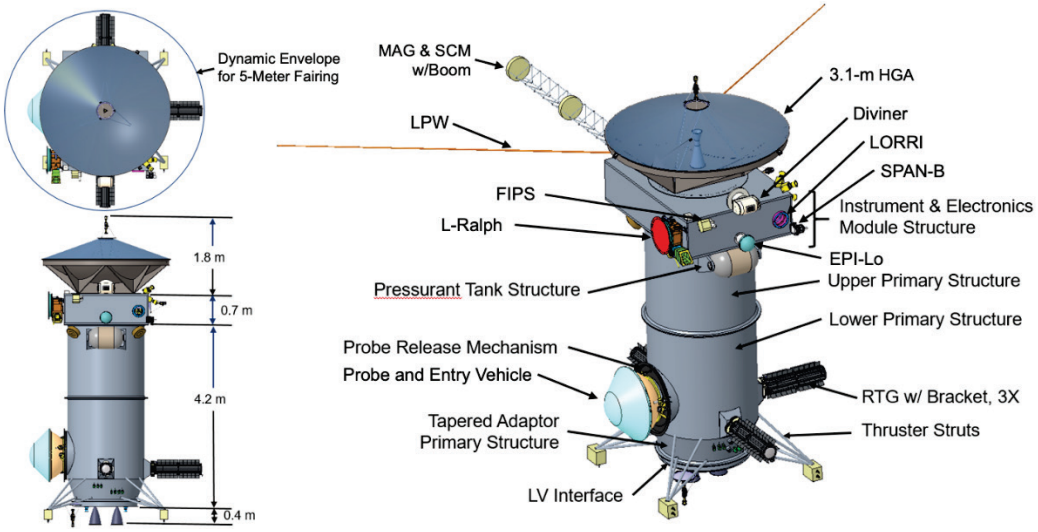

Exhibit 3-17. *Orbiter Layout with Dimensions and Instrument Configuration.*

Exhibit 3-18. *Orbiter and Probe Block Diagram (note: Probe portion is in upper right corner).*

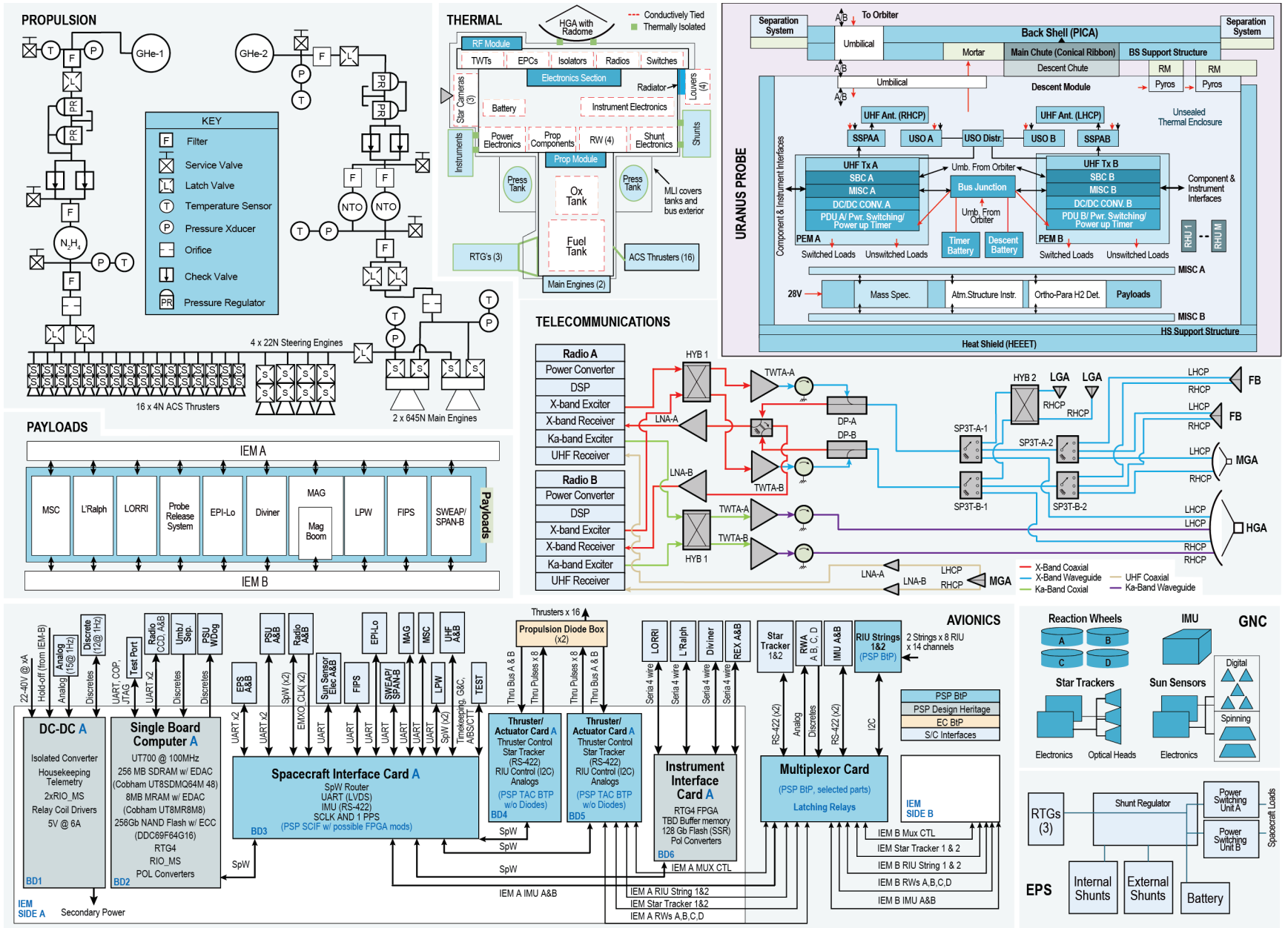

Orbiter Guidance & Control (G&C). The UOP Orbiter operates in two distinct modes, spin-stabilization and 3-axis, during the mission. The G&C subsystem provides spacecraft momentum axis control during the 13.4-year cruise phase, supporting passive control during hibernation periods, as well as active spin axis or active 3-axis control during Earth pointing and maneuver events. A spin axis inertial pointing accuracy of 0.5 deg is required to support cruise communications through the medium gain antenna (MGA). The Orbiter remains entirely in 3-axis mode from Uranus approach through to disposal. The G&C subsystem supports a three-axis inertial pointing accuracy of 0.06 deg (per axis) to support HGA pointing requirements for Ka band communications. During initial operations at Uranus, G&C controls burn vector steering during the UOI burn and provides stability during probe deployment and tracking for communications through the MGA during probe entry. During the science tour, G&C provides pointing control during satellite flybys, with any high-rate scans handled internally within the fixed-mounted instruments. A three-axis tracking accuracy of 0.06 deg (per axis) supports requirements for high-resolution imaging or radio science observations. The Orbiter is also capable of slewing to any inertial orientation via wheels or thrusters and provides for low jitter to satisfy imaging instrument accommodations.

The UOP G&C subsystem features a redundant hardware suite including star trackers, inertial measurement units (IMUs), sun sensors, and four reaction wheel assemblies.

Orbiter Electrical Power. UOP employs a direct energy transfer architecture, using three Mod-1 Next-Generation Radioisotope Thermoelectric Generators (NGRTG). Each 56-kg Mod-1 generator, expected to be available by 2029, provides 245 W of electrical power at fueling/beginning of life (BOL), with a maximum average annual power degradation of 1.9% per year throughout its lifetime. Fault tolerant linear shunt regulators provide RTG output power regulation, while block redundant power switching units provide switched, pulsed, and safety services for the spacecraft. Two 20 Ah 8s16p ABSL secondary batteries are included to support the DSM/UOI peak load case, and to meet the 30% margin requirement for the Momentum Dump case, both of which are thruster-intensive.

Orbiter Thermal. The Orbiter thermal subsystem is designed to maximize efficiency and minimize the use of electric heaters. Three thermal modes at varying solar distances were investigated: at Earth, 2AU, and Uranus. RTG waste heat is utilized to heat the main propellant tanks within the central cylinder via conduction through the mounting brackets. Thermal blankets and an HGA radome are used to cover as much surface area as possible to minimize heat leak to space. Radiators on the spacecraft bus sides are capable of rejecting up to 320 W of internal heat, with louvers used to release excess heat during early cruise and during Ka transmitter operation. Heat pipes are required to spread the Ka transmitter heat load. Externally mounted shunt elements scan be switched inside to heat the spacecraft as needed later in the mission.

Orbiter Avionics. The avionics subsystem, tasked with managing the spacecraft's command and data handling requirements is based on designs used on the Parker Solar Probe (PSP) and Van Allen Probes (VAP) missions, or planned for use on Europa Clipper. The single, internally redundant Integrated Electronics Module (IEM) leverages a slice-based architecture similar to the system used by PSP, with a multiplexer (MUX) joining the A and B sides for redundancy cross-strapping. Two single board computers (SBC) each provide 64MB of SDRAM, 8MB of MRAM (code storage), and 256Gb of flash memory with a UT700 100MHz processor. Additional PSP heritage-based components include a pair of Spacecraft Interface Cards (SCIF), four Thruster/Actuator Cards (TAC), two Instrument Interface Cards (IIF) each with 128Gb Solid State Recorders (SSR), and two DC/DC converters. Two strings of Remote Interface Units (RIUs) provide a total of 224 analog channels for temperature sensing. Four Propulsion Diode Boxes (PDB) planned for the Europa Clipper mission are used to mitigate electromagnetic interference effects caused during thruster firings.

Orbiter Flight Software. UOP uses onboard software to interpret uplinked commands and interface with various subsystems and related components while in flight. G&C software supports the Spin-Stabilized and 3-Axis attitude control modes previously described while providing precise pointing instructions to support science instrument observations. Command and data handling software handles all event-based (autonomous), time-tagged and macro commands provided to the system while managing the solid state recorder (SSR) functions, instrument data compression, memory scrubs, housekeeping data collection, and the data summary table. Command and data handling (C&DH) software is also responsible for the control of the heater system used to autonomously balance and maintain specific temperatures within the spacecraft bus. Testbed software will be used during ground operations to emulate system performance in various states during development, testing and integration.

Orbiter Telecommunications. The telecommunications system features a fully redundant design, including two radios, all necessary redundant RF cabling and switching, and two ultra-stable oscillators (USOs). The radios are connected to a suite of antennas that includes three low-gain antennas (LGAs), one MGA, two

fanbeam antennas, and a 3.1-m HGA. One of the three LGAs is dedicated to the ultrahigh frequency (UHF) link that receives probe telemetry during its descent into Uranus's atmosphere. The fanbeam antennas are positioned to provide coverage throughout UOI. Both USOs operate in an active cross-strapped configuration and will be powered on and available throughout the mission to provide a precision clock source for both radio science and communications. Both Ka- and X-band transmission will be supported by 100-W amplifiers (58-W RF). The spacecraft will communicate to the Deep Space Network's (DSN's) family of 34-m beam waveguide antennas. At Uranus, the Ka-band downlink will provide a 19.5-kbps link with the DSN.

Radiation Analysis. Radiation exposure for UOP consists of both natural and RTG-induced sources. The estimated total ionizing dose (TID) is estimated at 250 krad (Si) for components behind 100 mils Al with a radiation design margin (RDM) of 2. Contributions to this total include: ~15 krad for the radioisotope power system (RPS), ~16 krad for solar protons, ~95 krad for the Jupiter flyby at 6 R_J, and ~120 krad from the 4-year Uranus tour. Components for this study concept are selected to meet a 100 krad part hardness requirement, which requires ~240 mil Al equivalent shielding. Allocations for radiation shielding mass have been accounted for in the Orbiter master equipment list. The total non-ionizing dose (TNID) and single effect effects (SEE) are expected to be in family with other Jovian/long-duration missions. Consideration will need to be given for selecting detectors that would need to operate during the Jupiter flyby, such as star trackers. Detector noise and charging at Uranus is expected to be in-family with Earth-orbiting missions, but requires additional study given the limited knowledge of Uranus's radiation environment.

3.2.2. Probe Element

The UOP probe has a maximum expected value (MEV) mass of 267.5 kg. Nearly half of the mass is dedicated to the entry vehicle, which includes the aeroshell structure, parachute descent system, and Thermal Protection System (TPS). Within the aeroshell, the descent module houses and manages all science instruments and electronics, except for Engineering Science Investigation (ESI) instrumentation sensors that are embedded into the TPS itself. The orbiter separation mechanism provides spin stabilization of the probe during the approach and entry into the Uranus atmosphere.

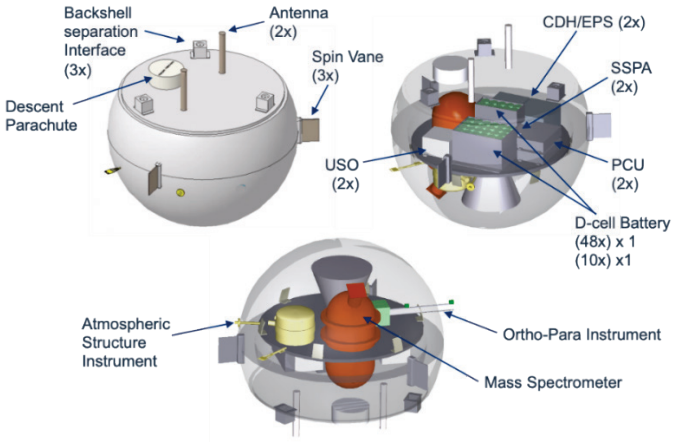

Exhibit 3-19. *Descent module configuration.*

The descent module is a truncated sphere for atmospheric stability and provides sufficient clearance margin to the interior of the TPS and the mortar-fired descent parachute attached to the backshell. Provisions for anti-spin vanes are included as the design matures. Both the descent module and heat shield have a load path through the backshell. Two sets of three separation mechanisms provide for separation of the heat shield from the backshell, and for the descent module from the backshell. Interior temperature of the descent module is maintained during the ~60-day approach using radioisotope heater units (RHUs) to alleviate battery capacity that would otherwise be needed for thermal control. Thermal switches to a radiator on the descent module shell provide for thermal management during cruise, approach, and descent.

During cruise to the Uranus system, the probe flight computer and individual components may be checked and updated using bus power provided by the orbiter; however, the majority of probe electronics are unpowered during cruise and Uranus approach except as needed for opportunistic cruise science. A redundant low-power timer circuit, triggered by orbiter separation, is powered during the ~60-day final approach and governs the sequencing of bus power-up based on the expected time of atmospheric entry. Instruments requiring warm-up are powered before entry, such as the USO supporting Doppler wind measurements. Instruments requiring calibration measurements before exposure to the atmosphere are powered before heat shield separation. Accelerometer and ESI data are recorded during the entry and high-g-load deceleration of the probe. Once the descent module separates from the aeroshell, the instruments begin recording science data to be relayed to the orbiter for eventual return to Earth. Ex. 3-19 shows the descent module configuration. Refer to Ex. 3-18 for the probe block diagram.

Probe Avionics. The UOP Probe avionics architecture is designed for block redundancy. The avionics hardware consists of SBCs and mission-specific cards (MiSC). This will take advantage of extensive use of heritage hardware from Parker Solar Probe and DART. C&DH, G&C, and spacecraft fault protection functions will be performed in a single radiation-hardened, quad-core, GR740 processor, same as the orbiter.

The MiSC will provide probe components and instrument interfaces as well as monitoring of temperature sensors. Because the probe will separate from the orbiter ~60 days before entering Uranus's atmosphere, a low-power and highly optimized timer circuit for power sequence is needed. This timer will work from a 5-V battery, consume no more than 250 mW, and be incorporated as part of the MiSC card design.

Probe Electrical Power. The electrical power subsystem (EPS) provides power distribution and energy storage for the probe. Block redundant power distribution is implemented using the same switch slices used in the Orbiter power switching unit (PSU). For the probe, these cards are not separate units, but instead are included in consolidated probe electronics modules. Two lithium thionyl chloride (LiSOCl2) primary batteries, selected for high energy density and long storage life, provide power to the probe. The first provides power only to a timer circuit activated when the probe is separated from the orbiter. The second provides power to the probe during descent operations. Before deployment, the probe electronics can be checked by supplying power from the orbiter. The primary batteries remain isolated during these periods.

Thermal batteries, secondary lithium-ion batteries, and other lithium primary chemistries with flight history were considered as part of this study. Thermal batteries have been qualified for 30 years of storage life but are designed for hours, rather than days, of operation after activation. Secondary cells provide lower energy density than primary cells and would require charge and balance electronics for maintenance through the long cruise. Therefore, lithium primary cells with flight heritage for longer performance were selected.

Probe Thermal Protection System. A variety of entry trajectory designs were evaluated for initial aerothermal environment and HEEET TPS sizing, resulting in selection of a –30.7° entry flight path angle as the best option for the probe, in terms of maximum acceleration, TPS sizing, and communication budget margin. Steeper entries yielded stagnation pressures that were beyond the capability of ground test facilities, and shallower entries resulted in degraded communications capability with the orbiter. Entry trajectory analysis was conducted using NASA Langley's POST2 software, and aerothermal environments were obtained via computational fluid dynamics (CFD) simulations using NASA Ames's Data Parallel Line Relaxation (DPLR) model. TPS sizing analysis was conducted using the NASA Ames developed materials response software, Fully Implicit Ablation and Thermal response (FIAT) [Chen and Frank 1999]. Additional information about the Probe entry analysis can be found in § 3.3.4.

3.2.3. Flight System Element Summary

A summary of mass and average power values per subsystem for the orbiter and probe flight elements (excluding science instruments) is provided in Ex. 3-20. A summary of flight system element parameters (also excluding science instruments) is shown in Ex. 3-21 and 3-22 Additional details can be found in Appendix C.

	Mass			Average Power			
Item	CBE (kg)	% Cont	MEV (kg)	CBE (W)	% Cont	MEV (W)	Comments *(See MEL in Appendix C for Heritage Basis)*
Structures and Mechanisms	668.5	21	811.5				
Propulsion	390.1	12	436.4	334.2	3	344.3	Power values applicable for DSM/UOI cases only
Guidance and Control	73.4	5	77.0	98.0	3	100.9	Includes 20 kg CBE radiation shielding allocation
Electrical Power	250.0	7	267.3	34.6	10	38.1	Includes 3 GFE RTGs, 30 kg CBE radiation shielding
Thermal	62.2	20	74.6	36.0	20	43.2	Power values listed are average at Uranus
Avionics	28.1	10	31.0	27.0	10	29.7	Includes 8.5 kg CBE radiation shielding allocation
Telecommunications	92.4	13	104.2	118.1	10	129.9	Includes 28.8 kg CBE radiation mini-vault
Harness	113.8	15	130.8				7% of total orbiter mass (includes instrument mass)
Orbiter Bus Total (w/o instruments)	**1678.4**	**15**	**1932.8**	**647.9**	**6**	**686.1**	*See PEL in Appendix C for phasing by power mode*
Probe Mechanical (Descent Module)	48.0	19	57.3				
Probe Avionics	2.4	10	2.6	22.8	15	26.2	
Probe Electrical Power	15.3	23	18.8	13.8	15	15.9	
Probe Thermal Control	4.6	19	5.5				RHUs are heat source
Probe RF Communications	4.7	12	5.3	59.3	9	64.8	
Probe-Orbiter Separation System	22.0	15	25.3				
Probe Harness	8.2	17	9.6				7% of Descent Module & Sep System. excludes EDS
Probe Entry and Descent System	108.0	12	121.2				0.4-m nose radius, 210 kg/m^2 ballistic coefficient
Probe Total (w/o instruments)	**213.2**	**15**	**245.6**	**95.9**	**12**	**106.9**	*See PEL in Appendix C for phasing by power mode*

Exhibit 3-20. *Flight system element (orbiter and probe) mass and power tables. Excludes science instruments.*

Flight System Element Parameters: Orbiter	Value / Summary / Units
General	
Design Life	222 months (18.5 years)
Structure	
Structures material	Machined aluminum cylinders, aluminum sheet-and-stringer cylinders, aluminum honeycomb panels
Number of deployed structures	One (probe). Instruments also have various antenna/boom or door/cover deployments.
Thermal Control	
Type of thermal control used	Thermal blankets: RTG waste heat: limited heaters; radiators/louvers, heat pipes, switchable shunts
Propulsion	
Estimated delta-V budget	2708 m/s
Propulsion type and associated propellants	Pressurized bi-propellant main engines, 350 psi MEOP, N2H4 and NTO-MON3: Monoprop ACS
Number of thrusters and tanks	2× 645-N bi-prop main engines, 4x 22-N monoprop steering, 16x 4-N Monoprop ACS, all fixed-mounted
Specific impulse, main engines	318 seconds
Attitude Control	
Control method	3-axis, wheels and thrusters; passive spin-stabilized during quiescent cruise
Control reference	Inertial, sun/earth safe mode
Attitude control capability	0.06 deg (3-axis, per axis); 0.5 deg (spin)
Attitude knowledge limit	Star Trackers: 6.3 arcsec, 3σ, of boresight; 49.6 arcsec, 3σ, about boresight
Command and Data Handling	
Spacecraft housekeeping data rate	1 kbps
Data storage capacity	256 Gbit non-volatile storage on SBC; 2x 128Gb buffers available on instrument interface cards
Power	
Power generation method	3x Next-Generation Mod 1 Radioisotope Thermoelectric Generators
Total Expected power generated	735 Watts at beginning of life (at fueling, 3-yrs pre-launch); 493 W available at end of mission
Battery type and storage capacity	2x 20 Ah 8s16p ABSL secondary batteries
Communications	
Bands supported	X-band uplink/downlink, with Ka band for science downlink; UHF for probe-to-orbiter uplink
Maximum transmit power	100-Watt TWTAs for X and Ka (58 Watts RF power)
Science data Earth return rate	19.5 kbps via Ka at Uranus on 3.1-m HGA

Exhibit 3-21. *Orbiter key characteristics. Excludes science instruments.*

Flight System Element Parameters: Probe	Value / Summary / Units
General	
Design Life	165 months (13.7 years)
Structure	
Structures material	Descent module: honeycomb w/composite facesheets; T300/PICA backshell, single-layer HEEET TPS
Number of deployed structures	4 (two parachute deployments, heatshield separation, backshell separation)
Aeroshell diameter	1.26 m
Thermal Control	
Type of thermal control used	Radioisotope Heater Units (RHUs) heat sources, with aerogel for thermal protection on entry
Attitude Control	
Control method	Passive spin on approach, released by release/spin-up mechanism on orbiter spacecraft
Command and Data Handling	
Data storage capacity	128 Gb non-volatile storage per each block-redundant side
Power	
Battery type and storage capacity	2x lithium thionyl chloride primary batteries, 468 A-h for 60-d approach, 32 Ah for 1-hr descent
Communications	
Orbiter-Probe uplink method and rate	Local UHF uplink to orbiter, 6 kbps

Exhibit 3-22. *Probe key characteristics. Excludes science instruments.*

3.3. Mission Design & Concept of Operations

The UOP concept involves many trajectory phases, each subject to their own set of challenging drivers (Ex. 3-23). The most significant challenge entails designing Earth-to-Uranus interplanetary trajectories due to competing objectives associated with RTG power degradation over time, Uranus's large heliocentric distance (18.9 AU on average), and time penalties associated with Δv-reduction strategies, such as gravity assists and relatively low Uranus approach velocities to enable chemical capture.

Despite these challenges, cruise trajectories for a Uranus orbiter and probe are favorable in the upcoming decade. These are further enabled by upcoming launch vehicles (e.g., Vulcan and Falcon Heavy Expendable) that offer significant performance advantages compared with the previous decade's options. The mission design team focused on a high-fidelity capture and probe deployment design to demonstrate feasibility based on multiple design iterations with NASA Langley EDL experts. This effort is a risk-reduction response to technical feedback on previous Uranus orbiter and probe reports.

A significant finding of this study is that major mission risk reduction is possible by separating Uranus orbit insertion and probe deployment while incurring minimal performance penalties. A wide array of compelling moon tour options is possible. This study presents one possible reference design in a high-fidelity model.

3.3.1. Interplanetary Cruise

A favorable Jupiter flyby geometry is fundamentally enabling in the 2031–2032 launch timeframe as it facilitates elimination of the cost and complexity associated with solar electric propulsion (SEP) and the thermal challenges associated with Venus gravity assists. In total, the interplanetary trajectories found in this study provide between 40–90% more launch mass capability when compared to previous studies [NASA 2017; McAdams et al. 2011]. In addition, the proposed baseline cruise reduces Δv requirements by 100–450 m/sec while reducing probe deployment risk[1].

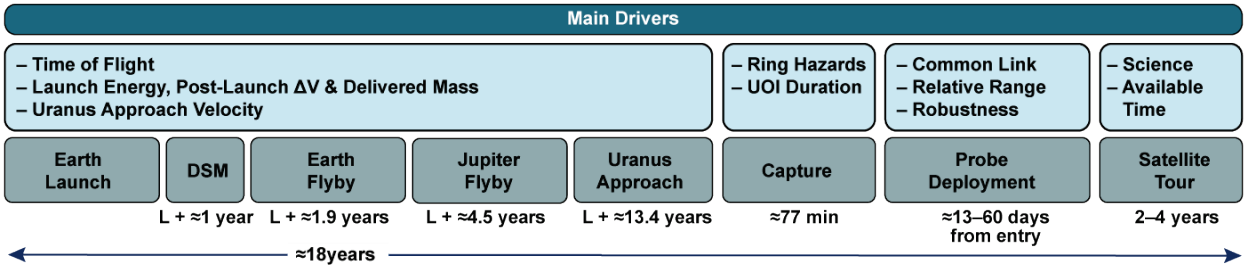

Exhibit 3-23. *High-level mission overview.*

Launch Date	C3 (km²/s²)	Path	DSM (km/s)	UOI (km/s)	PLΔV (km/s)	Post-UOI Mass (kg)	TOF (yrs)
9/30/2029	13.7	EVEEJU	0.00	1.221	1.221	7865.2	14.5
10/31/2029	11.3	EVEEJU	0.00	1.901	1.901	6665.4	13.1
3/7/2031	17.5	EVEEJU	0.05	1.722	1.771	6068.7	12.5
4/3/2031	28.6	E(DV)EJU	0.65	1.033	1.68	4934.7	13.5
6/13/2031	**27.1**	**E(ΔV)EJU**	**0.77**	**1.011**	**1.783**	**4919**	**13.4**
6/15/2031	27	E(ΔV)EJU	0.72	1.251	1.968	4643.5	12.7
7/18/2031	19.8	EVEJU	1.07	1.763	2.834	4089.3	11.6
8/1/2031	18	EVEJU	1.05	1.374	2.426	4855	12.3
8/9/2031	20.2	EVEJU	1.06	1.504	2.561	4433.5	12
4/29/2032	**28.8**	**E(ΔV)EJU**	**0.60**	**0.956**	**1.558**	**5111.5**	**12.8**
5/3/2032	29.2	E(ΔV)EJU	0.76	1.147	1.904	4527.2	12.2
8/15/2032	49.5	E(ΔV)EJU	0.42	1.302	1.726	3056.3	11.8
1/8/2033	*23.6*	*EVEEU*	*0.42*	*1.012*	*1.434*	*5933.3*	*15.3*
5/27/2034	*23.1*	*EVEEU*	*0.68*	*0.946*	*1.629*	*5626.4*	*15.2*
2/28/2036	*28.2*	*EVEEU*	*0.54*	*0.974*	*1.519*	*5240.5*	*15.3*
1/8/2038	*35.5*	*EVEEU*	*0.00*	*1.307*	*1.307*	*4812.3*	*14.2*

Exhibit 3-24. *Feasible launch opportunities with (2029–2032) and without (2033–2038) Jupiter gravity assists. Lighter colors = the best solutions. Bold = primary and backup baselines; italics show example windows without Jupiter flyby.*

[1] The comparison is based on normalizing Δv margins and statistical strategy reported in previous studies to that of this study. This study relies on conservative assumptions deemed typical of flagship missions.

The prime launch period opens on 9 Jun 2031, with a mission-driving C_3 of 29.36 km^2/sec^2 and closes on 30 Jun 2031, with a 13.4-year cruise (Ex. 3-25). The backup launch period occurs in Apr 2032 with a 12.8-year cruise; however, all performance is driven by the 2031 opportunity.

If launch readiness by 2031 is deemed infeasible, the Jupiter gravity assist can be replaced with opportune gravity assists from Earth and Venus, as shown in Ex. 3-24. These sequences extend launch availability through the mid- to late 2030's at the expense of increased overall mission duration and/or updating the spacecraft design to accommodate the thermal challenges associated with Venus flybys. Note also that the launch opportunities presented in the table constitute a hand-picked, representative sample from a vastly larger set of several hundred thousand solutions. The list as shown illustrates a range of potentially interesting trajectories, with the possibility of many other viable options being found through additional analysis.

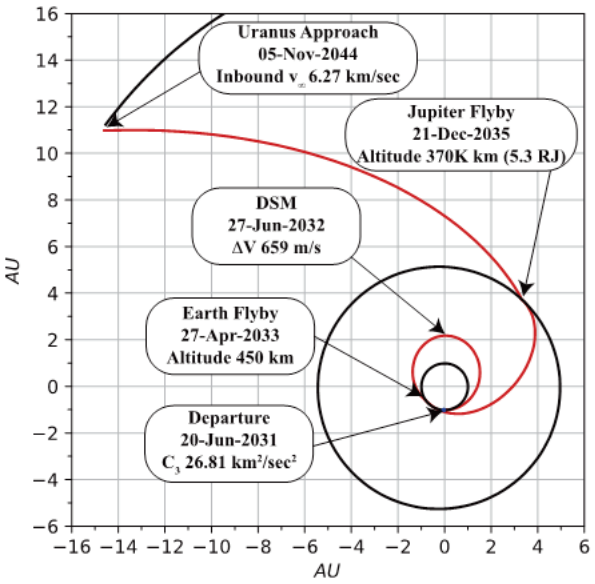

Exhibit 3-25. *Baseline interplanetary trajectory (launch period center case).*

3.3.2. Interplanetary Trade Space

The selection of prime and backup baseline interplanetary transfers is based on a patched-conic broad search over a feasible region of gravity-assisted interplanetary opportunities in the 2026–2038 timeframe and includes the possibility of v_∞-leveraging maneuvers and powered flybys. Gravity assist options include Earth, Venus, Mars, and Jupiter, while ignoring Saturn, which is out of phase for the majority of the given timeframe. The broad search does not consider trajectories based on the Space Launch System (SLS) or solar electric propulsion.

Post-UOI mass is a convenient optimization construct of the broad search process and is calculated in accordance with Ex. E-26. The reference launch vehicle for post-UOI mass assumes the FHE given that it is the

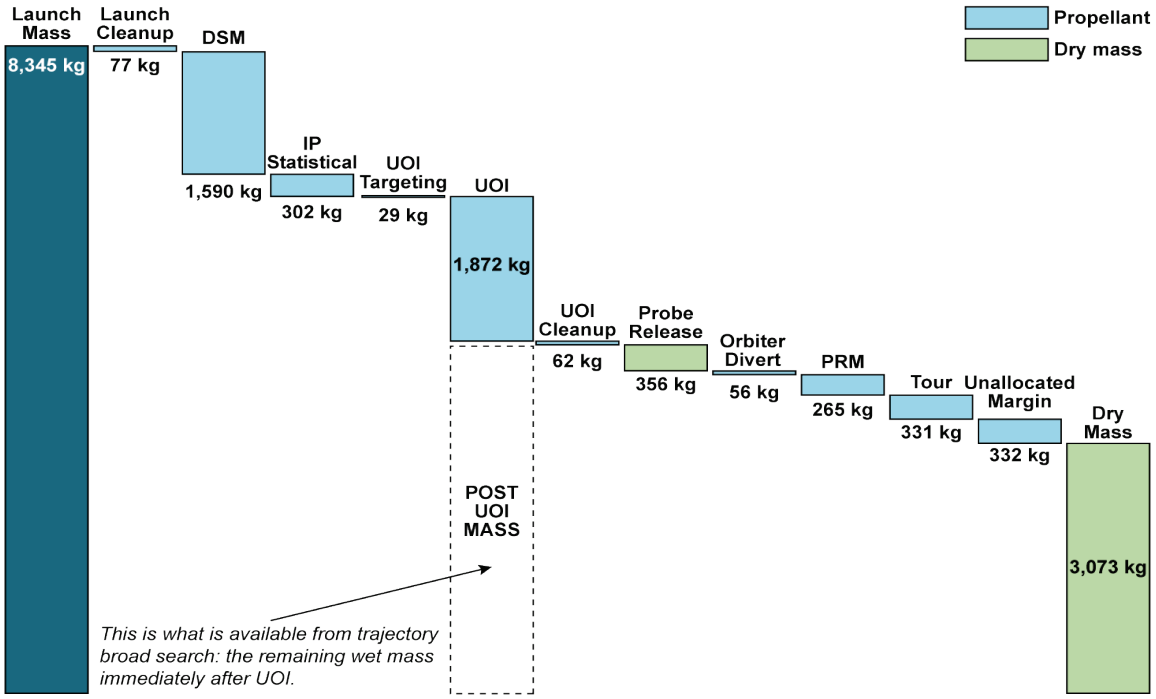

Exhibit 3-26. *General breakdown of available post-UOI mass and dry mass capability. For simplicity, the broad search analysis ignores launch cleanup, statistical, and targeting factors. The fully margined, MPV flight system dry mass (§ 3.3.6) is 2,756 kg.*

most capable option currently offered with performance parameters available in the NLS-II contract excluding the SLS (this assumption does not preclude feasible alternative launch vehicles). The broad search allows selection of an optimal trajectory among the competing objectives of time-of-flight (due to the limitations on expected RTG lifetime) and post-UOI mass. Additionally, an upper bound of 1.8 km/sec is imposed on the total ΔV for interplanetary maneuvers and UOI. Such an upper bound is consistent with a global ΔV below 3.0 km/sec (estimated limit for chemical missions) including the science tour and statistical cost.

Ex. 3-27 through 3-29 present the results of the broad search database, where the dotted red line represents the final design point for the UOP concept. Ex. 3-29 shows how the *EΔVEJU* sequence is enabling once a more aggressive maximum time-of-flight filter of 13.5 years is applied to Ex. E-27. Ex. 3-27 and 3-28 additionally demonstrate that enabling non-Jupiter sequences exist (e.g., *EVEEU*) beyond 2031, when Jupiter falls out of phase. The *EΔVEJU* interplanetary trajectory is selected because it represents a balanced choice that avoids Venus flybys, has qualitatively similar opportunities in both 2031 and 2032, and manageable total Δv and incoming speed at Uranus. While *VEEJU* trajectories can deliver better Δv performance, these require slightly longer duration and a Venus flyby, with the associated thermal challenges. Beyond the 2031–2032 launch opportunities, it is also possible to launch on the same launch vehicle without relying on a Jupiter flyby if the spacecraft uses an SEP stage, as baselined for the 2011 *Vision and Voyages Study* [National Research Council 2011].

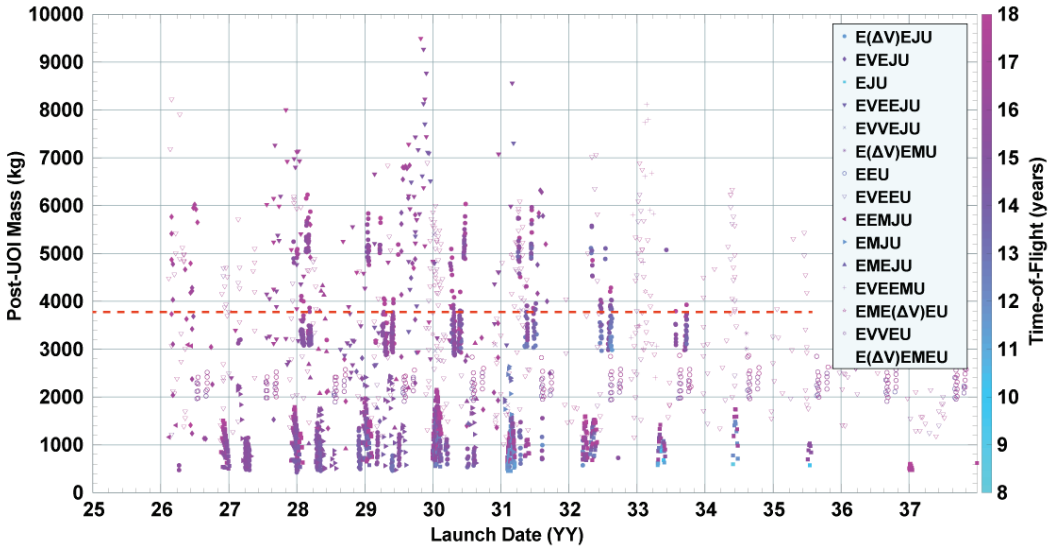

Exhibit 3-27. *FHE post-UOI available mass vs launch date w/ time-of-flight ≤ 18 years and interplanetary ΔV ≤ 1.8 km/s.*

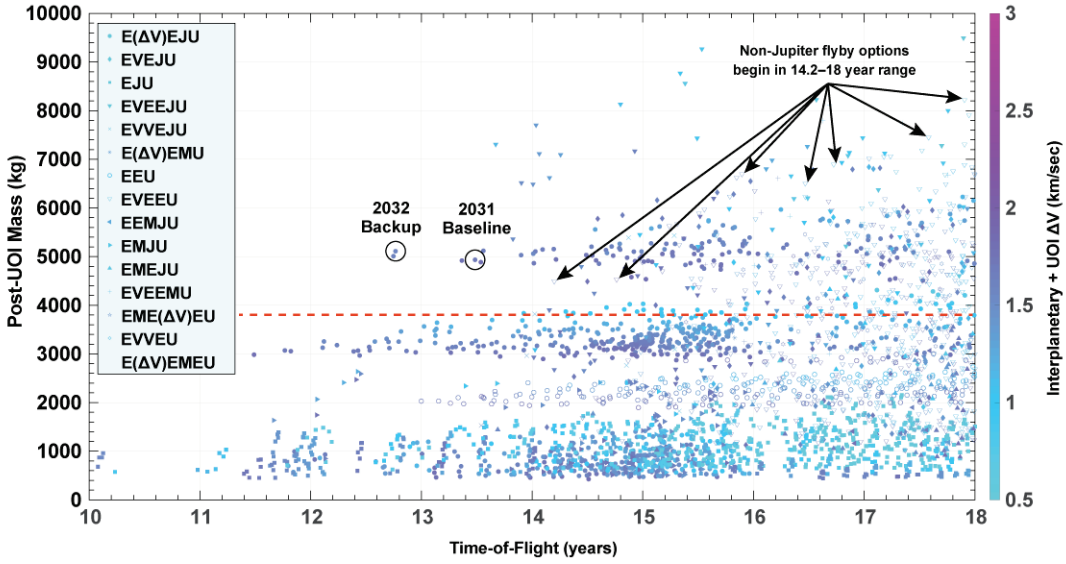

Exhibit 3-28. *FHE post-UOI available mass vs time-of-flight w/ time-of-flight ≤ 18 yrs and interplanetary ΔV ≤ 1.8 km/s.*

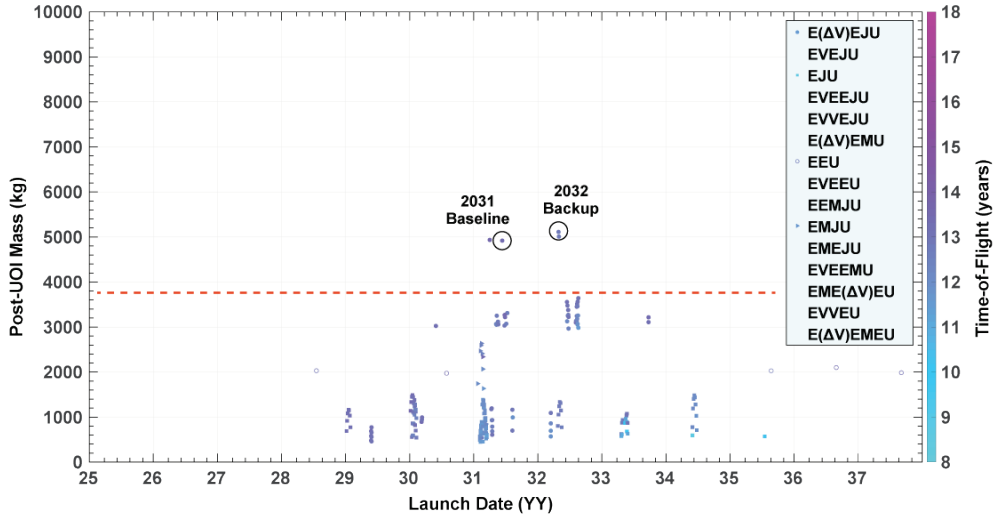

Exhibit 3-29. *FHE post-UOI available mass vs launch date w/ time-of-flight ≤ 13.5 yrs and interplanetary ΔV ≤ 1.8 km/s.*

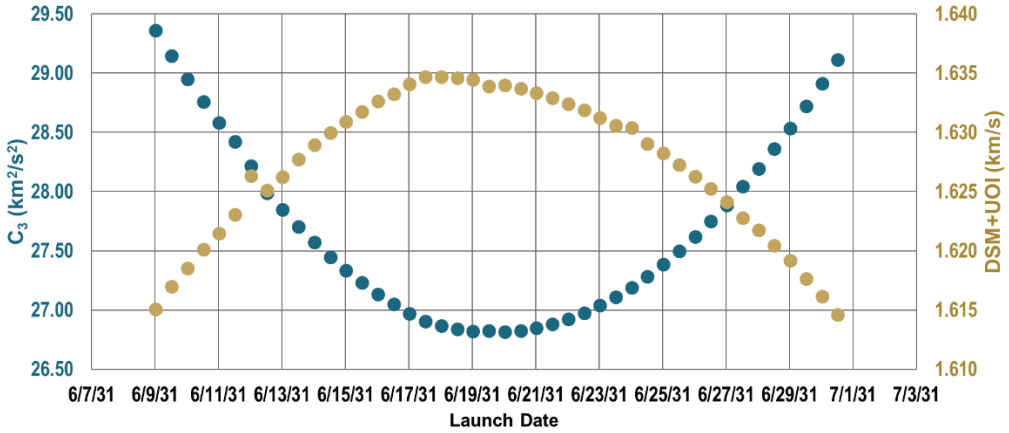

Exhibit 3-30. *Baseline launch period: 9 Jun 2031 – 30 Jun 2031. The driving date for maximum C_3 occurs on 9 Jun 2031 and the driving date for the ΔV budget occurs on 17 Jun 2031. The backup opportunity is not shown since the baseline is the driving case.*

3.3.3. High Fidelity Analysis

The 2031 *EΔVEJU* trajectory is modeled as a high-fidelity *n*-body problem and numerically integrated and optimized to obtain a 20-day launch period. The analysis yields a maximum C_3 of 29.36 km^2/s^2 and the driving interplanetary and UOI Δv for the mission budget (Ex. 3-30). The minimum Earth flyby altitude is set to 450 km, consistent with the Multi Mission Radioisotope Thermal Generator (MMRTG) Earth-biasing implementation on NASA's planned Dragonfly mission. The launch period exhibits a minimum Jupiter flyby altitude of 4.01 R_J, approximately equivalent to the radius of Io's orbit that is used as a driving case for radiation analysis (Ex. 3-31). Finally, the maximum possible value (MPV) launch mass for the final UOP point design is plotted against the portfolio of several possible launch vehicles

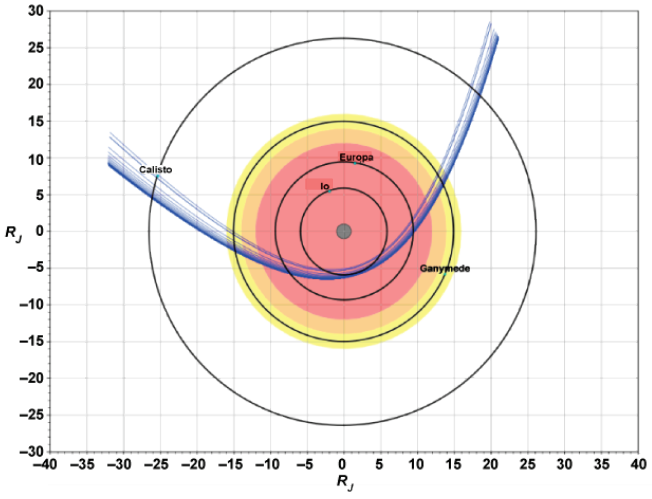

Exhibit 3-31. *All Jupiter flyby trajectories in the 2031 opportunity. Each trajectory spans 24 hours. Colors illustrate the strength of the Jupiter radiation environment.*

(Ex. 3-32). It is observed that the design is feasible with a Falcon Heavy Expendable and very close to the capability of a Vulcan Centaur configured with six solid rocket motors.

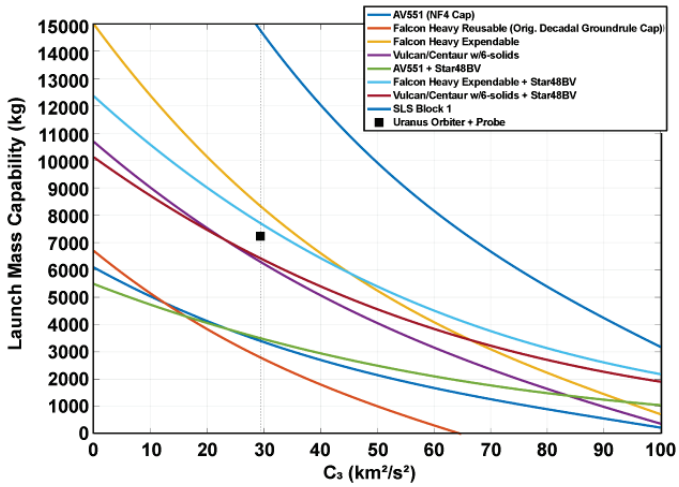

Exhibit 3-32. *Launch mass capability and the UOP point design.*

3.3.4. Uranus Capture & Probe Release

A major focus of this study was to identify an approach that enables deployment of a probe that penetrates Uranus's atmosphere and relays scientific data to the orbiter. The communication link is maintained for about one hour (the time need for the probe to reach an atmospheric pressure of 10 bar).

Previous studies are based on the *deployment on hyperbolic* approach paradigm (Ex. 3-33, left side), where the coupled orbiter and probe are placed in a trajectory that leads to prescribed atmospheric entry conditions prior to UOI, the probe is released for ballistic flight along this hyperbolic trajectory, and the orbiter is subsequently diverted via a comparatively small maneuver (15 m/s) that targets a favorable UOI location. The primary advantages of this approach are low ΔV requirements and negligible impact on overall mission duration. The main disadvantages are high probe entry velocity and ***the coupling of three critical events***: (1) targeting of probe entry conditions and UOI location, (2) establishment of probe communication link, and (3) UOI execution. This coupling leads to infeasibility as pragmatic operational constraints are included in the design, like ring avoidance constraints on UOI location, probe-orbiter geometry, link performance and telemetry margin, and ability to turn the spacecraft from probe link attitude to UOI attitude in a short amount of time.

In contrast, this study proposes a *deployment on elliptic post-capture* paradigm (Ex, 3-33, right side), where orbiter and probe remain coupled through UOI. After successful capture into Uranus's orbit, the targeting of probe entry interface, probe deployment, and orbiter divert ***are addressed independently***. Advantages of this approach include lower probe entry velocity, decoupling of critical events, and availability of backup opportunities for probe deployment. Disadvantages include slightly higher ΔV requirements and increase in overall mission duration by one period of the capture orbit (120 days).

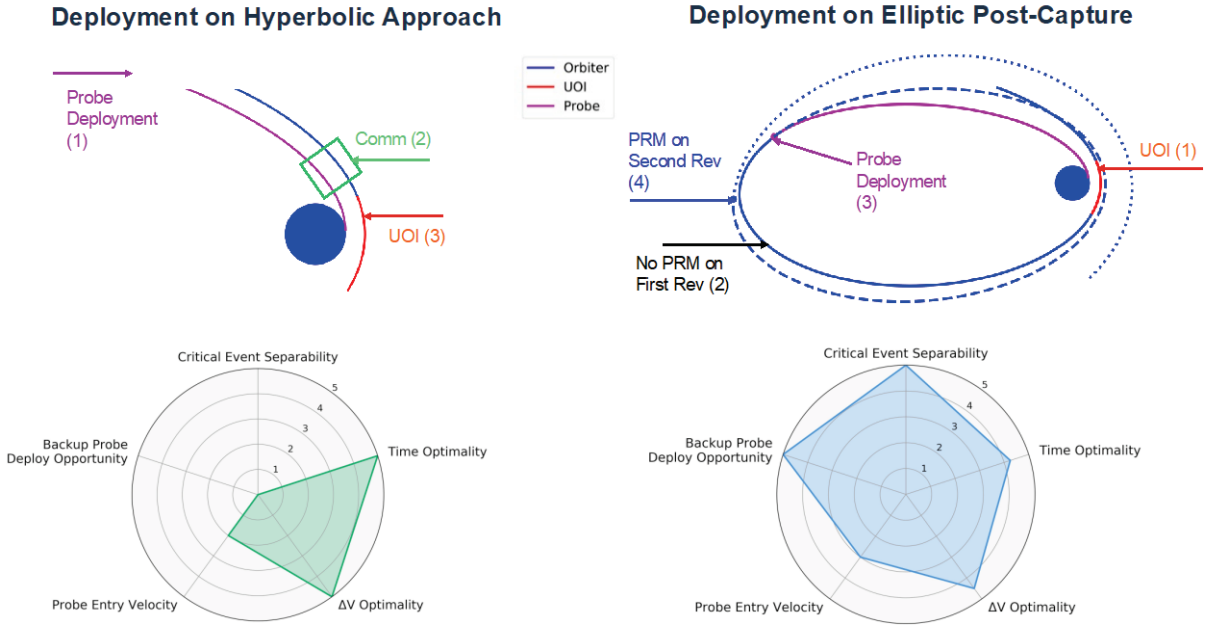

Exhibit 3-33. *Schematic comparison between probe deployment paradigms.*

Detailed aerothermodynamic analyses performed by NASA Langley and NASA Ames Research Centers (see Appendix C) show that feasible probe trajectories exist that can be targeted from the apoapsis of the capture orbit. These trajectories exhibit heat loads and heat rates well within the design margins of the probe heat shield and result in a descent profile that maintains favorable geometry with the orbiter. From subsequent detailed analyses it is determined that an orbiter-probe telecom link can be maintained with sufficient telemetry margin for the duration of the descent to 10 bar.

Probe entry analysis used an entry vehicle with a 1.26-m diameter, 45° half-angle sphere cone, with Pioneer Venus and Galileo (Jupiter) mission heritage. A blunt nose radius (0.4-m) was chosen to limit peak aerothermal environments near the stagnation point and thereby reduce the TPS thickness and mass required. Cases were run for a probe mass of 268 kg (MEV), and for up to ± 20 kg for sensitivity. Probe release is targeted for ~60 days prior to entry, with a relative entry flight path angle of –30.7° at entry interface altitude of 2000 km. The entry flight angle was determined after a trade of peak sensed acceleration, peak heat flux, peak stagnation pressure, TPS thickness based on total heat load, and telecommunication budget margin. In Uranus's thick atmosphere, the vehicle achieves maximum acceleration of 114 Earth g's ~3.5 min after atmospheric interface and achieves a peak heat flux of 1876 W/cm^2, which is within the expected capabilities of the single-layer HEEET TPS, which was recently developed by NASA for missions to outer-planet, Venus, and Mars Sample Return missions.

The entry vehicle reaches subsonic conditions 255 sec after entry, and at this point a mortar deploys a 2.5-m conical ribbon parachute at Mach 0.8, dynamic pressure of 2874 Pa, and an altitude of 63 km (0.069 bar). Conical ribbon parachutes have long heritage for planetary missions, having been used for Venus and Jupiter (EDL 3 and EDL 4), and the mortar deployment conditions are well within conditions seen in other planetary entries. The first parachute decelerates to low subsonic speeds, where the heat shield is jettisoned 15 sec after the parachute deployment at Mach 0.42. The first parachute is still attached to the backshell and the descent probe, allowing for a smaller ballistic coefficient while the heat shield and its higher ballistic coefficient vehicle can separate away at rates similar to other planetary entry missions.

After the heat shield has had sufficient separation from the rest of the vehicle, the descent probe and a second smaller, 1.8-m ringsail parachute separate from the backshell and first parachute system. The descent probe separation occurs 30 sec after the heat shield separation, at Mach 0.3, and an altitude of 54.7 km. Once again, the two stages have a positive separation rate because of ballistic coefficient difference.

Data start being received at the spacecraft ~5 min after atmospheric entry. After backshell separation, the probe descends under the second parachute until it reaches 1-bar pressure level at 13 min after entry. The probe continues to have good visibility to the orbiter throughout the remainder of its descent to the 10-bar level. Ex. 3-34 summarizes the probe trajectory and concept of operations, and Ex. 3-35 details the probe-orbiter communications link geometry during the descent.

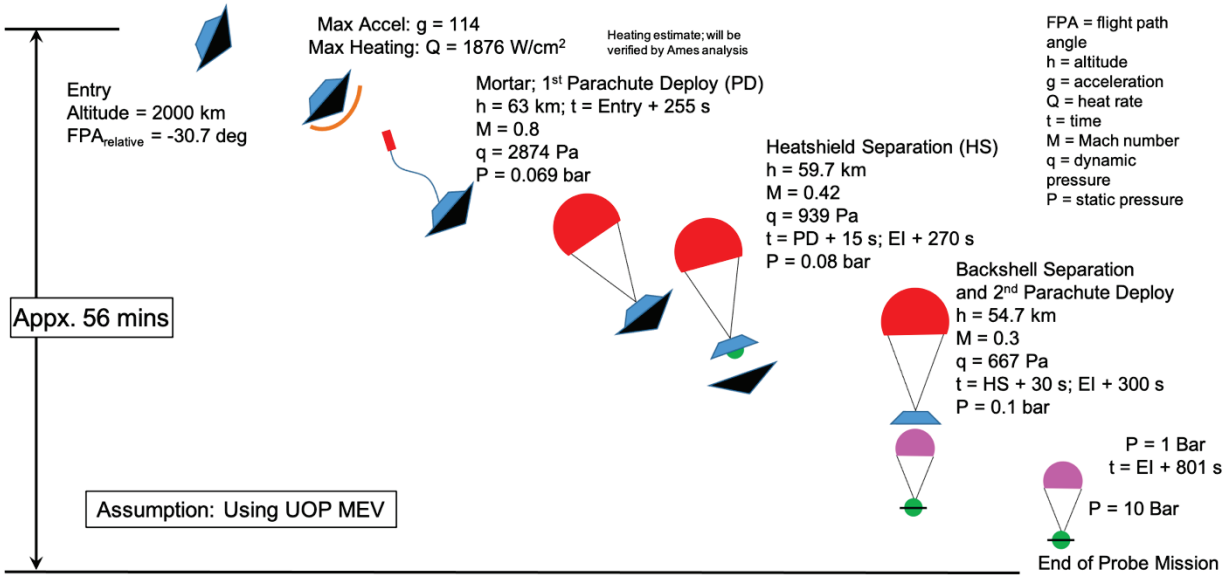

Exhibit 3-34. *Probe Trajectory Concept of Operations.*

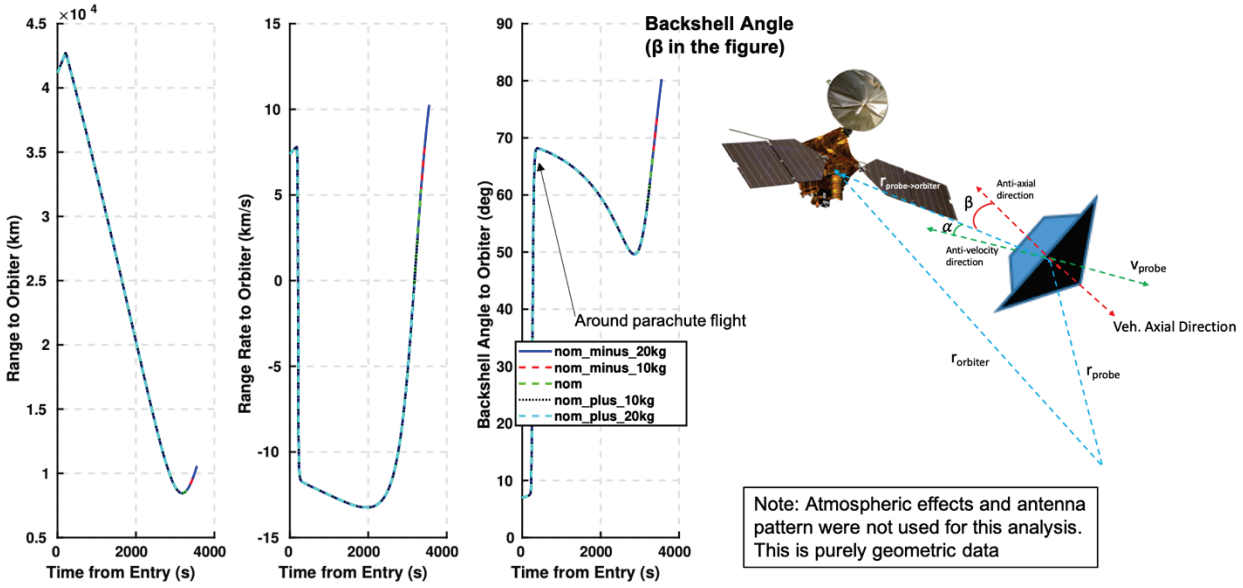

Exhibit 3-35. *Probe-Orbiter Communications Link Geometry.*

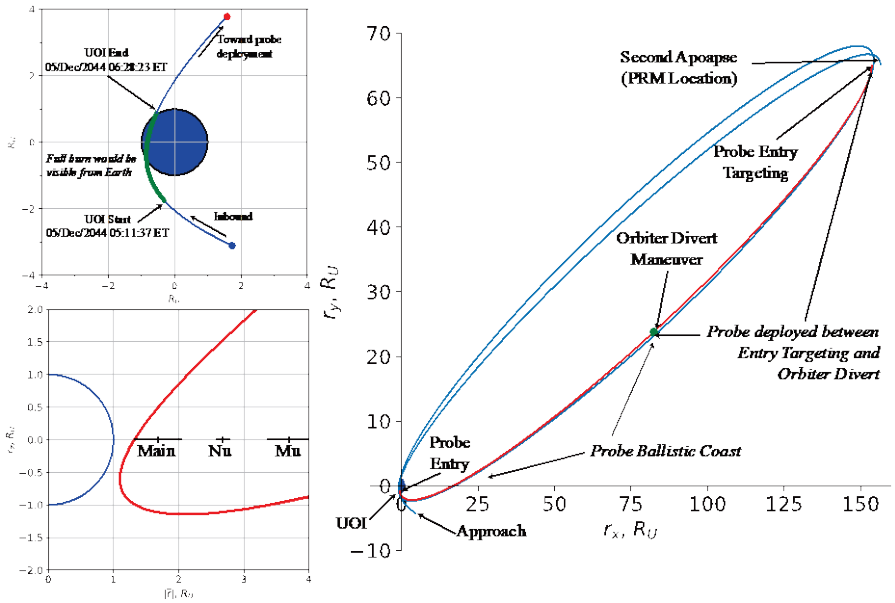

Exhibit 3-36. *Deployment on elliptic post-capture. UOI (top-left) is optimized for low altitude, avoiding ring hazards (bottom-left). Probe target/release, orbiter divert, and probe entry follow and leave the orbiter in favorable PRM location to start satellite tour (right).*

As shown in Ex. 3-36 probe deployment on elliptic post-capture results in a feasible paradigm that allows placing UOI at an advantageous location with altitude and duration constrained only by ring avoidance and target orbit period constraints. It is possible that any telemetry received after UOI could be processed on the ground to reduce uncertainty in the subsequent targeting of probe entry conditions and orbiter divert. After the orbiter finalizes the communication link with the probe, it reaches the second post-capture apoapsis and executes a period reduction maneuver (PRM) targeting the first flyby of the satellite tour.

3.3.5. Satellite Tour

It is possible to target any of the major moons of Uranus from the orbital location of the second post-capture apoapsis. The initial moon, inbound v∞, and flyby altitude determine which additional moons are reachable via subsequent resonant and non-resonant flybys aided by comparatively small spacecraft maneuvers. In practice, several subsequent flyby options emanate from a given flyby (between five and fifteen options are common), leading to a combinatorial explosion of alternatives.[2]

[2] If five downstream options were available on average (in practice there are more), there would be well over one billion 13-flyby tours.

Instead, given the limits available to the study team, an overall flyby strategy is devised that can be flown in practice, regardless of initial epoch or exact inbound conditions. This can be illustrated as a decision tree where high-level choices are made among available alternatives leading to a desired outcome. One path through one such decision trees is highlighted in Ex. 3-37; however, we stress that other choices are available and it is common practice in tour-based Flagship missions to analyze dozens of tours before committing to a flight-ready design.

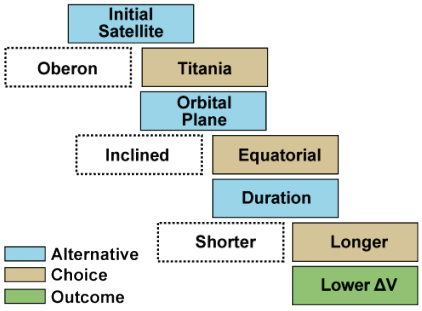

Exhibit 3-37 *One potential path through one potential tour-design decision tree.*

For this study, we select a strategy that relies on 15 resonant flybys of Titania (Ex. 3-38) to equatorialize the orbiter trajectory (Ex. 3-39). The advantage of this strategy is that a nearly equatorial orbit permits targeting of other satellites via non-resonant transfers (the major moons orbit Uranus near the equator). In this case, the orbiter targets eight non-resonant flybys of Umbriel, Oberon, and Ariel. Once the desired satellites are visited (more non-resonant flybys are possible), the orbiter relies on 11 resonant flybys of Ariel (Ex. 3-40) to reduce the Uranus-relative periapsis altitude until an end-of-life maneuver is executed to dispose of the orbiter into Uranus's atmosphere.

The equatorialization phase and subsequent non-resonant flybys are nominally ballistic (i.e., with no fuel expended) and the Ariel periapsis reduction phase entails a small deterministic component (17 m/s) before a large deorbit burn (216 m/s) is applied at the last apoapsis in the tour for controlled disposal of the orbiter in Uranus's atmosphere. Ex. 3-41 enumerates all targeted flybys. While no flyby of Miranda is reported in Ex. 3-41, the alternative sequence

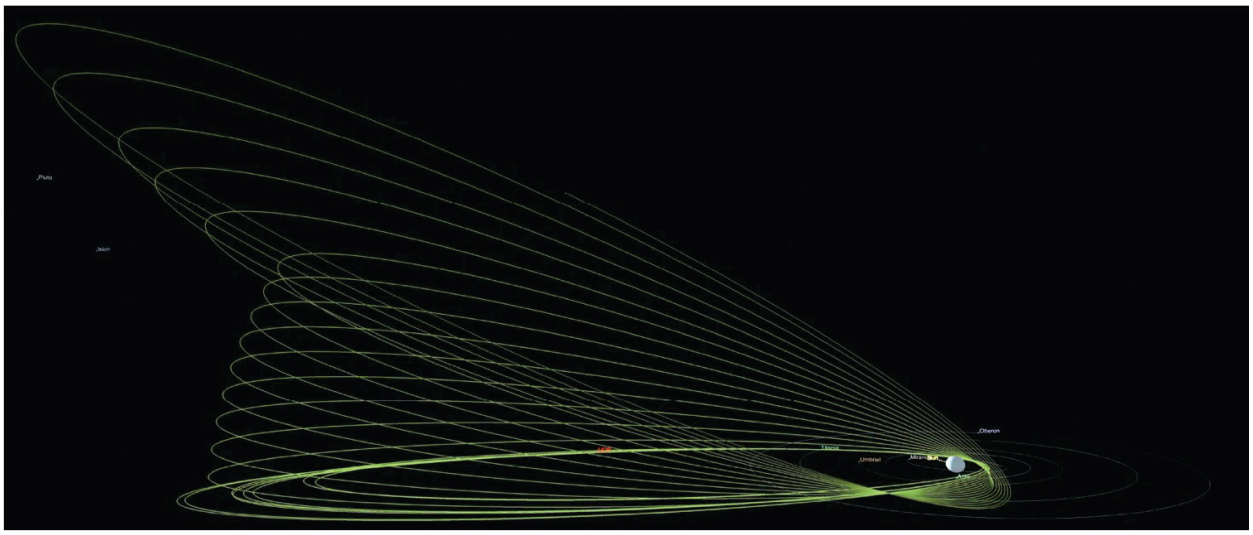

Exhibit 3-38. *Three-dimensional view of the equatorialization phase.*

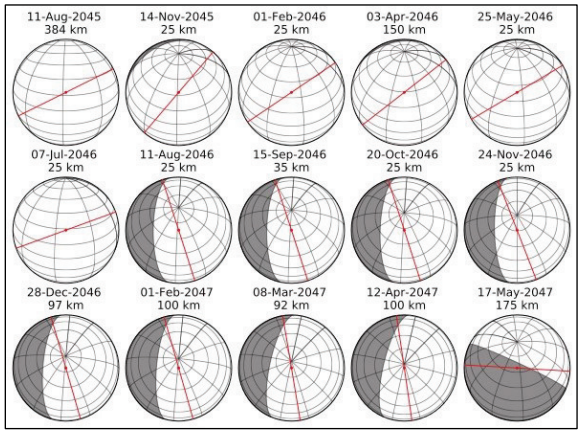

Exhibit 3-39. *Titania flybys used to equatorialize the orbiter trajectory.*

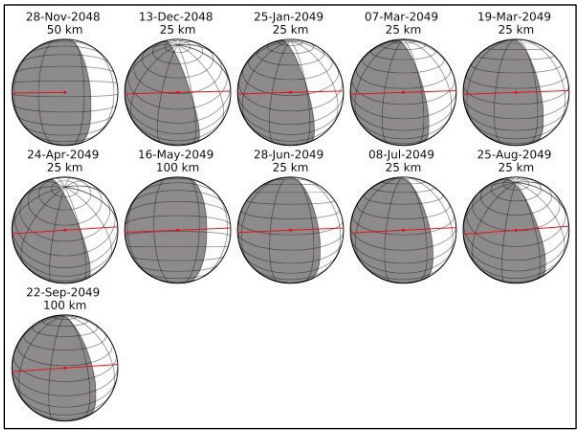

Exhibit 3-40. *Ariel flybys used to reduce Uranus-relative periapsis for subsequent spacecraft disposal.*

Body	Date	Phase (deg)	Altitude (km)	Speed (km/sec)	Lat (deg)	Lon (deg)
Titania	08/11/45	13.77	384.69	2.97	34.11N	91.07E
Titania	11/14/45	44.58	72.37	4.05	60.94N	64.46E
Titania	02/01/46	33.62	62.76	4.1	51.78N	81.93E
Titania	04/03/46	43.21	142.76	3.74	59.92N	75.09E
Titania	05/25/46	38.73	26.69	4.28	55.68N	84.30E
Titania	07/07/46	24.37	25.75	4.28	39.17N	98.21E
Titania	08/11/46	73.16	25.77	4.28	75.42N	3.27E
Titania	09/15/46	73.68	38.36	4.22	77.21N	3.27E
Titania	10/20/46	74.12	53.42	4.15	78.98N	3.56E
Titania	11/24/46	75.26	93.27	3.95	80.43N	359.60E
Titania	12/28/46	74.96	71.65	4.05	82.40N	4.92E
Titania	02/01/47	75.53	76.19	4.03	84.10N	5.20E
Titania	03/08/47	75.73	86.29	3.99	85.86N	11.02E
Titania	04/12/47	76.42	96.79	3.94	87.48N	12.85E
Titania	05/17/47	93.12	175.55	3.61	72.71N	294.23E
Umbriel	06/22/47	118.51	5354.46	0.52	1.79S	77.31E
Oberon	07/28/47	106.02	1038.56	1.62	4.16S	66.71E
Ariel	07/29/47	126.31	3786.72	0.76	0.18S	82.60E
Ariel	08/30/47	53.31	1821.57	1.39	0.19N	264.17E
Umbriel	10/03/47	118.14	3652.93	0.73	2.61N	76.52E
Titania	11/07/47	159.86	6505.63	0.47	1.88S	292.06E
Oberon	12/09/47	105.44	462.15	2.4	8.53N	65.78E
Ariel	01/10/48	44.24	1478.66	1.66	45.15N	99.27E

Exhibit 3-41. *Nominal equatorialization phase with initial non-resonant transfers to major satellites. Eleven additional flybys of Ariel occur during the remainder of the 4-year tour.*

Body	Date	Phase (deg)	Altitude (km)	Speed (km/sec)	Lat (deg)	Lon (deg)
Titania	08/10/45	21.35	500.02	2.67	41.41N	86.54E
Titania	11/14/45	33.33	400.02	2.89	52.77N	78.22E
Titania	01/31/46	27.06	200.02	3.49	44.90N	87.77E
Miranda	04/01/46	84.31	26791.71	0.04	43.38S	218.34E
Titania	04/02/46	42.83	133.1	3.74	60.32N	74.55E
Miranda	05/24/46	133.07	16713.25	0.06	38.13S	137.54E
Titania	05/25/46	38.03	52.01	4.11	54.97N	84.92E
Titania	07/07/46	65.24	556.85	2.55	74.88N	26.06E

Exhibit 3-42. *Alternative equatorialization sequence targeting Miranda prior to reaching equatorial plane.*

Phase	Maneuver Name	Δv (m/s) Deterministic	Δv (m/s) Statistical
Cruise	Launch Cleanup		20
	DSM	660	
	DSM Cleanup		30
	Earth Flyby Targeting/Bias		50
	Jupiter Flyby Targeting		30
	Phase Subtotal	**660**	**130**
Capture & Probe Release	UOI targeting		10
	UOI	1,087	
	UOI Cleanup		45
	Probe Targeting	15	
	Probe Separation		
	Orbiter Divert	29	
	Orbiter/Probe Statistical		5
	PRM	171	
	PRM Cleanup		20
	Phase Subtotal	**1,302**	**80**
Tour	Miranda Targeting	0	
	Miranda Statistical		6
	Ariel Targeting	17	
	Ariel Statistical		6
	Umbriel Targeting	0	
	Umbriel Statistical		6
	Titania Targeting	0	
	Titania Statistical		6
	Oberon Targeting	0	
	Oberon Statistical		6
	Phase Subtotal	**17**	**30**
Other	Disposal	216	
	Unallocated Margin	148	
	ACS		125
	Subtotal	**364**	**125**
Mission Total		**2343**	**365**
		2708	

Exhibit 3-43. *Notional mission ΔV.*

shown in Ex. 3-42 demonstrates that it is possible to target non-resonant Miranda flybys, return to the equatorialization phase, and continue toward the non-resonant transfers to the remaining major satellites.

A preliminary coverage analysis of the equatorialized trajectory, using instrument and sensor models with representative operational characteristics, reveals many opportunities to satisfy science observation objectives. Opportunistic satellite imaging is possible during the equatorialization portion of the tour, with more opportunities available once the spacecraft reaches the plane of Uranus's equator. Most of the required Uranus imaging takes place at fairly coarse scales and can be acquired far from the planet, where there are few competing targets for observation. Ring imaging can be accomplished at high inclinations during the equatorialization portion of the tour. Most of the Uranus flybys during this period are at relatively far distances so high-resolution imaging of the rings and satellites is not possible. Later, when the orbiter is in the ring plane and making close passes of Uranus, high resolution ring and satellite opportunities may be possible, but Uranus may be in the background. It would be desirable to have closer Uranus flybys early in the tour when the orbiter is at higher inclinations. Alternate tour strategies can be designed to accommodate this goal. See § 1.6 for discussion from the science perspective.

3.3.6. Mission Design Summary

Refer to Ex. 3-43 for a summary of the total mission ΔV, and Ex. 3-44 for the mission design table. Note that the flight system MPV launch mass of 7,235 kg, including 30% dry mass margin, fits well within the launch vehicle capability of 8,345 kg.

3.3.7. Mission Operations

UOP mission operations can be supported by a low-cost operations model, leveraging heritage facilities, infrastructure, tools, and experience for pre-launch, cruise, and science phases. There are no unique mission phases or spacecraft subsystems, ground system elements, tools, or staffing profiles required, and the optical navigation pipeline from downlink to processing is well established. The mission design is straightforward from an operations planning and support perspective (e.g., no solar conjunctions). Trajectory elements and critical events are similar to those in previous missions including MESSENGER, New Horizons, and Parker Solar Probe. The payload suite and corresponding science planning cycle and data pipeline architecture is comparable to scope and complexity of other similar missions. An enhanced operational focus will be placed on probe operations, with thorough testing, simulation, and rehearsals being conducted in pre-launch mission simulations and multiple times during flight.

Parameter	Value	Units
Prime Launch Period Open	9 Jun 2031	
Backup Launch Opportunity	Apr 2032	
Launch Site	Cape Canaveral AFS	
Launch Energy (C_3)	29.36	km^2/sec^2
Launch Vehicle	Falcon Heavy Expendable	
Mission Lifetime	18.5	years
Cruse Duration	13.4	years
Uranus Arrival	5 Dec 2044	
Probe Entry	6 Apr 2045	
Tour Start	6 Jun 2045	
Tour Science Phase Duration	4.5	years
Mission End / Orbiter Disposal	30 Dec 2049	
Stacked Dry Mass (Orbiter & Probe) MPV	2756	kg
Propellant Residuals and Pressurant Mass	111	kg
Usable Propellant Mass (N2H4 and Oxidizer)	4368	kg
Flight System MPV Launch Mass	7235	kg
Payload Adapter Mass (Leave Behind on LV)	45	kg
LV Capability (Falcon Heavy Expendable)	8345	kg
Unused Launch Vehicle Capability	1065	kg
Propellant Mass Fraction	60.4	%

Exhibit 3-44. *Mission Design Table. All performance is driven by the prime (2031) opportunity.*

UOP in-flight operations begin after launch in Jun 2031 with standard health assessment and the commissioning phase, which concludes in mid-Jul 2031 with the official start of Phase E and the beginning of the 13.4-year Cruise phase. In keeping with a low-cost operations model, the majority of Cruise is spent in a spin-stabilized hibernation mode. An initial transition period with three 4-hr tracks per week is planned prior to entering the first hibernation period at the end of Aug 2031. While in hibernation, weekly 2-hr DSN beacon tracks are planned for health checks, similar to those used for New Horizons. A proven response strategy is defined for red beacon tracks. Semiannual 3-axis wake up periods of two weeks each are scheduled to occur in March and September of each year. These periods consist of daily 8-hour DSN contacts. Activities can be recurring with system and payload health checks, or an alternating strategy may be employed. No science is baselined for Cruise, although instrument calibrations and stray light characterizations are not precluded for the flybys.

The spacecraft also awakens into 3-axis mode for approximately 7 weeks in 2022 to conduct the deep space maneuver (DSM). This window ensures adequate coverage for navigation with an appropriate data cutoff (DCO) for the final maneuver design, plus data downlink and reconstruction following the maneuver. The maneuver timing is flexible and may be split into two as a risk reduction measure.

Exits from hibernation are also planned to begin 100 days prior to each of the Earth and Jupiter gravity assists (EGA, JGA) and Uranus Orbit Insertion (UOI). This timing supports event preparations and approach maneuvers at –90d, –30d, –10d, and a clean-up at +20d. Eight weeks of DDORs, 2 per week, are scheduled for each approach. For EGA and JGA, the spacecraft returns to hibernation 8 days after the final clean-up maneuver, to accommodate all data downlink. There are no additional hibernation periods planned after UOI, and the Orbiter remains in 3-axis mode for the remainder of the mission.

Following post-UOI health checks, a 6-month transition and environment characterization period is planned supported by one daily 4-hour track. The key events during this period are the probe release/spacecraft divert maneuver and probe science, plus the periapsis raising maneuver (PRM).

All DSN contacts prior to the beginning of the prime mission science phase are supported by X-band. The 4-year science phase is supported by daily 8-hour Ka-band higher rate data downlinks. The first 2 years are focused on Uranus science and Titania while the orbit plane is brought into co-planar alignment, and the second 2 years are focused on the moons of the Uranian system. Single 34-m DSN supports are scheduled for all mission phases. The potential use of dual X-/Ka-band downlink for radio science is optional. Safe mode communications close with the chosen on-board antenna suite in all phases. Additional information on communications link performance can be found in Appendix C.

A preliminary analysis of data collection and return was conducted to estimate the potential data volumes that can be expected for operations at Uranus. For Probe operations, data will be streamed back to the Orbiter via UHF link and stored. While there is no requirement for the immediate return of Probe data to Earth, the total estimated data volume of 17 Mbits can easily fit within one of the initially scheduled 8-hour Ka-band downlinks. The data estimate for the science tour also assumes the use of one 8-hour Ka band downlink contact per Earth day. This provides a total, per-orbit downlink volume capability of 2.1 GB, at the available downlink rate of 19.475 kbps, assuming a 3dB link margin and the use of rate stepping. After applying an additional 5% margin for dropouts and overhead, the available science downlink data volume is estimated at 1.995 GB per orbit. The analysis further assumes that one orbit's worth of data would need to be downlinked within 30 days to clear the flash recorder for subsequent orbits. This cadence provides for sufficient margin in the event of unplanned situations such as DSN outages, since the Orbiter's 256 Gbit NAND storage can hold approximately 6 orbit's worth of science data.

Rough-order tour collection scenarios were developed using science team volume estimates organized into four different orbit types, each emphasizing a particular subset of the Orbiter instrument complement: (1) Uranus and rings remote sensing; (2) fields, particles, and magnetometer; (3) satellite flybys with remote sensing; and (4) multiple satellite flyby (equatorial phase). Compression factors of 2× are assumed, along with a 1 kbps spacecraft housekeeping data rate. Based on this preliminary analysis, the data return capability per orbit is sufficient to support science objectives for each of the four collection scenarios. An assumption of 26 orbits being completed during the tour phase, based on the mission design, yields the potential for 51.9 GB of total science data return. Refer to Appendix C for additional details.

3.4. Risk List

An assessment of potential risks for UOP, as summarized in Ex. 3-45 and 3-46, was conducted using APL's standard risk management process. The findings are consistent with study objectives to develop a low-cost, technologically ready mission concept. Only two of the identified risks (1, 2) are within the medium (yellow) range, with all others being classified as low (green). Mitigation strategies and approaches have been identified for each risk listed in the table, with several activities that could be initiated early in Phase A. Risks involving external factors, such as NEPA certification and predicted RPS power output, would need to be monitored but are currently assessed with low overall likelihoods of occurrence. Risks associated with uncertainties about Uranus's rings or atmospheric winds could be mitigated with additional observation and analysis, and/or through future mission design or spacecraft enhancement.

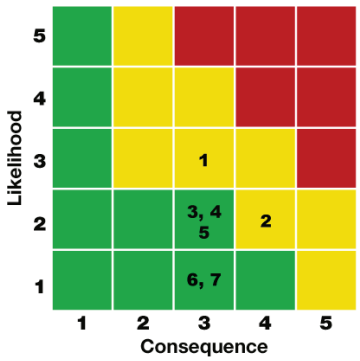

Exhibit 3-45. *UOP study 5×5 risk chart.*

#	Risk	Type	L	C	Mitigation
1	IF the reliability associated with a mission lifetime of >15 years cannot be demonstrated sufficiently, THEN spacecraft complexity and program cost may increase.	Cost, Technical	3	3	• Perform reliability analyses in Phase A and assess alternatives. • Reevaluate component/part selections as needed. • Conduct requalification or add redundancy where feasible.
2	IF launch vehicle NEPA certification is delayed for newer vehicle options, THEN the launch could also be delayed.	Schedule, Cost	2	4	• Start development of data books early for applicable LV options. • Select LV as early as possible, preferably around mission PDR.
3	IF expected peak entry acceleration loads for the probe cannot be met by the current system design, THEN additional effort would be required to remediate.	Cost	2	3	• Assess all systems for vulnerabilities in Phase A. • Qualify electronics and battery options for expected environments.
4	IF current knowledge/confirmation of ring locations and densities is updated, THEN the constraints for capture and tour trajectories may change, possibly with a ΔV cost.	Technical	2	3	• Attempt additional observations & modeling of Uranus's upper atmosphere and rings early in development to further characterize ring particle risk, and better confirm safe zones.
5	IF more detailed analysis indicates increased radiation hardness requirements, THEN higher parts cost could be incurred and/or additional shielding could be required.	Cost, Technical	2	3	• Conduct detailed radiation modeling and analysis in Phase A. • Allocate cost reserves for potential parts procurement increases. • Increase shielding mass allocations as needed.
6	IF uncertainties in Uranus upper atmosphere winds cause unexpected probe drift, THEN the orbiter could lose contact.	Technical	1	3	• Conduct detailed analysis and modeling/simulations to characterize coverage area relative to antenna beam widths. • Consider adding an active probe tracking capability.
7	IF the RPS estimated worst-case power output is lowered, THEN insufficient power margin may result.	Technical	1	3	• Revisit trade of # RTGs versus larger secondary battery. • Reduce pre-launch storage time from 2 to 3 years if possible.

Exhibit 3-46. *Top seven risks identified for the UOP concept study. L=likelihood (1–5), C=consequence (1–5).*

4. Development Schedule & Schedule Constraints

4.1. High-Level Mission Schedule

The UOP development schedule is based on previous schedules for relevant missions, proposed missions, and recent concept development efforts in the same class. The bar graph in Ex. 4-1 illustrates the sequence of key mission milestones for all mission phases. An 8-month Pre-Phase A, starting in Jan 2024, was included to allow for additional concept maturation and to accommodate the initiation of formal instrument procurements.

Additional details about the UOP development schedule and critical path can be found in Appendix C. Note that Probe development is in series with the start of Orbiter instrument system integration. Mission-level gateway milestones and key phases and durations are included in Ex. 4-2 and 4-3, respectively.

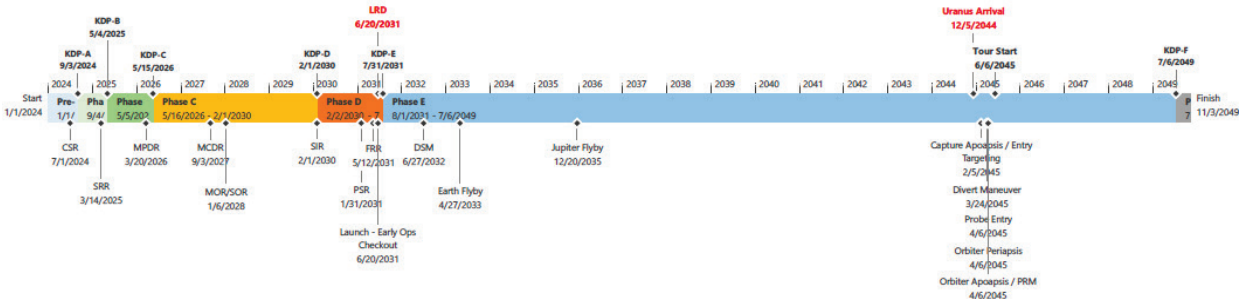

Exhibit 4-1. *High-Level Mission Schedule.*

Project Phase	Approximate Duration (mo.)
Phase A – Conceptual Design	8
Phase B – Preliminary Design	12
Phase C – Detailed Design	45
Phase D – Integration & Test	18
Phase E – Primary Mission Operations	216
Phase F – Extended Mission Operations	4
Start of Phase B to PDR	10
Start of Phase B to CDR	28
Start of Phase B to Delivery of Probe Instruments	47
Start of Phase B to Delivery of Orbiter Instruments	53
Start of Phase B to Delivery of Probe Aeroshell	54
Start of Phase B to Delivery of Probe Sphere Integrated	59
Start of Phase B to Delivery of Orbiter Bus	58
Start of Phase B to Delivery of Orbiter-Probe completed	60
System Level Integration & Test (From start of Probe System Integration through Orbiter System I&T/Environmental Test Program and Launch Site System Level Reintegration and Test)	23
Project Total Funded Schedule Reserve	7
Total Development Time Phase B–D	75

Exhibit 4-2. *Key Mission Phase Durations.*

Mission Level Milestones	Date
Concept Study Review (CSR)	7/1/2024
System Requirements Review (SRR)	3/14/2025
Mission Preliminary Design Review (PDR)	3/30/2026
Integrated Baseline Review (IBR)	11/5/2026
Critical Design Review (CDR)	9/1/2027
Mission/Science Operations Review (MOR/SOR)	1/4/2028
System Integration Review (SIR)	2/1/2030
Operational Readiness Review (ORR)	5/28/2030
Pre-Environmental Review (PER)	8/20/2030
Pre-Ship Review (PSR)	1/31/2031
Flight Readiness Review (FRR)	5/12/2031
Safety & Mission Success Review (SMSR)	6/11/2031
Launch Readiness Review (LRR)	6/14/2031
Launch Readiness Date (LRD)	6/20/2031

Exhibit 4-3. *Mission-Level Milestones.*

4.2. Technology Development Plan

The proposed baseline Orbiter and Probe designs are comprised entirely of heritage-based technology flown on recent, current, or planned space missions. All components have a test readiness level of 6 or higher and will require no additional technology development or funding to increase their TRL levels before the proposed launch date.

4.3. Development Schedule & Constraints

The development schedule assumes three Mod 1 NGRTGs are provided by the Department of Energy as Government Furnished Equipment (GFE), and that launch vehicle procurement is managed by NASA. The baselined launch window in 2031 is 21 days extending from 9 Jun 2031 to 30 Jun 2031, with a back-up opportunity in Apr 2032. Detailed Phase C/D and E scheduling information is provided in Appendix C. The schedule also incorporates the need to begin procurement of the custom propulsion tanks early during Phase A as long-lead items.

5. Mission Life Cycle Cost

5.1. Introduction

The cost estimate prepared for the UOP mission is of concept maturity level (CML) 4. The payload and spacecraft estimates capture the resources required for a preferred point design and take into account subsystem level mass, power, and risk. Our estimate also takes into account the technical and performance characteristics of components. Estimates for Science, Mission Operations, and Ground Data System elements whose costs are primarily determined by labor take into account the Phase A–D schedule and Phase E timeline.

The result is a mission estimate that is comprehensive and representative of expenditures that might be expected if the UOP mission is executed as described. The UOP mission cost, including unencumbered reserves of 50% (A–D) and 25% (E–F), is $2.8B in fiscal year 2025 dollars (FY$25), as shown in Ex. 5-1. Excluding all LV-related costs, the UOP Phase A–F mission cost is $2.6B FY25. Phase E costs are also shown.

WBS		Ph A–D	Ph E–F	Total	Notes
	Phase A	$7,628	—	$7,628	Assumption based on previous studies.
1	Program Management	$162,077	—	$162,077	A–D: wrap factor based on recent New Frontiers and APL missions E–F: bookkept with WBS 7
2	Systems Engineering				
3	Mission Assurance				
4	Science	$27,192	$233,668	$250,860	Average $13.3M per year during Phase E
5	Payload	$180,247	—	$180,247	Hardware estimated via parametric models (NICM, SEER Space)
6	Spacecraft (S/C)	$724,234	—	$724,234	Estimated via parametric models
7	Mission Operations (Mops)	$41,121	$299,053	$340,174	Ph E: DSN $21.3M, Average Ph Mops based on APL historical costs
8	Launch Vehicle	$236,000	—	$236,000	Falcon Heavy Expendable ($210M) + $26M NEPA
9	Ground Data System	$18,573	$19,313	$37,886	BOE
10	Integration & Test (I&T)	$114,869	—	$114,869	Based on APL historical I&T %, includes testbeds
	Reserves	**$634,157**	**$135,508**	**$769,665**	**Per Decadal guidelines: 50% A–D, 25% E–F. LV excluded**
	Total	**$2,146,097**	**$677,542**	**$2,823,640**	
	Total w/o LV	**$1,910,097**	**$677,542**	**$2,587,640**	

Exhibit 5-1. *Estimated Phases A–F UOP mission cost (FY$25K) by Level-2 WBS element.*

5.2. Mission Ground Rules & Assumptions

- Estimating ground rules and assumptions are derived from the *Decadal Mission Study Ground Rules* dated Feb 2021.
- Mission costs are reported using the Level-2 (and Level-3 where appropriate) work breakdown structure (WBS) provided in NPR 7120.5E.
- Cost estimates are reported in fiscal year 2025 (FY25) dollars.
- The NASA New Start inflation index provided by the Planetary Mission Concept Studies Headquarters (PMCS HQ) was used to adjust historical cost, price data, and parametric results to FY25 dollars if necessary.
- The mission does not require technology development dollars to advance components to TRL 6 because all UOP mission components will be at or above TRL 6 when required.
- A launch vehicle of sufficient capability to support the UOP mission is in development. Our assumption is that a launch vehicle meeting mission requirements will be available by 2030. Launch vehicle costs are estimated based on the expected capability.
- This estimate assumes no development delays and an on-time launch in Jun 2031.
- Phase A–D cost reserves are calculated as 50% of the estimated costs of all components excluding the launch vehicle. Phase E–F cost reserves are calculated as 25% of the estimated costs of all Phase E elements excluding DSN charges.

5.3. Cost Benchmarking

The cost and scope of the UOP concept corresponds well with NASA Flagship-class missions (Ex. 5-2). The estimated cost to develop and operate UOP compares favorably to current Flagship missions under development as well as past Flagship missions with an average cost of $3.1B, excluding launch vehicle costs, as shown in red.

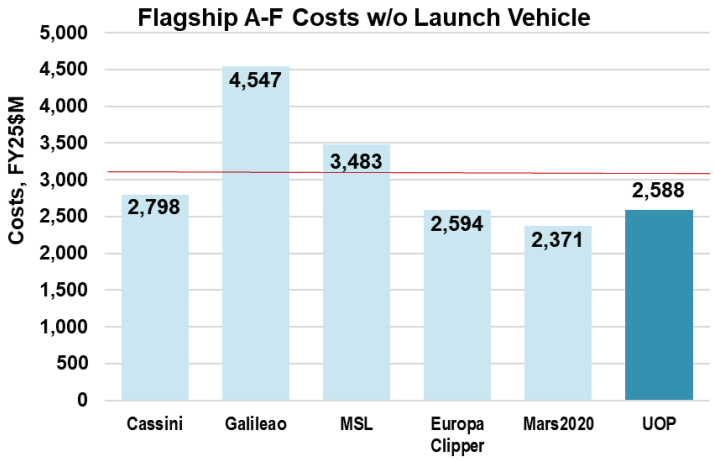

Exhibit 5-2. *Mission-level cost comparison (FY$25K) to other Flagship missions.*

5.4. Costing Methodology & Basis of Estimate

The UOP CML 4 mission cost estimate is a combination of high-level parametric and analog techniques and incorporates a wide range of uncertainty in the estimating process. No adjustments were made to remove the historical cost of manifested risk from the heritage data underlying the baseline estimate. Therefore, before reserves are applied, the estimated costs already include a historical average of the cost of risk. This approach is appropriate for capturing risk and uncertainty commensurate with early formulation stages of a mission. The following describes the basis of estimate for each element.

WBS 1, 2, 3: Project Management, Systems Engineering, Mission Assurance (PMSEMA). Because these functions depend on multiple mission- and organization-specific characteristics [Hahn 2014], cost analogies to comparable historical missions are preferred over cost model output, which does not take the mission into account. Existing analyses demonstrate that hardware costs are a reliable predictor of these critical mission function costs. APL has conducted thorough and rigorous analyses of PMSEMA costs, both for historical APL missions and for analogous missions. The PMSEMA estimate for UOP relies on APL's analysis of historical PM, SE, and MA practices on Van Allen Probes (VAP), Parker Solar Probe (PSP), and New Horizons (NH). VAP and PSP in particular include costs associated with current NASA requirements (e.g., Earned Value Management System (EVMS), 7120.5E). UOP's total mission PMSEMA cost is 15.9% of the flight system (payload + spacecraft + I&T). This percentage is allowed to vary along with hardware costs as part of the mission cost risk analysis, discussed below, to capture uncertainty (particularly given CML-4-level design phase).

WBS 4: Science. This element covers the managing, directing, and controlling of the science investigation. It includes the costs of the Principal Investigator (PI), Project Scientist (PS), science team members, and activities. The Phase A–D and E–F science estimate is an analogous estimate based on the cost per month of NH, MESSENGER, Cassini, Dragonfly, OSIRIS-REx, and Juno. MESSENGER is APL's most recent historical data point for planetary orbital science and Cassini is a recently completed outer planets flagship mission. The analogy costs are representative of expenditures for science on a typical New Frontiers or Flagship mission. The estimate reflects the manpower needed to create various data products as well as to ensure closure to science objectives.

WBS 5: Payload. The WBS 5 estimate includes a science payload of 8 instruments on the orbiter and 3 instruments on the probe and payload-level PMSEMA (Ex. 5-3). The USOs for both the orbiter and probe are bookkept with their spacecraft elements. The 8.2% cost-to-cost factor for estimating payload PMSEMA costs is based on the VAP, NH, MESSENGER, and PSP payload suite cost data with PMSEMA costs estimated as a percentage of the payload hardware. Technical management and systems engineering costs for individual instruments are carried in their respective instrument development costs.

Given the early design phase, multiple approaches are used to estimate each instrument to capture the potential range in cost. This includes two parametric estimates that rely on different sets of input variables (SEER Space and NICM 9), and historical analogous costs to specific heritage instruments where available. The orbiter payload draws heritage from MESSENGER, NH, LRO and PSP. Specifically, the Magnetometer and Electrons instruments are similar to MESSENGER/MAG and FIPS. The NAC and pieces of the Fields & Particles package are analogous to NH/LORRI and PEPSSI. The Ions and Energetic Particles instruments are analogous to PSP SPAN-B and EPI-Lo. The Probe payload is analogous to Rosetta and a subset of the Galileo sensors. An average of the two parametric estimates are used as the point estimate to prevent estimate bias (high or

	Cost (FY$25)	Notes
Payload	**$180,247**	**Hardware estimated via parametric models (NICM, SEER Space)**
Payload Mgmt	**$13,660**	**Based on VA, NH, MESSENGER, PSP**
Orbiter Payload	**$140,501**	
Magnetometer	$4,781	
Narrow-Angle Framing Camera	$27,283	
Thermal IR Camera	$38,242	
Fields & Particles Package	$29,803	
Plasma 1 (Electrons)	*$8,357*	
Plasma 2 (Ions)	*$7,106*	
Plasma 3 (Energetic Particles)	*$10,147*	
Waves	*$4,194*	
Radio Science / USO	—	USO carried under orbiter comms costs
Vis/NIR Imaging Spectrometer + WAC	$40,393	
Probe Payload	$26,087	
Mass Spectrometer	$18,661	
Atmospheric Structure Instrument	$4,153	
UltraStable Oscillator (USO)	—	USO carried under probe RF costs
Hydrogen Ortho-Para Sensor	$3,274	

Exhibit 5-3. *WBS 5 (payload) costs in FY$25K.*

	Cost (FY$25)	Notes
Spacecraft	**$724,234**	**Estimated via parametric models**
Orbiter	**$445,873**	**3 NGRTGs ($70M, $25M *2), SEER Space (prop and SW via ROM)**
Probe	**$233,131**	**SEER Space (FSW via ROM)**
EDL/Aeroshell	**$45,219**	**Price TruePlanning estimate**

Exhibit 5-4. *WBS 6 (spacecraft) costs in FY$25K.*

low) and are compared to historical analogies. These estimates are subject to a cost risk analysis (discussed below) to further quantify uncertainty.

WBS 6: Spacecraft. The WBS 6 estimate includes the orbiter, probe, aeroshell and 3 NGRTGs (Ex. 5-4). Spacecraft PMSEMA is carried in WBS 1, 2, and 3 consistent with APL in-house builds [Hahn 2015]. The basis of estimate relies primarily on parametric models. The exceptions to this are the propulsion system and FSW, estimated via a ROM by propulsion and FSW subject-matter experts based on recent experience, as well as the RTGs, in accordance with Decadal guidelines. Two parametric estimates are used as the point estimate. SEER Space is one of the primary estimating methodologies because it was designed specifically for missions in early formulation stages. TruePlanning is also utilized as it provides a cost estimate at the component level for the aeroshell. No major technology development is required for the spacecraft.

WBS 7 & 9: Mission Operations (MOps) & Ground Data Systems (GDS). The MOps estimate includes mission operations planning and development, network security, data processing, and mission management. The pre- and post-launch mission operations estimate are based on the cost per month of NH, PSP, and OSIRIS-REx. NH and PSP represent typical APL expenditure on pre-launch MOps for projects of comparable scope and complexity. The GDS estimate is a BUE from a ground data systems subject matter expert. The UOP Ground Data system provides full life cycle support for subsystem test, observatory I&T, hardware simulator control, & flight operations. The cost estimate is based on extensive reuse of PSP, Dragonfly, and DART Ground Software via APL's Mission Independent Ground Software (MIGS), as well as use of the existing Building 21 Mission Operations Center (MOC).

WBS 8: Launch Vehicle and Services. The mission requires a launch vehicle that does not correspond with any of the options currently described in the Decadal guidelines. As such, the figures used in this estimated are based on an evaluation of current best estimates of the cost of the capability that will be required. The price of a LV with Falcon Heavy Expendable-type capabilities, based on past pricing to NASA missions of EELVs, would be at least $210M for a launch using a standard sized fairing. NEPA and Nuclear Launch Approval costs are covered by the cost of the RTGs in WBS 6. The $26M RTG surcharge is included.

WBS 10: System Integration and Testing (I&T). This element covers the efforts to assemble and test the

spacecraft and instruments. The UOP I&T effort is estimated as 12.7% of the hardware. This percentage is based on a detailed analysis of cost actuals from previous APL missions, including MESSENGER, NH, STEREO, VAP, and PSP. This percentage is allowed to vary along with hardware costs as part of the mission cost risk analysis to capture the risk historically manifested during I&T.

Deep Space Network (DSN) Charges. This element provides for access to the DSN infrastructure needed to transmit and receive mission and scientific data. Mission charges are estimated using the Jet Propulsion Laboratory (JPL) DSN Aperture Fee tool. The DSN cost estimate covers pre- and post-contact activity for each linkage.

5.5. Confidence & Cost Reserves

The cost risk ranges by major WBS element as inputs for the UOP probabilistic cost risk analysis to quantify total cost risk are found in Ex. 5-5 and are described below.

PMSEMA. Given the use of cost-to-cost factors to estimate these functions, both the CER and underlying cost drivers are allowed to range so that all sources of uncertainty can be quantified.

Science, Ground Data Systems & Mission Ops. These are low-risk cost elements but are subject to cost growth as part of the cost risk analysis.

Payload. The average of the 70th percentile estimates of the two parametric model estimates is used to inform the UOP payload risk model to capture the uncertainty given the CML-4-level design phase.

Spacecraft. Each subsystem is subject to a data-driven risk analysis based on historical APL cost growth. Mass input also varies in the SEER space model consistent with early design programs to 30% over current best estimate.

WBS	Cost Element	Point	High
1,2,3	PMSEMA	$162,077	$217,559
4	Science	$250,860	$313,575
5	Payload	$180,247	$242,855
6	Spacecraft w/o RTGs	$604,234	$851,250
	RTGs	$120,000	$120,000
7	Mission Ops	$340,174	$425,217
8	Launch Vehicle	$236,000	$236,000
9	Ground Data System	$37,886	$47,358
10	I&T	$114,869	$154,191

Exhibit 5-5. *Inputs to cost distributions in FY$25K.*

Description	Value (FY$25K)	Confidence Level
Point Estimate	$2,053,975	47%
Mean	$2,297,629	
Standard Deviation	$900,550	
Cost Reserves	$769,665	
PIMMC	$2,823,640	78%

Exhibit 5-6. *Cost-risk analysis.*

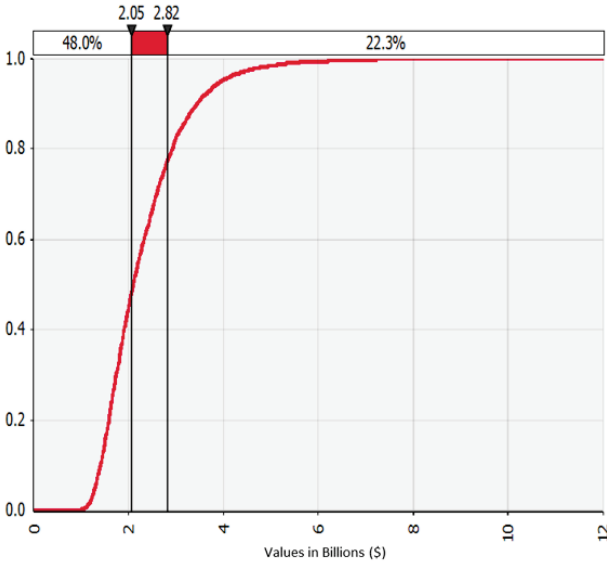

Exhibit 5-7. *S-curve summary of cost-risk analysis.*

Integration &Test. I&T as a percentage of the payload and spacecraft from the point estimate is used to inform the risk analysis, allowing I&T to vary with hardware cost.

Per the PMCS guidelines, the estimate includes unencumbered cost reserves of 50% of the estimated costs of all Phase A–D elements except for the launch vehicle. A probabilistic cost risk analysis shows 77.7% confidence that the Phase A–D mission is achievable within the estimated costs of this study (Ex. 5-6 and 5-7). The high confidence level is driven primarily by the large cost reserves for this pre-proposal concept. Given a typical competitive pre-Phase A NASA environment with 25% reserves on Phase A–D elements, the probabilistic cost risk analysis shows 67.1% confidence that the Phase A–D mission would be achievable. A 50th- to 70th-percentile confidence level is expected and reasonable for a pre-Phase A concept with this level of reserves.

A coefficient of variation (standard deviation/mean) of approximately 39% indicates appropriate levels of conservatism given the early formulation phase. The model confirms the point estimate and provides a reasonable basis for the UOP CML-4 study.

UOP's development plan includes ample cost reserves (50% on Ph B-D). However, should cost reduction be necessary due to budgetary constraints, there are several viable descope options available that would result in cost savings. Ex. 5-8 summarizes the resulting cost savings. The list provides reasoned descope options that can be implemented without affecting the threshold mission (see Ex. 1-10).

	Descope Option	Cost Savings (FY25 $K)	Mass Savings	Date to Realize Savings
1	Reduce length of Orbital Tour from 4 years to 2 years	$81,814	N/A	Start of Ph E
2	Remove WAC from Orbiter	$19,029	12 kg	PDR
3	Remove ortho-para sensor from Probe	$4,626	1 kg	PDR

Exhibit 5-8. *UOP Descope options and resulting cost savings.*

The estimated cost savings for removal of the WAC and ortho-para sensor instruments include hardware costs, as well as associated efforts for project management, systems engineering, mission assurance, payload management, and integration and test costs. The estimated cost savings for a reduced Orbital tour from 4 years to 2 years is derived from reducing the cost estimate for prime mission operations activities, as well as reducing ground data systems and science estimates by the same duration of time. All estimated cost savings for descopes are mutually exclusive.

.

Appendix A: Acronyms & Abbreviations

ACE	APL Concurrent Engineering
ACS	Attitude Control System
AO	Announcement of Opportunity
APL	(Johns Hopkins) Applied Physics Laboratory
ARC	Avionics Redundant Controller
AU	Astronautical Unit
BOE	Basis of Estimate
BOL	Beginning of Life
BUE	Bottom-Up Estimate
BWG	Beam Waveguide
C/A	Close (Closest) Approach
C&DH	Command and Data Handling
Catbed (Heaters)	Catalyst Bed (Heaters)
CBE	Current Best Estimate
CDR	Critical Design Review
CER	Cost Estimating Relationship
cFE	Core Flight Executive
CFD	Computational Fluid Dynamics
CFDP	CCSDS File Delivery Protocol
CG	Center of Gravity
CLPS	Commercial Lunar Payload Services
CML	Concept Maturity Level
CMOS	Complementary Metal Oxide Semiconductor
COTS	Commercial Off the Shelf
ΔV	Delta (Change in) Velocity
DART	Double Asteroid Redirection Test
DC/DC	Direct-Current to Direct-Current (Converter Card)
DCO	Data Cutoff
DD	Dust Detector
DDOR	Delta Differential One-Way Ranging
DMA	Direct Memory Access
DOE	Department of Energy
DOR	Differential One-Way Ranging

DPLR	Data Parallel Line Relaxation
DSM	Deep Space Maneuver
DSN	Deep Space Network
DSS	Digital Sun Sensor
DTE	Direct to Earth
DTM	Digital Terrain Model
DVR	Digital Video Recorder
E(ΔV)EJU	Earth-(Delta-V)- Earth Jupiter Uranus
EC	Electrical Conductivity
EDS	Entry & Descent System
EELV	Evolved Expendable Launch Vehicle
EFH	Expendable Falcon Heavy
EOL	End of Life
EOM	End of Mission
EPC	Electronic Power Conditioner
EPS	Electrical Power Subsystem
ESI	Engineering Science Investigation
ESA	European Space Agency
EVEEU	Earth-Venus-Earth-Earth-Uranus
EVEEJU	Earth-Venus-Earth-Earth-Jupiter-Uranus
EVMS	Earned Value Management System
F&P	Fields & Particles (Instrument Suite)
FIAT	Fully Implicit Ablation and Thermal response
FIPS	Fast Imaging Plasma Spectrometer
FOV	Field of View
FPGA	Field-Programmable Gate Array
FSS	Fine Sun Sensor
FSW	Flight Software
FY	Fiscal Year
G&C	Guidance and Control
GDS	Ground Data System
GFE	Government Furnished Equipment
GNC	Guidance, Navigation & Control
HEEET	Heatshield for Extreme Entry Environment Technology
HGA	High-Gain Antenna

I&T	Integration and Test
I^2C	Inter-Integrated Circuit
IBR	Integrated Baseline Review
IEM	Integrated Electronics Module
IIF	Instrument Interface (Card)
IMU	Inertial Measurement Unit
INMS	Ion & Neutral Mass Spectrometer
IR	Infrared
IT	Information Technology
IVO	Io Volcano Explorer (Proposed Discovery Mission in Step 2)
JGA	Jupiter Gravity Assist
JPL	Jet Propulsion Laboratory
JSC	Johnson Space Center
KBO	Kuiper Belt Object
L'Ralph	Lucy (Mission) Ralph (Instrument)
L/W	Launch Window
LEOP	Launch and Early Operations Phase
LGA	Low-Gain Antenna
LNA	Low-Noise Amplifiers
LORRI	(New Horizons) Long Range Reconnaissance Imager
LPW	(MAVEN) Langmuir Probe & Waves (Instrument)
LRD	Launch Readiness Date
LRM	Low-Reflectance Material
LRR	Launch Readiness Review
LV	Launch Vehicle
LVS	Low-Voltage Sensor
Ma	Million Years
MA	Mission Assurance
MAG	Magnetometer
MatISSE	Maturation of Instruments for Solar System Exploration
MEL	Master Equipment List
MEOP	Maximum Expected Operating Pressure
MER	Mars Exploration Rovers
MESSENGER	MErcury Surface, Space ENvironment, GEochemistry, and Ranging
MEV	Maximum Expected Value

MGA	Medium-Gain Antenna
MiSC	Mission-Specific Cards
MIGS	Mission Independent Ground Software
MIMU	Miniature Inertial Measurement Unit
MLI	Multi-Layer Insulation
MMH	Monomethylhydrazine
MMRTG	Multi-Mission Radioisotope Thermal Generator
MOC	Mission Operations Center
MOCET	(Aerospace Corp.) Mission Cost Estimating Tool
MON-3	Mixed Oxides of Nitrogen (Nitrogen Tetroxide)
MOps	Mission Operations
MOR	Mission Operations Review
MPV	Maximum Possible Value
MRAM	Magnetoresistive Random-Access Memory
MRR	Mission Readiness Review
MSC	(TRACERS) Search Coil Magnetometer
MSL	Mars Science Laboratory
MUX	Multiplexer
MY	Million Years
NAC	Narrow Angle Camera
NASA	National Aeronautics and Space Administration
NEPA	National Environmental Policy Act
NGRTG	Next-Generation (RTG)
NH	New Horizons
NICM	NASA Instrument Cost Model
NIR	Near Infrared
NOI	Neptune Orbit Insertion
NPR	NASA Procedural Requirement
NRC	National Research Council
NRE	Non-Recurring Engineering
OPAG	Outer Planets Assessment Group
ORR	Operational Readiness Review
OSIRIS-REx	Origins, Spectral Interpretation, Resource Identification, Security-Regolith EXplorer
PAF	Payload Adapter Fitting
PDB	Propulsion Diode Boxes

PDR	Preliminary Design Review
PDU	Power Distribution Unit
PER	Pre-Environmental Review
PICA	Phenolic-Impregnated Carbon Ablator
PIMMC	Principal Investigator Managed Mission Cost
PIMS	Plasma Instrument for Magnetic Sounding
PM	Project Management
PMCS	Planetary Mission Concept Studies
PMSEMA	Project Management, Systems Engineering, Mission Assurance
POST2	Program to Optimize Simulated Trajectories II
PPS	Pulse Per Second
PPU	Power Processing Unit
PRM	Periapsis Reduction Maneuver
PSP	Parker Solar Probe
PSR	Pre-Ship Review
PSI	Planetary Science Institute
PSU	Power Switching Unit
Q&A	Question & Answer
RDM	Radiation Design Model
RF	Radio Frequency
RHU	Radioisotope Heater Unit
RIO	Remote Input/Output
RIU	Remote Interface Unit
ROM	Rough Order of Magnitude
RPM	Rotations/Revolutions per Minute
RPS	(NASA) Radioisotope Power System(s)
RS	Radio Science
RTG	Radioisotope Thermoelectric Generator
RW	Reaction Wheel
S/C	Spacecraft
S&MA	Safety & Mission Assurance
SBC	Single Board Computer
SCIF	Spacecraft Interface
SE	Systems Engineering
SEE	Single Effect Effects

SEER	System Evaluation and Estimation of Resources
SEIS-SP	Seismic Experiment for Internal Structure-Short Period
SEP	Solar Electric Propulsion
SIR	System Integrations Review
SLS	Space Launch System
SMSR	Safety and Mission Success Review
SOC	Science Operations Center
SOR	Science Operations Review
SPHERE	Spectro-Polarimetric High-contrast Exoplanet REsearch
SPS	Sun Pulse Sensor
SRAM	Static Random-Access Memory
SRR	System Requirements Review
SRU	Shunt Regulator Unit
SSIRU	Scalable Space Inertial Reference Unit
SSPA	Solid State Power Amplifier
SSR	Solid-State Recorder
STM	Science Traceability Matrix
SWAP	(New Horizons) Solar Winds Around Pluto
SWAPI	(IMAP) Solar Winds and Pickup Ions
T-OWS	Triton Ocean World Surveyor
TAC	Thruster/Actuator Card
TCM	Trajectory Correction Maneuver
TID	Total Ionizing Dose
TNID	Total Non-Iodizing Dose
TOF	Time of Flight
TPS	Thermal Protection System
TRACERS	Tandem Reconnection and Cusp Electrodynamics Reconnaissance Satellites
TRL	Technology Readiness Level
TT&C	Tracking, Telemetry and Control
TWTA	Travelling Wave Tube Amplifier
UHF	Ultra-High Frequency
UMOD	Uranian Model
USO	UltraStable Oscillator
UV	Ultraviolet
UVIS	Ultraviolet Imaging Spectrometer

V&V	Validation & Verification
VAP	Van Allen Probes
VDA	Vacuum Deposited Aluminum
Vis/NIR	Visible and Near-Infrared (Imaging Spectrometer Instrument)
VLT	Very Large Telescope
WAC	Wide-Angle Camera
WBS	Work Breakdown Structure
WT	Traveling Wave Tube

Appendix B: References

Arridge, C.S. et al. (2011). Uranus Pathfinder: Exploring the Origins and Evolution of Ice Giant Planets. *Exp. Astron.,* **33,** 753–791. doi:10.1007/s10686-011-9251-4

Arridge, C.S. et al. (2014). The science case for an orbital mission to Uranus: Exploring the origins and evolution of ice giant planets. *Plan. & Space Sci.* **104***,* 122c140. doi:10.1016/j.pss.2014.08.009

Atreya, S.K. et al. (2020). Deep Atmosphere Composition, Structure, Origin, and Exploration, with Particular Focus on Critical in situ Science at the Icy Giants. *Space Sci Rev* **216**, 18. doi: 10.1007/s11214-020-0640-8

Bagenal, F. (1992). Giant Planet Magnetospheres. *Annual Rev. Earth Planet. Sci*. **20**, 289

Bagenal, F. (2013). Planetary Magnetospheres. In *Planets, Stars and Stellar Systems Vol. 3*, pp 251–307, Springer.

Bailey, E. & Stevenson, D. (2021). Thermodynamically Governed Interior Models of Uranus and Neptune. *Planet. Sci. Journal* **2**, 64

Cartwright, R. et al. (2018). Red material on the large moons of Uranus: Dust from the irregular satellites? *Icarus* **314,** 210–231. doi :10.1016/j.icarus.2018.06.004

Cassidy, T. et al. (2010). Radiolysis and Photolysis of Icy Satellite Surfaces: Experiments and Theory. *Space Sci Rev* **153**, 299

Cao, X., and C. Paty (2017). Diurnal and seasonal variability of Uranus's magnetosphere. *J. Geophys. Res. Space Physics* **122**, 6318. https://doi.org/10.1002/2017JA024063

Chen, Y-K., and Frank S. Milos (1999). Ablation and thermal response program for spacecraft heatshield analysis. Journal of Spacecraft and Rockets 36.3: 475-483

Clark, R.N. et al. (2019). Isotopic ratios of Saturn's rings and satellites; implications for the origin of water and Phoebe. *Icarus* **321** 791-802.

Cowley, S.W.H. (2013). Response of Uranus' auroras to solar wind compressions at equinox. *J. Geophys. Res. Space Physics* **118**, 2897. https://doi.org/10.1002/jgra.50323

de Kleer, K., I. de Pater, A.G. Davies, and M. Adamkovics (2013). Near-Infrared Spectra of the Uranian Ring System. *Icarus* **226**, 1038

Dumas, C., B.A. Smith, and R.J. Terrile (2003). Hubble Space Telescope NICMOS Multiband Photometry of Proteus and Puck. *Astron. J.***126**, 1080

Feuchtgruber, H., E. Lellouch, G. Orton, et al. (2013). The D/H ratio in the atmospheres of Uranus and Neptune from Herschel-PACS observations. *Astron. Astrophys.* **551**, A126. doi: 10.1051/0004-6361/201220857

Fletcher, L., H. Ravit, E. Roussos, et al (2020). Ice Giant Systems: The scientific potential of orbital missions to Uranus and Neptune. *Planet. Space Sci*. **191**, 105030. doi:10.1016/j.pss.2020.105030

Fletcher, L.N., I. de Pater, G.S. Orton, et al. (2020). Ice Giant Circulation Patterns: Implications for Atmospheric Probes. *Space Sci. Rev.s* **216**, article ID 21. https://arxiv.org/abs/1907.02901

Frelikh, R. and R. Murray-Clay (2017). The formation of Uranus and Neptune: fine tuning in core accretion. *Astron. J.* **154,** 98–106. https://doi.org/10.3847/1538-3881/aa81c7

French, R.S. and M. Showalter (2012). Cupid is doomed: An analysis of the stability of the inner Uranian satellites. *Icarus* **220**, 911–921. doi 10.1016/j.icarus.2012.06.031

French, R.G., R.I. Dawson, and M.R. Showalter (2015). Resonances, Chaos, and Short-term Interactions Amon the Inner Uranian Satellites. *Astron. J.* **149,** 142. doi 10.1088/0004-6256/149/4/142

Friedson, A.J. and E.J. Gonzalez (2017). Inhibition of ordinary and diffusive convection in the water condensation zone of the ice giants and implications for their thermal evolution. *Icarus* **297,** 160-178. doi:10.1016/j.icarus.2017.06.029

Fuller, J. (2014). Saturn ring seismology: Evidence for stable stratification in the deep interior of Saturn. *Icarus* **242**, 283.

Guillot, T. (1995). Condensation of methane, ammonia, and water and the inhibition of convection in giant planets. *Science* **269**, 1697-1699. doi:10.1126/science.7569896

Guillot, T., et al. (2018). A suppression of differential rotation in Jupiter's deep interior. *Nature* **555**, 227

Guillot, T., et al. (2020). Storms and the Depletion of Ammonia in Jupiter: II. Explaining the Juno Observations. *Journal of Geophysical Research: Planets* **125**, arti id. e06403

Hammel, H., I. de Pater, S. Gibbard, et al. (2005). Uranus in 2003 : zonal winds, banded structure, and discrete features. *Icarus* **175**, 534-545. doi :10.1016/j.icarus.2004.11.012

Helled, R., Anderson, J. D., & Schubert, G. (2010). Uranus and Neptune: shape and rotation. *Icarus* **210**, 446

Helled, R., Anderson, J. D., Podolak, M., & Schubert, G. (2011). Interior Models of Uranus and Neptune. *ApJ* **726**, 1. Doi: 10.1088/0004-637x/726/1/15

Helled, R. & Stevenson, D. (2017). The Fuzziness of Giant Planets' Cores. *ApJL* **840,** L4

Helled, R., Nettelmann N, Guillot T. (2020). Uranus and Neptune: Origin, Evolution and Internal Structure. *Space Sci. Rev*. **216**, 38.

Helled, R. & Fortney, J. (2020). The interiors of Uranus and Neptune: current understanding and open questions. *Phil. Trans. R. Soc. A.* **378,** art. ID 20190474. Doi: 10.1098/rsta.2019.0474

Herbert, F. (2009). Aurora and magnetic field of Uranus *J.Geophys.Res*. **114**, A11206. Doi: 10.1029/2009JA014394

Hesselbrock, A. and Minton, D. (2017). An ongoing satellite-ring cycle of Mars and the origins of Phobos and Deimos. *Nature Geoscience* **10**, 266

Hueso, R. and Sanchez-Lavega, A. (2019). Atmospheric Dynamics and Vertical Structure of Uranus and Neptune's Weather Layers. *Space Sci. Rev*. **215**, 52

Hueso, R., Guillot, T., Sanchez-Lavega, A. (2020). Convective storms and atmospheric vertical structure in Uranus and Neptune. *Phil. Trans. of the Royal Society A* 378, art id.20190476

Iess, L. et al. (2014). The Gravity Field and Interior Structure of Enceladus. *Science* **344**, 78

Ip, W. (2006). On a ring origin of the equatorial ridge of Iapetus. *Geophys. Res. Lett.* **33,** L16203

Karkoschka, E. (2001). Comprehensive Photometry of the Rings and 16 Satellites of Uranus with the Hubble Space Telescope. *Icarus* **151**, 51.

Karkoschka, E. (2003). Sizes, shapes, and albedos of the inner satellites of Neptune. *Icarus* **162**, 400

Kaspi, Y. et al. (2013). Atmospheric confinement of jet streams on Uranus and Neptune. *Nature* **497**, 344

Kaspi, Y. et al., (2018). Jupiter's atmospheric jet streams extend thousands of kilometres deep. *Nature* **555**, 223

Kegerreis, J. et al., (2018). Consequences of Giant Impacts on Early Uranus for Rotation, Internal Structure, Debris, and Atmospheric Erosion. *ApJ* **861,** 52

Lainey, V. et al., (2009). Strong tidal dissipation in Io and Jupiter from astrometric observations. *Nature* **459**, 957-959

Lamy, L., et al. (2012). Earth-based detection of Uranus' aurorae. *Geophys. Res. Lett*. **39**, L07105.

Leconte, J. et al. (2017). Condensation-inhibited convection in hydrogen-rich atmospheres . Stability against double-diffusive processes and thermal profiles for Jupiter, Saturn, Uranus, and Neptune. *Astron. & Astrophys*. **598**, A98

Li, C. et al. (2017). The distribution of ammonia on Jupiter from a preliminary inversion of Juno microwave radiometer data. *Geophysical Research Letters* **44**, 5317

Lissauer, J. et al. (2009). Models of Jupiter's growth incorporating thermal and hydrodynamic constraints. *Icarus* **199**, 338

Mahaffy, P. et al. (2000). Noble gas abundance and isotope ratios in the atmosphere of Jupiter from the Galileo Probe Mass Spectrometer. *Journal of Geophysical Research* **105**, 15061

Mandt, K. et al. (2020). Tracing the Origins of the Ice Giants Through Noble Gas Isotopic Composition. *Space Science Reviews* **216**, article ID 99

Mankovich, C. et al. (2018). Cassini Ring Seismology as a Probe of Saturn's Interior. I. Rigid Rotation. *ApJ* **871**, 1

McAdams, J., Scott, C., Guo, Y., and Dankanich, J., *Conceptual Mission Design of a Polar Uranus Orbiter and Probe*, Advances in the Astronautical Sciences, 2011

Moore, K. et al. (2019). Time variation of Jupiter's internal magnetic field consistent with zonal wind advection. *Nature Astron*. **3**, 730.

Moses, J. et al. (2020). Atmospheric chemistry on Uranus and Neptune. *Phil. Trans. of the Royal Society A* **378**, article id.20190477

Mousis, O. et al. (2020). Key Atmospheric Signatures for Identifying the Source Reservoirs of Volatiles in Uranus and Neptune. *Space Science Reviews* **216**, article id.77

National Aeronautics and Space Administration, *Ice Giants Pre-Decadal Survey Mission Study Report*, June 2017

Nettelmann, N. et al. (2013). New indication for a dichotomy in the interior structure of Uranus and Neptune from the application of modified shape and rotation data. *Planetary Space Sci*. **77**, 143.

Nicholson. P. et al. (2018). The Rings of Uranus. In *Planetary Ring Systems*, pp. 93–111. Cambridge University Press

Niemann, H. et al. (1998). The composition of the Jovian atmosphere as determined by the Galileo probe mass spectrometer. *J. of Geophysical Res*. **103**, 22831

Orton, G.S. et al. (2016). Constraints on the Bulk Composition of Uranus from Herschel PACS and ISO LWS Photometry, SOFIA FORCAST Photometry and Spectroscopy, and Ground-Based Photometry of its Thermal Emission. EGU General Assembly 2016, id. EPSC2016-5041

Pappalardo, R., Reynolds, S., Greeley, R. (1997). Extensional tilt blocks on Miranda: Evidence for an upwelling origin of Arden Corona. *J. Geophys. Res*. **102**, 369

Peterson, G., Nimmo, F., Schenk, P. (2015). Elastic thickness and heat flux estimates for the uranian satellite Ariel. *Icarus* **250**, 116.

Podolak, M., Weizman, A., & Marley, M. (1995). Comparative models of Uranus and Neptune. *Planet. Space Sci.* **43**, 1517

Podolak, M., Helled, R., Stevenson, D. (2019). Effect of non-adiabatic thermal profiles on the inferred compositions of Uranus and Neptune. *Monthly Notices of the Royal Astro. Society* **487,** 2653.

Reinhardt, C. et al. (2020). Bifurcation in the history of Uranus and Neptune: the role of giant impacts. *Monthly Notices of the Royal Astro. Society* **492**, 5336

Rosenblum, E. et al. (2011). Turbulent Mixing and Layer Formation in Double-Diffusive Convection: Three-Dimensional Numerical Simulations and Theory. *Astrophysical Journal* **731**, 66

Schenk, P. et al. (2011). Plasma, plumes and rings: Saturn system dynamics as recorded in global color patterns on its midsize icy satellites. *Icarus* **211**, 740.

Schenk, P. and Moore, J. (2020). Topography and geology of Uranian mid-sized icy satellites in comparison with Saturnian and Plutonian satellites. *Phil. Trans. R. Soc. A* **378**, article ID: 20200102

Scheibe, L. Nettelmann, N., Redmer, R. (2019). Thermal evolution of Uranus and Neptune I. Adiabatic models. *Astronomy & Astrophysics* **632**, A70.

Selesnick, R. S., and McNutt, R. L., Jr. (1987). Voyager 2 plasma ion observations in the magnetosphere of Uranus. *J. Geophys. Res.* **92**, 15,249

Showalter, M. (2020). The rings and small moons of Uranus and Neptune. *Phil. Trans. of the Royal Society A* **378**, article id 20190482

Smith, B.A. et al. (1986). Voyager 2 in the Uranian System: Imaging Science Results. *Science* **233**, 43

Soubiran, F. & Militzer, B. (2015). Miscibility calculations for water and hydrogen in giant planets. *ApJ* **806,** 228

Soubiran et al. 2017). Properties of hydrogen, helium, and silicon dioxide mixtures in giant planet interiors. *Physics of Plasmas* **24**, 041401

Sromovsky, L.A., Fry, P., Kim, J. (2011). Episodic bright and dark spots on Uranus. *Icarus* **215**, 292

Stanley, S., J. Bloxham (2004). Convective-region geometry as the cause of Uranus' and Neptune's unusual magnetic fields. *Nature* **428**, 151

Stanley, S., J. Bloxham (2006). Numerical dynamo models of Uranus' and Neptune's magnetic fields. *Icarus* **184**, 556

Teanby, N. et al. (2020). Neptune and Uranus: ice or rock giants? *Phil. Trans. of the Royal Society A* **378**, article id.20190489

Toth, G., Kovacs, D., Hansen, K.C, Gombosi, T. (2004). Three-dimensional MHD simulations of the magnetosphere of Uranus. *J. Geophys. Res.* **109**, A11210

Sohl, F. et al. (2010). Subsurface Water Oceans on Icy Satellites: Chemical Composition and Exchange Processes. *Space Sci Rev* **153**, 485

Weiss, B. et al (2021). Searching for Subsurface Oceans on the Moons of Uranus Using Magnetic Induction. 52nd Lunar and Planetary Science Conference 2021, Abs. 2096

Valletta, C. & Helled, R. (2019). The Deposition of Heavy Elements in Giant Protoplanetary Atmospheres: The Importance of Planetesimal–Envelope Interactions. *ApJ* **871,** 127

Vasyliunas, V. M. (1986). The convection-dominated magnetosphere of Uranus. *Geophys. Res. Letters* **13**, 621

Vazan, A. and Helled, R. (2020). Explaining the low luminosity of Uranus: A self-consistent thermal and structural evolution. *Astron. & Astrophys* **633**, A50

Vision and Voyages for Planetary Science in the Decade 2013-2022, National Academies Press (National Research Council. 2011. Vision and Voyages for Planetary Science in the Decade 2013-2022. Washington, DC: The National Academies Press. https://doi.org/10.17226/13117)

Voigt, G H., Behannon, K.W., Ness, N.F. (1987). Magnetic field and current structures in the magnetosphere of Uranus. *J. Geophys. Res*. **92**, 15337

von Zahn, U., Hunten, D., Lehmacher, G. (1998). Helium in Jupiter's atmosphere: Results from the Galileo probe Helium Interferometer Experiment. *J. Geophys. Res*. **103**, 22815

Appendix C: Additional Details

See separate file for Appendix C details.